ECOLE POLYTECHNIQUE FEDERALE DE LAUSANNE
SCHOOL OF LIFE SCIENCES

Master project in Life Sciences and Technology

IMPLEMENTATION OF A HUMAN FEEDBACK-BASED LOCOMOTION AND ITS CONTROL BY MEANS OF A FEEDFORWARD COMPONENT INSPIRED BY CENTRAL PATTERN GENERATORS

Carried out in the laboratory of BioRob
at EPFL
Under the supervision of Jesse Van den Kieboom

Done by

FLORIN DZELADINI

Under the direction of
Prof. Auke Ijspeert
In the laboratory of BioRob
EPFL

External Expert Dr. Hugo Gravato Marques

LAUSANNE, EPFL

January 2013

Abstract

Bipedalism is considered as one of the first distinctive feature developed by the early hominids, compared to their cousins apes. This unique characteristic of human beings has always intrigued scientists and thus has been extensively studied. In the past decades, modeling of human walking has gained particular interest in research, with the venue of computers and increasing computational power. Modeling of human walking is of particular interest in the biomechanical and medical field, as it can give insights in the design of limb prosthesis, providing crucial information regarding the movement of the limb. Moreover, it is also important for the design of limb orthoses, devices used to modify the skeletal and neuromuscular systems, which are used in rehabilitation by assisting movement of people with walking difficulty (e.g. due to neurodegenerative diseases, such as multiple sclerosis or due to spinal cord injury), or assisting people with injuries during their rehabilitation.

To grasp the context of this project, it is necessary to introduce animal movement modeling. Animal movement can be modeled as a system of differential equations, coupled trough interactions of the system with the environment (i.e. sensors to send information to the system, and actuators send information to the environments). In this framework, walking can be viewed as a limit cycle; the system oscillates, its trajectory is confined around the mean of the system trajectory. This limit cycle possesses a relative resistance to perturbations, i.e., the walking can be more or less stable.

Walking gaits of various animals have been modeled using this framework of differential equations, and more specifically, using network of coupled oscillators. In these models, oscillators are coupled among themselves and thus influence each other. Nerve signals generating swimming in the Lampreys have been modeled using such a system. When the lamprey swims, nerve influxes are observed as activity burst, repeated at defined intervals. These bursts are observed along the spinal cord, with a delay in the burst onset that is proportional to the position along the spinal cord. These neural oscillatory networks are called central pattern generator (CPG), and have also been observed in the locomotion of other animals, such as the salamander or the cheetah.

These oscillatory networks were successfully used to model several swimming animals. However, results obtained with walking animals have been rather disappointing, except for the salamander, whose movements are relatively simple and slow. This is not surprising, since this system does not take into account interaction with the environment for shaping the movement, which should be more important for walking animals.

To show the importance of interaction with the environment, work by H. Geyer and his group (2010) should be introduced. They have developed a human walking model solely based on reflexes (i.e. interactions between the body and the environment). This model includes limb dynamic information (muscles, tendons and sensors) and shows the importance of reflexes pathways in movements shape. Applied to the human, this model, based on simple reflex rules, is capable of producing a stable gait, comparable to the real human gait.

In an adaptation of the model made by J. Wang (2012), both walking and running were obtained by simply varying the parameters of the system. Implementing both the H. Geyer (referred to as the FBL model, for Feedback Based Locomotion) and the J. Wang model (referred to as FBL+) is the purpose of the first part of this project.

The presented FBL model shows the importance of the interaction between the body and the environment. Biologically, it is known that reflex loops do exist, but a walking 100% based on reflexes is not possible. The presence of a feedforward component allowing control of gait parameter (such as speed, frequency, step size) seems obvious. The question is therefore: What is the feedforward component and how can it be integrated to the existing model? It is plausible - though extensively debated and unproven - that a CPG component acting on locomotion exist in the human spinal cord. In this project we make the hypothesis of the presence of such a component. Since reflexes can generate signals that place the system in a limit cycle, and taken into account the hypothesis that a feedforward component exist, we can make the new hypothesis that the feedforward component must be hidden behind those reflex signals.

The analysis of the signals generated by the reflex loops of the FBL model is the starting point of the second part of this report, where it is demonstrated that when the FBL model produces a stable locomotion, most of the signals oscillate at a quasi constant frequency, with only slight variation in shape. Most stable signals are then modeled as oscillators that can generate waves of arbitrary shapes and/or basal constant input.

We then test the properties of such a system by combining/replacing some reflex loops by their feedforward counterparts (either as a basal input or as a CPG). We show that, not only those new models are stable with characteristics close to the original model, but with online control they showed a clear increase of the robustness compared to the FBL and FBL+ models. Moreover, modifications of some general parameters of the feedforward component allow easy changes in gait characteristics, such as gait speed.

Nomenclature

General abbreviations

CNS	Central nervous system
CPG	Central pattern generator
FBL	Feedback based walking
FBL+	Feedback based walking extension inspired by [30]
IN	Interneuron
MN	Motoneuron
IN_{CPG}	CPG interneuron
IN_{FF}	Feedforward interneuron
IN_{SD}	State dependent interneuron
IN_{SEN}	Sensory interneuron
cFOOT	Contraleteral Foot
iFOOT	Ipsilateral Foot
ANKLE	Ankle joint
HIP	Hip joint
KNEE	Knee joint
GLU	Hip extensor muscle
HF	Hip flexor muscle
VAS	Knee extensor muscle
GAS	Ankle extensor muscle
TA	Ankle flexor muscle
HAM	bi-articular hip extensor and knee flexor muscle
SOL	bi-articular knee flexor and ankle extensor muscle
EC	Solution evaluation criterion
PSO	Particle swarm optimization
SC	Solution run stopping criterion

Muscles components

be	muscle parallel passive element 1 (buffer elasticity)
ce	muscle contractil element
pe	muscle parallel passive element 2 (parallel elasticity)
se	muscle serial passive element (serial elasticity)

Muscles variables

F_{ce}	*ce* force
F_{mtu}	MTU force
F_{se}	*se* force
l_{ce}	*ce* length
l_{mtu}	MTU length
l_{se}	*se* length

Muscles parameters

θ_{max}	Joint angle at which for a given MTU $t_{\theta\to\tau}$ is maximum
θ_{ref}	Reference joint angle which corresponds to the angle of the joint at the initialisation of the MTU
$c = log(0.05)$	
F_{max}	MTU maximum force
$K = 1.5$	
l^0_{mtu}	Initial muscle length
$N = 5.0$	
$pennetation$	Factors accounting for fibers muscle orientation bias
v_{max}	*ce* maximum shortening velocity

Joint variables

θ	Joint angle
$t_{\theta\to\tau}$	MTU Force to joint torque transfer function

Joint parameters

δ_{max}	Maximum joint angle before soft limit engages
δ_{min}	Minimum joint angle before soft limit engages
r_0	Moment arm for a given MTU joint connection

Optimization criterion

C_{angles}	Criterion used for similarity with human angle maximization
C_{left_right}	Criterion used for left right assymetry minimization
$C_{steplengths}$	Criterion used for step lengths variability minimization
C_{trunk}	Criterion used for minimizing trunk leaning
$C_{speed}(v_{opt})$	Criterion used for optimization toward a given speed v_{opt}
$C_{steplength}(s_{opt}$	Criterion used for optimization toward a given steplength s_{opt}

Feedbacks

MFF	Muscle Force Feedback
MLF	Muscle Length Feedback
GCF	Ground Feedback
GIF	Ground & Stability Feedback
OPF	Joint over extension prevention Feedback

Contents

Part I

Feedback based walking (FBL) model

Chapter 1

Introduction

In the first part of the report we will describe a walking model inspired by the work of H.Geyer [9, 8] and J. Wang [30].

In 2010, the H. Geyer group designed a bipedal walking model based on a simple reflex loop, that was able to produce stable walking gait using sensory information solely [9]. This model is hereafter referred to as FBL; feedback-based locomotion. Sensory modalities from muscles (i.e. the Golgi tendon and muscle spindle), from feet (pressure sensors) and from the vestibular system were modeled as simple system (muscle spindle were modeled has an affine transform of the muscle length, Golgi tendon as being proportional to the muscle forces, pressure sensors under each foot being proportional to the reaction force with the ground and finally sensory modalities from the vestibular system were modeled as a simple PD control which tries to bring the angle of a joint (e.g. the trunk) toward a reference angle). Muscle activity was then obtained as a linear combination of the different sensors. The coefficients of the sensors-muscles linear map were determined using optimization algorithms. This methodology led to gaits of various characteristics, some resembling the human gait, others totally unnatural. However, with carefully chosen optimization criteria, the results - both in term of muscle activation pattern and movements - were comparable to real human walking.

An important feature of the H.Geyer model is its link with biological structures. The different biological structure captured by the FBL model are presented below. The detail concerning the modeling is described in section 2.1.3.

1.1 Biological muscle

Skeletal muscles are made of multiple bundles named the fascicles, each of which contains many muscle fibers, the individual muscle cells. Within the muscle cells are the myofibrils, which are the muscle contractile units. They are themselves made of repeating units: the sacomeres, which consist of organized actin and myosin filaments which, by sliding along each other shorten the fiber, provoking the muscle contraction (see figure 1.1). The active force generated by the contraction of the sarcomeres can be modeled at the muscles level by a bell shaped curve with a maximum occuring close to muscle resting length. When stretched behond a certain length, the elastical property of a protein called titin (which is part of sarcomere) generates, at the muscle level, a passive repealing force in the opposite direction (e.g. acting against its elongation) [10].

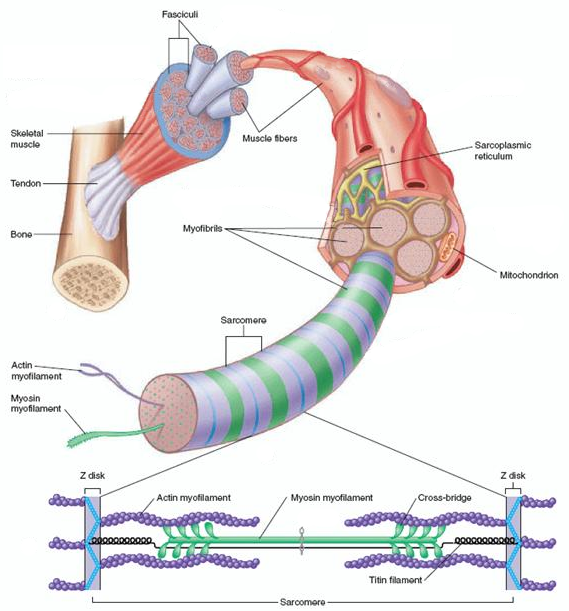

Figure 1.1: Illustration of the skeletal muscle anatomy and contraction process. Adapted from [25]

1.1.1 Force-length relationship

The relation between the length of a muscle and the force generated can be understood by looking at the property of sarcomeres to generate an active force with a bell shaped profile and a passive repealing force when stretched beyond a certain length. The resulting shape of the muscle force-length relationship is shown in figure 1.2, left panel.

1.1.2 Force-velocity relationship

The relationship between the shortening velocity during concentric contractions (shortening contractions) and the force generated by the muscle represents the dynamic property of the actin - myosin interaction cycle. The force-velocity profile has a inverted sigmoidal shape. The force generated is maximum when the muscle is lengthening and goes to zeros when the muscle is shortening [11]. The right panel of figure 1.2 shows a plot of the force-velocity relationship.

1.1.3 Muscle contraction

Muscle contraction occurs when receiving signals from efferent nerves from the central nervous system. There are three different types of contractions: concentric contraction (i.e. when contraction occurs while muscle is shortening), eccentric contraction (i.e. when contraction occurs while muscle is lengthening, meaning that the force generated by the muscle is less than the tension applied to the muscles) and isometric contraction (i.e. when the muscles generate force without changing its length, for example, when gripping an object). During walking, mainly concentric and eccentric contractions occurs.

1.1.4 Muscle fibers types

Skeletal muscles are composed of two types of fibers: the type I and type II fibers, called slow and fast twitch fibers, respectively. Fast twitch fibers are activated faster than slower ones and can produce more energy but they fatigue more quickly. This difference is

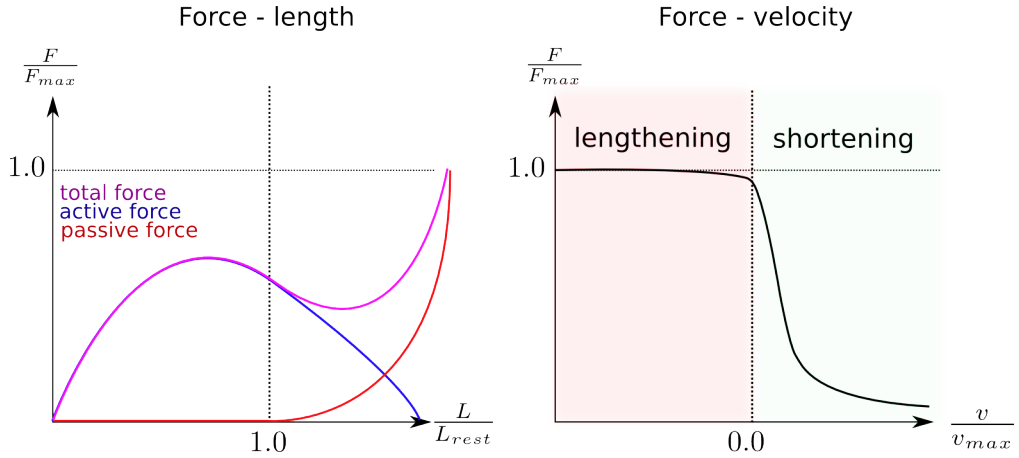

Figure 1.2: LEFT PANEL: muscle force-length relationship. RIGHT PANEL: muscle force-velocity relationship. F refers to the force generated by the muscle, F_{max} is the maximal force that can be generated by the muscle, L is the muscle length, L_{rest} is the muscle reference length, v is the muscle contractile velocity, v_{max} is the maximum muscle velocity.

due to the fiber composition; slow twitch fibers composition favors aeorobic metabolism (i.e. they contain many mitochondria and are surrounded by many capilllaries), whereas fast twitch fibers have a composition which favors anaeorobic metabolism (mostly lactic acid fermentation) [27]. In order to understand why the type II fibers contract faster but fatigue quicker than the type I fibers we have to look at the mechanisms by which cells produce energy. Cells produce energy mainly by regenerating their stock of Adenosine triphosphate (ATP) from Adenosine di and monophosphate (respectively ADP and AMP). In animal cells, this can be achieved through different processes, depending on the presence or absence of oxygen. One of the main reaction chain used in both aerobic (with oxygen) and aneorobic (without) conditions to regenerate the ATP is the transformation of oxygen into pyruvate. This is done through a reaction chain called glycolysis. The overall chemical reaction of glycolysis is:

$$\mathrm{Glu} + 2\,\mathrm{NAD}^+ + 2\,\mathrm{P}^\mathrm{i} + 2\,\mathrm{ADP} \longrightarrow 2\,\mathrm{Py} + 2\,\mathrm{NADH} + 2\,\mathrm{ATP} + 2\,\mathrm{H}^+ + 2\,\mathrm{H}^2\mathrm{O} + \mathrm{heat}$$

Where, Glu is the gluscose, Py the pyruvate, ADP the adenosine dyphosphate, ATP the adenosine triphosphate.

Then, in the presence of oxygen, the pyruvate will be transformed to acetyl-CoA and enter in the krebs cycle (a chain of 10 reactions that involves many different compounds) while in absence of oxygen, pyruvate undergoes a process of fermentation which oxidizes the NADH by-product of glycolysis back to NAD^+, thus regenerating the NAD^+ needed by the glycolysis.

Therefore, what makes the muscles fibers II faster than fibers I is the fact that the fermentation is much faster in regenerating the NAD^+ stock than the electron transport chain. However the fermentation process produces lactic acid which accumulates and makes prolonged effort painful.

1.1.5 Muscle spindles

Muscles spindles are sensory receptors found in the central part of the muscles, which provide sensory feedback information to the central nervous system (CNS). They are composed of two different afferent fibers called primary and secondary nerve fibers. The firing rate of the primary fibers is mainly related to changes in muscle velocity, while the

firing rate of the secondary fibers is mainly related to changes in muscle length [20]. The response of the primary and secondary fibers muscle spindles to change in velocity and length, respectively, can be modulated by efferent neurones called γ motoneurons.

1.1.6 Tendon

The tendon is a viscoelastic structure connecting muscles to bones. It is composed of parallel collagen fibers. At the junction between the muscles and the tendon, is the golgi tendon organ, which is a proprioceptive structure conveying the muscle force information to the CNS.

Chapter 2

Methods

2.1 Modeling

The FBL model is presented in the two next sections. In the first section, the different subcomponents of the model are presented (muscle models, sensors models). In the second section, the different subcomponents are combined into a physical model of the lower part of a human body (implemented in Webots), where the muscles of both limbs and the trunk are represented; each limb is modeled by seven muscles that acts on three joints (hip, knee and ankle) and a model allowing the gait generation is then added to the lower limb model, where the activity of each muscles is generated by different feedback rules.

This model is able to produce stable locomotion at different speed, with characteristics close to human walking, by solely using sensory information. In short, a direct mapping is created between a set of sensors (the different sensors modeled are: muscle sensors (length and force sensors), joint sensors, ground sensors) to the muscle input.

2.1.1 Humanoid subcomponents modeling

2.1.1.1 Muscle model

The muscle model presented here is based on the Hill model and was developed by the H. Geyer group published in 2004 in *Neural Systems and Rehabilitation Engineering* [8]. In this model, the muscle is modeled together with its respective tendon and is called a muscle tendon unit (MTU). An active, contractile element (ce) with two passive parallel elements (buffer elasticity be and parallel elasticity pe) form the muscle, see figure 2.1. The active element represents the muscle contraction, while the two passive elements simulates the physical properties of the muscle fibers. The be element prevent muscle from collapsing, while the pe prevent muscle length from going beyond a certain length. The tendon is modeled as a passive element in series with the muscle, called series elasticity (se), see figure 2.1.
In the normal state, only the ce and se element are active. pe and be engages only when the muscle is slack (i.e if $l_{mtu} - l_{ce} < l_{slack}$) or stretches beyond its optimal length (i.e if $l_{ce} > l_{opt}$).

General equations
Because of the physical connection between the muscle and the tendon (se), the total force of the MTU is equal to the force coming from the tendon (se) and will always equal the

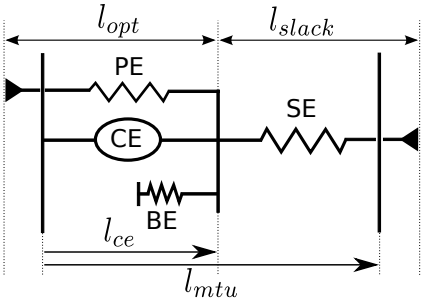

Figure 2.1: Schematic view of a muscle tendon unit (MTU) adapted from [9]. In the normal state, only the serial element (*se*) and the contractile element (*ce*) are active. Two other passive elements are added in parallel of *ce*: *be* that engages if tendon is slack (i.e if $l_{mtu} - l_{ce} = l_{se} < l_{slack}$), preventing muscle collapse, and *pe*, that engages when the muscle stretches beyond its optimal length (i.e if $l_{ce} > l_{opt}$), preventing the muscle to extend beyond a certain length.

contribution from the muscle. We thus have :

$$F_m = F_{se} \tag{2.1}$$
$$= F_{ce} + F_{pe} - F_{be} \tag{2.2}$$

The contribution of the *be* is opposite to the action of *ce* because it acts against the contraction, as *be* acts to prevent the muscle from collapsing. Conversely, the contribution of the *pe* is positive as it acts in the same direction as the muscle contraction. The force of the muscle depends on its activity (A), on its length through the f_l function and on its velocity through the f_v function. The three functions are restricted to the $[0; 1]$ interval, and the maximum muscle force (F_{max}) is reached, obviously, when the three functions are equals to one. The equation governing the muscle force is given by :

$$F_{ce} = A \cdot F_{max} \cdot f_l(l_{ce}) \cdot f_v(v_{ce}) \tag{2.3}$$

with:

$$f_l(l_{ce}) = exp\left(c\left|\frac{l_{ce} - l_{opt}}{l_{opt} w}\right|^3\right) \tag{2.4}$$

$$f_v(v_{ce}) = \begin{cases} \frac{v_{max} - v_{ce}}{v_{max} + K v_{ce}} & \text{if } v_{ce} < 0 \\ N + (N-1)\frac{v_{max} + v_{ce}}{7.56 K v_{ce} - v_{max}} & \text{if } v_{ce} \geqslant 0 \end{cases}. \tag{2.5}$$

$$\frac{dA}{dt} = \tau(S(t) - A) \tag{2.6}$$

The activity of the contractile element A is modeled as a first order differential equation of the stimulation S sent to the muscle accounting for neural delay. The f_l function has a bell shaped profile. It models the relationship between the active force generated by the muscle and the length of the muscle. The f_v function has an inverted sigmoid shape given by biological muscles force - velocity relationship, see section 1.1.2. The passive force of the muscle is modeled by the *pe* spring. The *be* is added to prevent muscle to reach zero length. The *pe* element engages when muscle extends beyond its optimal length ($l_{ce} > l_{opt}$) and the *be* element engages when muscle is slack ($l_{mtu} - l_{ce} > l_{slack}$). The passive elements *be*, *pe* and *se* are modeled as unidirectional non linear spring damper, acting in one direction. They are modeled as monotonical non-linear functions. *be* acts

against muscle contraction movement and engages only when muscles is close to minimal length, its force should monotonically increase as the muscle length decreases. *pe* acts against muscle elongation and models the macroscopic effects of titin molecules present in each sarcomeres (see section 1.1). The equations of the two passive parallel elements (*pe* and *be*) are given by :

$$F_{be} = \begin{cases} F_{max}(\frac{l_{opt}-w-l_{ce}}{l_{opt}w/2})^2 & \text{if } l_{mtu}-l_{ce} > l_{slack} \\ 0 & \text{else} \end{cases}. \tag{2.7}$$

$$F_{pe} = \begin{cases} F^*_{pe} \cdot f_v(v_{ce}) = F_{max}(\frac{l_{ce}-l_{opt}}{l_{opt}w})^2 \cdot f_v(v_{ce}) & \text{if } l_{ce} > l_{opt} \\ 0 & \text{else} \end{cases}. \tag{2.8}$$

The tendon is function of the tendon length (l_{se}) and acts against its elongation. It is active only if it extends beyond its slack length ($l_{se} > l_{slack}$) and its force should monotonically increase as the length of the tendon increases. There is also a constraint that the maximum force generated by the tendon should not exceed the maximum force of the muscle F_{max}. Here the tendon force is modeled as a square function of the normalized tendon length $\varepsilon(l_{se}) = \frac{l_{se}-l_{slack}}{l_{slack}}$:

$$F_{se} = \begin{cases} F_{max} \cdot (\frac{\varepsilon}{\varepsilon_{ref}})^2, & \text{if } \varepsilon > 0 \\ 0 & \text{else} \end{cases}. \tag{2.9}$$

The general equations used in the model are summarized in table 2.1.

Force calculation

In order to simulate an MTU, we need to compute the force for a given MTU state, which is given by its muscle length (l_{ce}) and speed (v_{ce}) and the corresponding tendon length (l_{se}). The resolution of the MTU is done in three steps:

1. Solve the general muscle force equation 2.1 for f_v

   (a) Compute F_{se}, F^*_{pe}, F_{be} using:

$$F_{se} = \begin{cases} F_{max} \cdot (\frac{\varepsilon}{\varepsilon_{ref}})^2, & \text{if } \varepsilon > 0 \\ 0 & \text{else} \end{cases}. \tag{2.10}$$

$$F_{be} = \begin{cases} F_{max}(\frac{l_{min}-l_{ce}}{l_{opt}w/2})^2 & \text{if } l_{mtu}-l_{ce} > l_{slack} \\ 0 & \text{else} \end{cases}. \tag{2.11}$$

$$F^*_{pe} = \begin{cases} (\frac{l_{ce}-l_{opt}}{l_{opt}w})^2 & \text{if } l_{ce} > l_{opt} \\ 0 & \text{else} \end{cases}. \tag{2.12}$$

   (b) Replace in eq. 2.1 :

$$F_{ce} = F_{se} - F_{pe} + F_{be} \tag{2.13}$$

$$= F_{se} - F^*_{pe} \cdot f_v + F_{be} \tag{2.14}$$

   (c) Then, compute f_l and the activation A. Since F_{pe} depends linearly on f_v we can easily solve the equation for f_v. Using equations 2.3 and 2.14 we obtain:

$$f_v = \frac{F_{se} + F_{be}}{F_{max}(A \cdot f_l(l_{ce}) + F^*_{pe})} \tag{2.15}$$

Table 2.1: Main equations of the muscle model from H.Geyer.

Main equations

Name	Equation	Signification
F_{mtu}	$F_m = F_{se} = F_{ce} + F_{pe} - F_{be}$	Force of generated by the MTU
F_{se}	$F_{se} = \begin{cases} F_{max} \cdot (\frac{\varepsilon}{\varepsilon_{ref}})^2, & \text{if } \varepsilon > 0 \\ 0, & \text{else} \end{cases}$.	Force generated by the tendon
F_{pe}	$F_{pe} = \begin{cases} F_{max}(\frac{l_{ce}-l_{opt}}{l_{opt}w})^2 \cdot f_v(v_{ce}) & \text{if } l_{ce} > l_{opt} \\ 0 & \text{else.} \end{cases}$	Force of the parallel element preventing muscle overextension
F_{be}	$F_{be} = \begin{cases} F_{max}(\frac{l_{opt}-w-l_{ce}}{l_{opt}w/2})^2 & \text{if } l_{mtu} - l_{ce} > l_{slack} \\ 0 & \text{else} \end{cases}$.	Force of the parallel element preventing muscle to collapse
F_{ce}	$F_{ce} = A \cdot F_{max} \cdot f_l(l_{ce}) \cdot f_v(v_{ce})$	Force generated by the muscle (ce)
A	$\frac{dA}{dt} = \tau(S(t) - A)$	Muscle activation is equal to the integral of the input signal $I(t)$. Biologically, the input signal can be viewed as the normalized frequency of neuronal spike that reaches the muscle (i.e. restricted to the $[0; 1]$. interval). The activation is thus also limited to this interval.
$f_l(l_{ce})$	$f_l(l_{ce}) = exp(c\left\lvert\frac{l_{ce}-l_{opt}}{l_{opt}w}\right\rvert^3)$	Muscle force - muscle length relationship function (function of the muscle length (l_{ce})
$f_v(v_{ce})$	$f_v(v_{ce}) = \begin{cases} \frac{v_{max}-v_{ce}}{v_{max}+Kv_{ce}} & \text{if } v_{ce} \geqslant 0 \\ N + (N-1)\frac{v_{max}+v_{ce}}{7.56Kv_{ce}-v_{max}} & \text{if } v_{ce} < 0 \end{cases}$.	Muscle force - muscle velocity relationship function (function of the muscle velocity (v_{ce})
$v_{ce}(f_v)$	$v_{ce}(f_v) = \begin{cases} v_{max} \cdot \frac{1-f_v}{1+K*f_v} & \text{if} f_v < 1.0 \\ v_{max} \cdot \frac{f_v-1}{7.56K(f_v-N)+1-N} & \text{else} \end{cases}$.	Inverse of the muscle force - velocity function. This function is used for the resolution of the muscles equations.
l_{ce}	$l_{ce} = \frac{dv_{ce}}{dt}$	Muscle (ce) length
l_{se}	$l_{se} = l_{mtu} - l_{ce}$	Tendon (se) length
l_{mtu}	$l_{mtu} = l_{slack} + l_{opt} + \Delta l_{mtu}$	MTU length
Δl_{mtu}	$\Delta l_{mtu} = pennation \cdot r_0 \cdot \int_{\theta_{ref}}^{\theta} t_{\theta \to \tau}(\theta, \theta_{max})$	MTU length changes from MTU slack length

2. Using the inverse of the muscle force - velocity relationship defined in eq. 2.4, we get the muscle contraction speed v_{ce}:

$$v_{ce}(f_v) = \begin{cases} v_{max} \cdot \frac{1-f_v}{1+K*f_v} & \text{if } f_v < 1.0 \\ v_{max} \cdot \frac{f_v-1}{7.56K(f_v-N)+1-N} & \text{else} \end{cases}. \tag{2.16}$$

3. Integrating the muscle speed we get the muscle length l_{ce}. At each time step, the changes in length of the contractile element dl_{ce} is related to the contraction speed by $dl_{ce}/dt = v_{ce} = [f_v(v_{ce})]^{-1}$, which is integrated using a runge-kutta fourth order resolution method.

4. Using the total force $F_{mtu} = F_{ce}$ of the muscle we can deduce the torque that will generate the changes in angle of joint(s) on which the muscle is acting. This is done through the webots controller by numerically solving the physical constraints.

5. Finally, the new angle θ is used to compute l_{mtu} (length of the muscle-tendon unit) using eq. 2.24, which gives the length of the serial element l_{se} through the relation $l_{mtu} = l_{se} + l_{ce}$. (See 2.1.1.1 for details on the calculation of l_{mtu}.)

Torque generation
Each MTU contributes to the movement of one or two joints depending on the type of muscles ("normal" vs "bi-articular" muscles). In the original article of H.Geyer [8], the torque is calculated as:

$$\tau = t_{\theta\to\tau}(\theta) \cdot F_{mtu} \tag{2.17}$$

Where $t_{\theta\to\tau}$ is a function limited to the interval $[0; 1]$ that translates the ability of the muscle in rotating the joint onto which it acts. The function $t_{\theta\to\tau}$ is maximal at the angle θ_{max}, which corresponds to the angle at which the torque generated by the muscle on the joint is maximal. The $t_{\theta\to\tau}$ function used in [9] is defined as:

$$t_{\theta\to\tau} = 1 \tag{2.18}$$

for the hip joints and

$$t_{\theta\to\tau} = cos(\theta - \theta_{max}) \tag{2.19}$$

for ankle and knee joints.

Note on the calculation of $t_{\theta\to\tau}$
When approximating a muscle as a straight line, an exact transfer function can be easily derived using the sine and cosine laws. The resulting transfer function is :

$$t_{\theta\to\tau} = \frac{sin(\theta)}{(1 + a^2 - 2a \cdot cos(\theta))^{1/2}} \tag{2.20}$$

Where $a = cos(\theta_{max})$ (see below for calculation detail). This function is, under the assumption made on the muscle shape, a geometrically correct version of the function defined in equation 2.19. As expected, when comparing the two functions (see figure 2.2), the major features are the same (i.e. maximum at θ_{max} and monotonically decreasing on each side of the maximum). Furthermore in the range of action of the joints during human walking the error is negligible between the two functions. Both 2.18 and 2.19 can

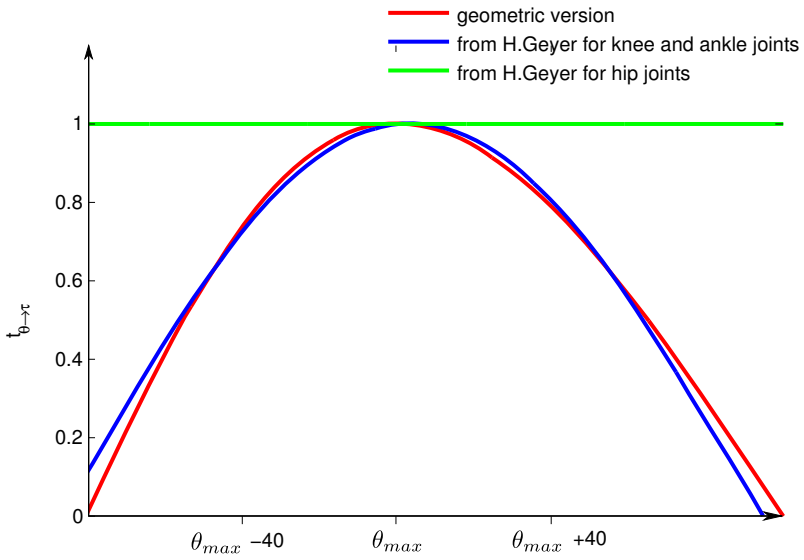

Figure 2.2: Comparison of the different $t_{\theta\to\tau}$ functions. All functions are normalized by r_0. In blue the transfer function used by H.Geyer for knee and ankle joints (see eq. 2.19), in green the one used for hip joints and in red the function derived in this section.

be viewed as approximation of the function just defined. Concerning the hip joints tranfer function, the fact that the range of the hip joint is small is a good justification in the choice made by H.Geyer to choose a constant transfer function $t_{\theta\to\tau}$.

Below we give the detail of the calculation of $t_{\theta\to\tau}$.

We are looking at the force that contributes to the joint torque τ (see figure 2.3) and thus only the component perpendicular to the the displacement vector r_0 (i.e. the vector from the point from which torque is measured to the point where force is applied) contributes to the force.

$$\tau = F \cdot t_{\theta\to\tau} = F \cdot x$$

with

$$x = r_0 \cdot sin(\alpha)$$

then, from the sine and cosine laws:

$$\begin{aligned} \frac{sin(\alpha)}{l_0} &= \frac{sin(\theta)}{l_{mtu}} \\ l_{mtu} &= (r_0^2 + l_0^2 - 2 l_0 r_0 cos(\theta))^{1/2} \end{aligned}$$

It follows

$$t_{\theta\to\tau} = x/r_0 = \frac{sin(\theta)}{l_{mtu}} \cdot l_0 = \frac{sin(\theta)}{(r_0^2 + l_0^2 - 2 l_0 r_0 cos(\theta))^{1/2}} \cdot l_0 \tag{2.21}$$

To compare with the H. Geyer model, we should express l_0 as a function of θ_{max}. θ_{max} corresponds to the angle at which the force generated by the muscles is maximum. If we assume that the muscle fibers are parallel to the vector formed by the attached point of the muscle on the bones, the angle formed by the closest anchor point to the joint and the

muscle would be close to 90 degrees as noted in fig. 2.3. Therefore, we can approximate that $cos(\theta_{max}) = \frac{r_0}{l_0}$ and eq. 2.21 becomes:

$$\begin{aligned} t_{\theta\to\tau} &= \frac{sin(\theta)}{((r_0/l_0)^2 + (l_0/l_0)^2 - 2l_0r_0/(l_0^2)cos(\theta))^{1/2}} \cdot l_0/l_0 \\ &= \frac{sin(\theta)}{((r_0/l_0)^2 + 1 - 2(r_0/l_0)cos(\theta))^{1/2}} \\ &= \frac{sin(\theta)}{(1 + a^2 - 2a \cdot cos(\theta))^{1/2}} \end{aligned}$$

Where $a = cos(\theta_{max})$.

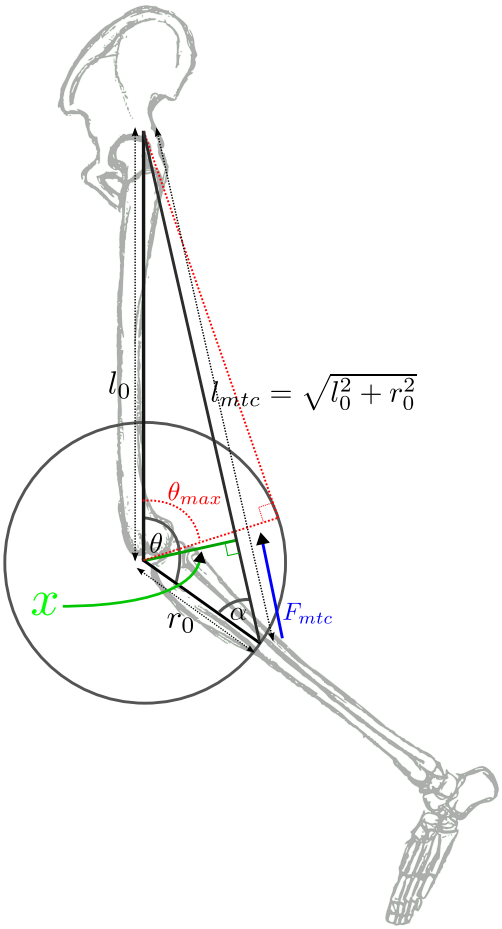

Figure 2.3: Geometric approximation of the Biceps femoris (the muscle responsible for knee flexion) muscle attachment. The muscle is approximated by a straight rigid body attached at a position r_0 from the knee in the tibial bone and at a position l_0 from the knee in the femur bone. The Force generated by the muscle is assumed to be parallel to the rigid body (the force vector is in blue). When the angle formed by the femur and the tibial is θ_{max} the torque is maximum ($||\tau|| = ||F_{mtu}||$).

MTU length calculation

The approach used for the calculation of the MTU length (l_{mtu}) is based on an estimation of the changes in the MTU length based on changes in joint angles. The change in MTU length dl_{mtu} can be modeled as follow :

$$dl_{mtu} = r_0 \cdot t_{\theta\to\tau} \tag{2.22}$$

Intuitively, this modeling is justified by the property of $t_{\theta\to\tau}$. Indeed this function is maximal (equals one) when all the force generated by the MTU contributes to changes in joint angle. This happens when the angle formed by the MTU and the joint is equal to $pi/2$, which corresponds to the joint angle $\theta = \theta_{max}$. We thus have - as expected for $\theta = \theta_{max}$ - a change in muscle length of $dl_{mtu} = r_0$.

Given a joint angle θ and a reference angle θ_{ref}, changes in the length of an MTU can be calculated by integrating $t_{\theta\to\tau}$, the function defined in the previous paragraph (eq. 2.18 and eq. 2.19).

$$\Delta l_{mtu} = pennation \cdot r_0 \cdot \int_{\theta_{ref}}^{\theta} t_{\theta\to\tau}(\theta, \theta_{max}) \tag{2.23}$$

then, the total length of an MTU is given by

$$l_{mtu} = l_{slack} + l_{opt} + \Delta l_{mtu}. \tag{2.24}$$

The *pennation* factor is added to take into account the fact that muscle fibers are not perfectly aligned with the muscle attachment position.

Initialization
To initialize an MTU, its length (l_{mtu}) must be calculated using the eq. 2.24.
From the MTU length, both the length of the contractile element (l_{ce}) and the length of the serial element l_{se} can be derived. The initial speed of contraction/elongation (v_{ce}) as well as the activation level (A) are assumed to be equal to zero. The MTU length depends on whether the MTU is slack or not. If the MTU is slack (e.g. $F_{se} = 0$), then

$$l_{ce} = l_{opt} \tag{2.25}$$
$$l_{se} = l_{mtu} - l_{ce} \tag{2.26}$$

If the MTU is not slacked then $F_{se} > 0$ and since $F_{ce} = 0$, we have

$$F_{pe} = F_{se} \tag{2.27}$$
$$(\frac{l_{ce} - l_{opt}}{l_{opt} w})^2 \cdot f_v(v_{ce}) = (\frac{\varepsilon}{\varepsilon_{ref}})^2 \tag{2.28}$$

From which we can get:

$$l_{se} = l_{slack} \frac{l_{opt} w + \varepsilon_{ref}(l_{mtu} - l_{opt})}{l_{opt} w + \varepsilon_{ref} l_{slack}} \tag{2.29}$$
$$l_{ce} = l_{mtu} - l_{se} \tag{2.30}$$

2.1.1.2 Biological sensors models

There are four informations sensors that sends signal to the muscles (shown in figure 2.4):

1. **Muscle sensors.** There are two muscle feedbacks types. A muscle length feedback, modeling the muscle spindle, and a muscle force feedback, modeling the Golgi tendon. The muscle length feedback equation for a given MTU m ($Fb_l(m)$) is defined as follow:

$$Fb_l(m) = \frac{l^m_{ce}}{l^m_{opt}} - l^m_{offset} \tag{2.31}$$

   Where,

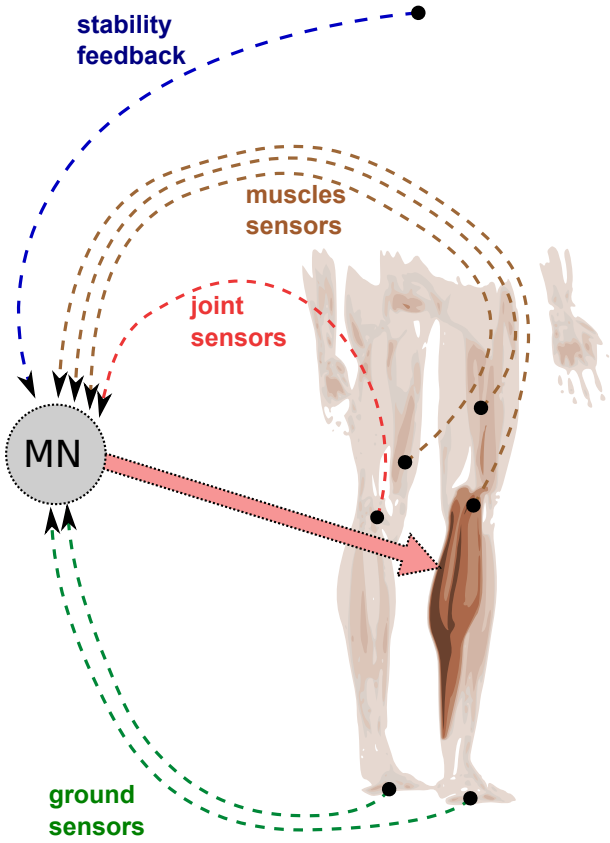

Figure 2.4: In the FBL model, the walking cycle is divided in three different part (swing (sw), stance (st) and stance end st_{end}). The activity of a muscle in each cycle part is governed by a linear combination of signal from different sources: muscles length and force sensors, joint sensors and ground sensors.

- the exposant m refers to a specific MTU
- l^m_{offset} is a parameter found by optimization
- l^m_{ce}, l^m_{opt} are respectively the ce length and the ce optimal length of MTU m.

The muscle force feedback equation for a given MTU m ($Fb_f(m)$) is defined as follow:

$$Fb_f(m) = \frac{F^m_{mtu}}{F^m_{max}} \tag{2.32}$$

Where,

- F^m_{mtu} corresponds to the current force generated by the mtu m
- F^m_{max} corresponds to the maximum force that can be generated by the mtu m

2. **Joint overextension prevention sensors.** This sensor is used to prevent knee joint overextension. It is modeled as a simple correction term proportional to the differences between max tolerated angles ϕ^{off} and actual joint angle ϕ. The sensors output for a joint j is given by:

$$Fb_o(j) = \begin{cases} (\phi_j - \phi^{off}_j) & \text{if } \Delta\theta > 0, \omega/\omega_{ref} > -1 \\ 0 & \text{else} \end{cases} \tag{2.33}$$

3. **Ground sensors.** There are two ground sensors that feel the reaction forces on the ground; one located at the toe and one at the heel level. In order to ensure a smooth variation of the sensors values, the output of the sensors is modeled as linear differential functions of the reaction forces. For instance, the equation governing the toe sensor output is given by

$$\frac{dF}{dt} = \tau f \tag{2.34}$$

Where,

- F is the sensors feedback
- f is the reaction force
- $\tau = 100$ is the convergence speed

The ground feedback (Fb_g) on side s is defined as being equal to the sum of the two ground sensors normalized by the total weight of the model:

$$Fb_g(s) = k_{bw}\frac{F^s_{toe\_ground} + F^s_{heel\_ground}}{M \cdot g} = k_{bw}\frac{F^s_{ground}}{M \cdot g} \tag{2.35}$$

Where,

- g is the gravity
- M the mass of the model
- s is the side (i.e ipsilateral if feedback acts on motoneurone of the same side and contralateral otherwise)
- k_{bw} is a parameter found by optimization.

4. **Stability feedback.** The stability sensors are used to insure stability. They work by trying to bring a joint toward a reference angle using a PD control adapted to act at the muscle level.The feedback acts on the muscles in order to bring the angle of a joint toward a reference angle δ_{ref}. The feedback is given by :

$$Fb_s \quad = \quad \left\{k_p \cdot (\delta - \delta^{ref}) + k_d\dot{\delta}\right\}_{\pm} \tag{2.36}$$

Where,

- δ corresponds to the actual joint angle we want to bring toward a reference angle
- δ_{ref} is the reference angle.

The sign of the brackets depends on the action of the muscles on the trunk; Negative if the action of the muscle is in the direction of positive angle changes and positive otherwise [30].

In the FBL model, this feedback is used to maintain the trunk straight. This is done by sending a signal to hip muscles (i.e. GLU, HAM and HF) during stance phase (st). In order to account for the fact that only the leg in contact with the ground can be used to stabilize the trunk, the stability feedback signal is combined with the ground sensors of the same leg, allowing the leg bearing most of the weight (i.e. more stable) to be used to maintain the trunk. It has be shown that this combination of the stability feedback and ground sensors is not necessary if during double stance support the stability feedback is applied only to muscles of the leg in stance end

phase (st_{end}) [30], see section 2.1.2.3 for description of cycle phases description. The exact same kind of feedback rule is used by J. Wang to bring the hip and knee joint toward a target reference angle during the end of the swing phase (see section 2.1.3 for details).

A biological link with the function of the cerebellum can be made. Indeed, as seen in 5.1.2, one of the function of the cerebellum is to adapt to perturbation by reducing the error that it induces. Note that for the trunk joint, δ and δ_{ref} are angles calculated in a global reference frame (i.e. with respect to the vertical axes). If this kind of feedback exists it should not only involve the cerebellum but also the vestibular system. Indeed, as it can feel the gravity, a vertical global reference frame could emerge from structure having afferent from the vestibular system. It is thus likely that this kind of feedback would emerge from the reticular formation as it integrates information from both the cerebellum and the vestibular system (see section 5).

2.1.2 Humanoid modeling

2.1.2.1 Lower limbs description

In order to obtain a walking human model, the MTUs previously defined must be associated to form a working lower body. The lower limb model is defined as a two dimensional system composed of seven degrees of freedom, corresponding to the seven joints of the lower limbs: one degree of freedom for the trunk and one degree of freedom for each ankle, knee and hip joint of both limbs. In those seven MTUs per limb, five are normal MTUs and two are bi-articular MTUs (acting on two joints simultaneously). The hip joints are driven by two normal MTUs: the gluteus (GLU) and the hip flexor (HF) MTU permittingF respectively extension and flexion of the joints. The ankle joints are also driven by two normal MTUs: the gastrocnemius (GAS) and the tibialis (TA) MTUs, permitting extension and flexion of the joints, respectively. The knee joints are driven by only one normal MTUs: the vasilus (VAS) MTU, permitting the joint extension. The knee flexion is ensured by two bi-articular MTU: the hamstring (HAM) and the soleus (SOL), generating knee flexion and respectively hip and ankle extensions. The MTUs and joints corresponding to the MTUs and the values of their associated parameters are given in table 2.2. A schematic view of the system is presented in figure 2.5.
The physical model used as starting point was implemented on webots by Steve Berger during its master thesis at BioRob in 2011. The weight and length of the different segments are based on anthropometric data from [31] (see table 2.2).

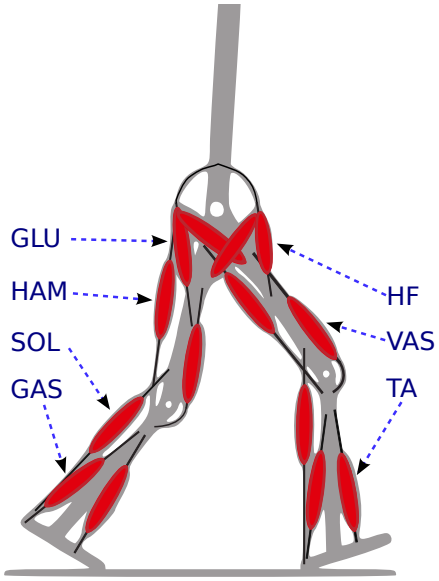

Figure 2.5: View of the lower limb model with the 14 MTUs and the joints onto which they act, figure inspired from [9].

2.1.2.2 Muscles to Joints mapping

The torque acting on one joint is given by the combination of the action of the different muscles that can act on it. The torque at joint J is thus defined as :

$$\tau_J = \sum_{M \epsilon J} \tau_J^M = \sum_{M \epsilon J} r_0^M \cdot t^M_{\theta_J \to \tau}(\theta) \cdot F^M_{mtu} \tag{2.37}$$

Where,

- J represents a joint
- M represents a MTU
- F^M_{mtu} the force generated by M
- r_0^M the moment arm of M on J
- $t^M_{\theta_J \to \tau}(\theta_J)$ the transfer function that account, given a joint angle θ_J for the contribution of M to τ_J
- τ_J the actual torque acting on J.

The action of one muscle on a joint has been described in detail in section 2.1.1.1.

Joint Soft limit

The model previously described does not take into account the effect of ligaments. Ligaments form the joint that maintains two bones together and also keep the angle formed by the joined within a given range. Its action is against the movement and engages only when the angle is beyond certain limit, which depends on the joints (see table 2.3). Here we model the ligament as non linear spring damper acting as soft limit on the joints [9, 26] that is added to τ_J, if the joint angle is outside its normal range.

When the angle goes beyond the limit of the joint and the angular speed is not big enough to bring back the joint in its normal range a force is generated. The resulting torque τ acting on the joint is modeled as :

$$\tau = \begin{cases} k \cdot \Delta\theta \cdot (1 - \omega/\omega_{ref}) & \text{if } \Delta\theta > 0, \omega/\omega_{ref} > -1 \\ 0 & \text{else} \end{cases} \tag{2.38}$$

Where,

- $k = 17.19[Nm/rad]$ is the spring damper stiffness.
- $\omega_{ref} = 1.74 \cdot 10^{-2}[rad/s]$ is the reference angular speed, used to normalize the joint angular speed.
- $\Delta\theta$ is the angle by which the joint limit is exceeded (i.e. difference between the actual angle and the limit angle). Note that the axes are chosen so that $\Delta\theta > 0$ when the joint limit is passed.
- $\omega[rad^{-1}]$ is the angular speed. Note that the axes of rotation are chosen so that $\omega > 0$ when the angle is going toward the joint limit angle.
- τ is the torque acting on the joints. The direction of the torque is chosen in order to maintain the joint angle in its range of operation.

Note that this model of non linear spring damper is also used in the model of H.Geyer to model the ground reaction forces to foot contact. Here the contact of the robot with the ground are managed by the physical simulator of webots, thus we use this model only for modeling the ligaments.

2.1.2.3 Sensors to muscles mapping

Cycle phase description
In the FBL model the activity of the motoneurons depends on the cycle phase. In the model of H.Geyer the cycle is divided in three parts :

- Stance (st) phase
- Swing (sw) phase
- Stance end (st_{end}) phase

The ground sensors - as defined in eq. 2.34 - are used to detect the state of the limb (i.e. st / sw). A threshold is put on the summed signals from toe and heel ground sensors. If reached, the limb is assumed to be in st phase. The st_{end} phase corresponds to the double stance support phase when the contralateral limb just touched the ground.

Figure 2.6 shows a schematic view of the FBL model regarding the cycle phase separation.

Feedback rules
The FBL model developed by H.Geyer is a pure feedback model (i.e. it has no feedforward component). In the FBL, the activity of each MTU depends solely on a delayed weighted sum of different sensory inputs (called reflexes or feedbacks).

For each muscle, a signal $S_M(t)$ is generated as a basal activity (S_M^0), plus a linear combination of the weighted feedback signals $Fb_{i,j}(t)$. The signal $S_M(t)$ can be viewed as the normalized spiking frequency of the motoneurons pool of a muscle M or, in other words, its normalized "activity":

$$S_M(t) = \begin{cases} S_M^0 + \sum_{i \epsilon muscles} \sum_{j \epsilon sensors} W_{i,j} \cdot Fb_{i,j}(t) & \text{if } 0 \leqslant S_M(t) \leqslant 1 \\ 0 & \text{if } S_M(t) < 0 \\ 1 & \text{if } S_M(t) > 1 \end{cases} . \quad (2.39)$$

Note that, for each muscle, only a small part of the sensors are used; most of the weight $W_{i,j}$ are equals to zero (see table 2.4 for detailed reflex equations for each muscle). Information about the sensors used by each muscle is based on the work of H. Geyer.

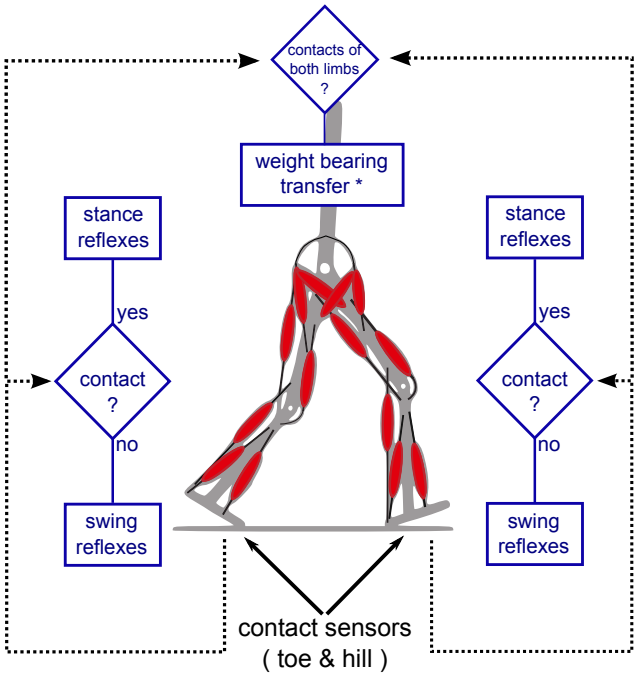

Figure 2.6: Schematic view of the reflex based walking model from H.Geyer. Ground sensors are used to detect whether the limb is on stance or swing phase. Then, depending on whether the limb is in contact with the ground, different reflex rules are generated (all reflex rules are shown on table 2.4). An extra term is added to the hips flexor (i.e. HF) and hips extensor (i.e. GLU) to facilitate the weight bearing transfer during the end of the stance, when the other limb touches the ground (i.e. during the double stance support). Figure inspired from [9].

The motoneurons output $S_M(t)$ is related to the muscle activity $A_M(t)$ through the first order linear equation :

$$\frac{d}{dt}A_M = \tau(S_M(t) - A_M(t)) \tag{2.40}$$

This differential equation models the delay that exists between the firing of motoneurons and their action on the muscle contraction. The delay is modeled as a first order differential equation. The law governing the activities of each muscles during the different cycle phases are presented in table 2.4. This model uses the 2D physical model of lower limbs described in the previous section, and adds the MTU activity rules.
The input to a motoneuron can be different depending on the limb cycle phase. There is a set of rules for st phase (s_M^{st}) and another for the sw phase (s_M^{sw}). There is also an extra term added to the hips flexor (i.e. HF) and hips extensor (i.e. GLU) motoneurons signals during the st_{end} phase, this extra term is added to facilitate the weight bearing transfer. The table 2.4 shows all the different s_M input signal to motoneurons associated to each muscles.

Model parameters

All muscles parameters and joints ranges are taken from [9]. Parameters of the lower limbs are based on anthropometric data taken from [31]. The only parameters that are optimized are the parameters associated with the sensors-muscles mapping, whose rules are shown in table 2.4. There are 28 parameters (5 for stability feedback, 6 for muscle force feedbacks, 6 for muscle length feedbacks, 7 for basal muscle activity and 4 other parameters) which are

found by optimization, the table 2.5 presents the parameters together with their respective range. In this project, we used the Particle Swarm Optimization PSO method (described in section 2.2) to found optimal parameters values.

2.1.2.4 Energy consumption model

One of the main feature used as optimization criterion is the energy consumption of the system. The energy consumption model is inspired from [3], as used in [30]. The model also separates the activation heat rate and the maintenance rate in two terms: one for slow twitch fibers, and one for fast twitch fibers. Slow twitch fibers are activated more slowly than fast twitch fibers (see section 1.1.4 for details). The full model of energy of one MTU M with :

- m : mass
- t_I : type I fiber percentage
- s : neural stimulation
- a : muscle activity
- F : active force generated by the muscle
- F_t : the total force generated by the MTU

can be written as:

$$E = A + M + S + W \tag{2.41}$$

Where:

- $A = m \cdot f_A(s)$ is the activation heat rate, with :

$$f_A(s) = 40 \cdot t_I \cdot sin(\pi/2 \cdot s) + 133 \cdot t_I I \cdot (1 - cos(\pi/2 \cdot s) \tag{2.42}$$

- $M = m \cdot g(l_{ce}/l_{opt}) \cdot f_M(a)$ is the maintenance heat rate, with :

$$g(l) = \begin{cases} 0.5 & \text{if } 0.0 \leqslant l \leqslant 0.5 \\ 1 & \text{if } 0.5 < l \leqslant 1.0 \\ -2l + 3 & \text{if } 1.0 < l \leqslant 1.5 \\ 0 & \text{else} \end{cases} \tag{2.43}$$

$$f_M(a) = 74 \cdot t_I \cdot sin(\pi/2 \cdot a) + 111 \cdot t_I I \cdot (1 - cos(\pi/2 \cdot a) \tag{2.44}$$

- $S = \begin{cases} 0.25 \cdot F_t \cdot v_{ce} & \text{if } v_{ce} > 0.0 \\ 0.0 & \text{else} \end{cases}$ is the shortening heat rate,
- $W = \begin{cases} F \cdot v_{ce} & \text{if } v_{ce} > 0.0 \\ 0.0 & \text{else} \end{cases}$ is the work rate. v_{ce} is the shortening speed, l_{ce} the muscle length and l_{opt} : the optimal muscle length.

The change in energy consumption at time t is given by:

$$dE = dt \cdot \sum_{m \epsilon \text{muscles}} E_m, \text{ with } E_m = A_m + M_m + S_m + W_m$$

2.1.3 FBL model extension inspired from J. Wang

In this section we describe an extension of the FBL model implemented for comparison robustness comparison purpose. The extended model is referred to as FBL+ in the rest of the report and is inspired by work of J. Wang [30]

The main difference is the addition of a fourth cycle phase; in addition to the sw, st, sw_{end} phases a swing end (sw_{end}) phase is added. During this phase, three new stability feedback rules are added (see eq. 2.36). Two rules control the hip joint through the HF and GLU muscles and the last rule controls the knee joint through the VAS muscle. Theses rules aim at directing the KNEE and HIP joint angles toward a reference angle during the sw_{end} phase, thus adjusting the limb position before touching the ground. Both HF and GLU stability rules share the same δ^{ref} reference angle. Theses rules adds 8 parameters to be optimized (see table 2.6).

The other differences with the FBL model is how it enters in the sw_{end} and st_{end} phases. Instead of simply entering the st_{end} phase when the other limb touches the ground (i.e. during the double stance support), it can also enter when the horizontal distance (normalized by the foot length) between the center of gravity of the model and the toe reaches a certain threshold. The same method is used to define the criterion for entering in sw_{end} phase.

The two threshold parameters are optimized, as well as the parameters associated with the new feedback rules. We thus have 10 new parameters to optimize. The new parameters and their associated range are given in table 2.6.

2.2 Optimization

Optimization can be viewed as finding one particular solution of a subset of solutions that satisfies some criteria. Most of the optimization problems can be formulated mathematically as finding the minimum of a given fitness function or objective function, i.e.

$$[x \in A, \forall y \in A, f(x) = min(f(y))], \;\; f(x) : A^n \rightarrow \mathbb{R}, A \in \mathbb{R}$$

In order to use the framework of iterative optimization algorithms, we need a) a set of parameters, usually from a subset of the multidimensional space of real numbers (noted A in the previous equation, often referred to as the search space) that controls the behavior of the system and b) a way to evaluate the system.

Various optimization techniques can be used, such as genetic algorithm, particle swarm optimization (PSO) or gradient descent algorithm. Here we chose PSO because it has been shown to give good results in the same kind of problems (see work of Steve Berger, former master student at Biorob [2]), and because its computational cost is small and implementation easy.

2.2.1 PSO algorithm

PSO algorithm is a method used for the optimization of non linear continuous functions, but adaptations to discrete space exists [29, 28, 13]. It is inspired by the movement of swarm observed in nature, hence the name. The PSO algorithm is an iterative optimization algorithm. It starts with a set of solution (randomly chosen or not) in the search space A. After each iteration, the performance of each particle is evaluated using an objective function f, then each particle moves in the search space with a speed direction and amplitude that takes into account

- personal best performance noted x_{pb}
- the best performance of the whole swarm so far x_{gb}

At each iteration, the whole swarm moves in the search space and particles smoothly influence each other. The speed v_i and the position x_i of particle i at iteration t are given by [22]:

$$v_i(t+1) = \omega v_i(t) + c_1 \text{rnd}()(x_{pb} - x(t)) + c_2 \text{rnd}()(x_{gb} - x(t)) \quad (2.45)$$

$$x_i(t+1) = v_i(t+1) + x_i(t) \quad (2.46)$$

Where,

- v_i and x_i are respectively the speed and the position in the search space A of particle i
- c_1 and c_2 are the "cognitive factor" and the "social factor", respectively. If c_1 is too large compared to c_2, each particle will converge to another direction and the whole swarm will not converge to a specific solution. If c_2 is too large compared to c_1, the algorithm will converge prematurely. Here $c_1 = c_2 = 2.05$ (adapted from [22])
- ω is the constriction factor. $w < 1.0$ and prevent failure to converge due to unbounded increase of the speed. Here we take : $w = 0.729$. We further limit the maximum normalized velocity v_n to 0.3, where the component on dimension d of v_n is given as $v_{nd} = v_d/|max(A_d) - min(A_d)|$.

2.2.1.1 Multi-objectives functions evaluation

The objective function often combines different criteria. The consequence is that it is not always easy to manage interactions between the different criteria (see section 2.2.3. A simple solution is to prevent interaction by using multiplicative parameters of different order of magnitudes for each objective (criteria with highest magnitude order parameters (C_{high}) will be optimized first, while criteria with lowest magnitude order parameters (C_{low}) will be optimized last). However in presence of noise, some criteria might not be optimized. In practice, it is very unlikely - and difficult to verify - that the C_{low} will be optimized at all. Indeed, if any criterion has a variability bigger than the magnitude order of the next criteria, those criteria will never be optimized.

2.2.1.2 Stage PSO

The stage PSO algorithm is a simple extension added to the PSO algorithm (developed by Jesse Van den Kieboom at BioRob) which aims at facilitating the optimization process with multi-objectives functions. Instead of using one global evaluation function that combines all the different objectives, the optimization is split into different stages. At each stage a simple objective function is used to evaluate the solution (i.e. traveled distance, energy consumption, speed, step length or similarity with human gait). To enter a stage the particle should satisfy a criterion called entrance criterion. All stages have a entrance criterion except the first one. All the particle are initialized in the first stage. At each iteration, a particle at stage N is evaluated for all previous stages, and the next stage (i.e. $n \leqslant N + 1$), and is set at n^*, the lowest stage whose entrance criterion was not validated. At the next iteration, this particle, now at stage n^*, will be evaluated for all stages $n \leqslant n^* + 1$, and will be set at a the lowest stage whose entrance criterion was not validated.

2.2.2 Robot evaluation

2.2.2.1 Initial conditions

The choice of the model initial state is crucial for the subsequent optimization to be effective. We tested two starting conditions:

- Start in standing position
  With the FBL model, starting from a standing position is possible. Indeed, there is an immediate feedback from the ground (since the feet are in contact with the ground) and the stability feedback from the trunk (as the trunk starts falling). Those two feedbacks permit the first foot to detaches from the ground and activates other feedbacks, generating locomotion.
  Although stable locomotion can be found following optimization, the first steps are highly instable; the robot starts stumbling before entering in a limit cycle. This stumbling phase can be greatly reduced by a) intializing the ground sensors to 100 N value, b) filter the information from ground sensors using a first order differential equation (see eq. 2.34).

- Start with an non-zero initial velocity
  Here we propose to start with a walking gait (obtained from optimization with the standing position as initial condition), and then change the parameters after a few steps (when the limit cycle of the starting gait is reached). This solution presents the advantage of minimizing the initial perturbation to the system.

After evaluation of the two initial states, we decided to use this initial state in our experiments.

Evaluation criterion (EC)

The evaluation of the robot is based on different criteria, which make use of different variables summarized below:

- d: distance traveled in [m]
- v: mean speed [m/s]
- t: duration of the run in [s]
- E: energy consumed as defined in section 2.1.2.4
- c: number of cycles
- $\bar{\theta}_{trunk}$: mean trunk angle with regards to vertical axes
- $corr_{ankle}$: correlation of ankle angle produced by the model with human data from [31]
- $corr_{knee}$: correlation of knee angle produced by the model with human data from [31]
- $corr_{hip}$: correlation of hip angle produced by the model with human data from [31]
- sl_{SNR}: step length stability based on signal to noise ratio (SNR) measurement.
- $left\_right$: step length left right similarity criterion based on SNR measurement.

The criteria are described in details in section 2.2.3 and summarized in table 2.7.

Stopping criterion (SC)

Each set of parameter is evaluated on the Webots physical simulator. The run is stopped if the robot falls or if the SC is reached. The following SCs were investigated:

- Distance limit: the run is stopped when the robot reaches the distance limit (d_{lim}).

- Time limit: the run is stopped when the robot has walked without falling longer than the time limit (t_{lim}).
- Energy limit: the run is stopped when the energy spent by the robot reaches E_{lim}.

The SCs are chosen big enough to ensure that the robot has entered in a limit cycle. If not specified $d_{lim} > 30$[m] is chosen. The corresponding time limit $t_{lim} > 23$[s], assuming that the walking speed is 1.3[m/s]. E_{lim} is estimated based on the energy consumption of a human of 70 [kg] walking at 1.3 [m/s] ($\sim 210[J/m]$ data from [33]). If not specified the stopping criterion d_{lim} is used.

2.2.3 Objective function

IN PSO, the objective function evaluates multiple criteria at the same time. Not only the robot should be able to walk, but the gait should also resemble the human gait both in term of energy consumption and in term of gait shape. The objective function should thus take into account human gait characteristics, such as step length or speed.

Here we build the objective function step by step. Starting with an objective function able to produce stable walking gait, several constraints are subsequently added:

1. Generate a stable walking gait with energy minimization constraints
   In this simple initial objective function, two criteria are satisfied at the same time: the robot should walk, but at the least energy cost. Several objective functions can produce a solution that walks; any measure of distance, such as the number of steps or the distance traveled, is enough to make the solution walk. Here we decided to use d as the objective function parameter. In order to optimize for minimal energy consumption E is also added. With d_{lim} as stopping criterion the function can be written as :

   $$F = d - \alpha \cdot E \quad \text{with } SC = d_{lim} \tag{2.47}$$

   Where α is a parameter to be carefully determined. Indeed the optimization process should first optimize for the distance d, thus ensuring that the solution walks, and then only the energy consumption should be optimized. The term corresponding to the energy (i.e. $\alpha \cdot E$) should therefore be small compared to the distance. Note that this works because the distance is limited to d_lim, thus once the model walks without falling the noise on d will be extremely small in the magnitude of the distance that can be traveled in 0.001[s] (the duration of one time step).

2. Increase similarity with human gait
   When optimizing using the objective function described above, the produced gait can significantly differ from human gait (see section 3.1.2), both in terms of joint angles and produced torques. In order to increase resemblance with human gait, a similarity criterion was introduced: the correlation *corr* between joint angle data of walking human (data from [31]) and joint angle of the robot.

   $$corr(X, Y) = \frac{cov(X, Y)}{\sqrt{var(X)var(Y)}} \tag{2.48}$$

   Where:

   - The covariance between to dataset of the same length is given by :

   $$cov(X, Y) = \frac{1}{N-1} \sum_{i=1}^{N} \left(X_i - \bar{X}\right)\left(Y_i - \bar{Y}\right) \tag{2.49}$$

- The variance of a dataset is given by :

$$var(X) = \frac{1}{N}\sum_{i=1}^{N}(x_i - \bar{x})^2 \tag{2.50}$$

The *corr* is calculated for each joint of one arbitrarily chosen limb (we assume that the gait is symmetric) over the last full walking cycle. Note that because the correlation is calculated between two sequences of the same length, the angles extracted from the robot are linearly interpolated to have the same length as the human angle sequence. The final criterion is the minimum correlation of the three joints. Because the measure of correlation is not sensitive to the mean of the signal, the difference in mean angle between robot and human could be added in the criterion. The optimizations with and without the criterion accounting for the difference in mean angle between robot and human joints shows no real improvement in the resulting gait. The similarity is finally simply chosen as:

$$\mathrm{C}_{angles} = \min\{corr_{ankle}, corr_{knee}, corr_{hip}\} \tag{2.51}$$

The objective function used becomes :

$$F = d - \alpha \cdot E + \beta \cdot \mathrm{C}_{angles} \quad \text{with } SC = d_{lim} \tag{2.52}$$

Since the correlation is comprised between 0 and 1, it will have little effect at the beginning of the optimization. Thus the optimization will first find a solution that is able to walk with minimal energy consumption and then optimize for maximizing the resemblance between robot and human gait.

3. Increase step length stability
In order to avoid step length variation, a measure of the stability of the step lengths is used: the signal to noise ratio (SNR) of the step length during the trial is calculated. The SNR is defined as:

$$\mathrm{SNR} = log(\frac{\bar{X}}{var(X)}) \tag{2.53}$$

Where $\bar{X}$ is the mean of the vector X and $var(X)$ is the variance of the vector X
The criterion for step length stability is given as :

$$\mathrm{C}_{steplengths} = \mathrm{SNR}(sls) \tag{2.54}$$

Where sls is the vector of all the step lengths.
The fitness function becomes:

$$F = d - \alpha \cdot E + \beta \cdot \mathrm{C}_{angles} + \gamma \cdot \mathrm{C}_{steplength} \quad \text{with } SC = d_{lim} \tag{2.55}$$

4. Control gait speed & step length size
Here, constraints on gait characteristics - speed and step length - are added. In both cases, the function chosen should present a unique maximum at the desired speed $v_{desired}$ or step length $sl_{desired}$. The simplest function presenting this characteristic is the absolute function. The constraint for speed are thus written as :

$$C_{speed} = -|v_{desired} - v| \tag{2.56}$$

where v is the mean of the step lengths during one run. Similarly, the constraint for step length are written as

$$C_{steplength} = -|sl_{desired} - sl| \tag{2.57}$$

where sl is the mean of the step lengths during one run.

The final objective function can be written as a sum of all the constraints :

$$\begin{aligned} F &= d - \alpha \cdot E \\ &+ \beta \cdot \mathrm{C}_{angles} \\ &+ \delta \cdot \mathrm{C}_{speed} \\ &+ \zeta \cdot \mathrm{C}_{steplength} \quad \text{with } SC = d_{lim} \end{aligned}$$

with the distance limit d_{lim} as SC.
A similar objective function can be written for the other stopping criteria. For example, with the energy limit E_{lim} as SC, the objective function becomes :

$$\begin{aligned} F &= d \\ &+ \beta \cdot \mathrm{C}_{angles} \\ &+ \delta \cdot \mathrm{C}_{speed} \\ &+ \zeta \cdot \mathrm{C}_{steplength} \quad \text{with } SC = E_{lim} \end{aligned}$$

Other criteria have been developed for specific use and are described here for completeness purpose.

1. Minimizing cost of transport
   This criterion is used as last stage (see stage PSO) when optimizing for robustness. It takes into account not only the energy expenditure but also the traveled distance so that its better to go further but only if the increase in energy consumption rate is not to high. The criterion to maximize is defined as :

   $$\mathrm{C}_{cot} = \frac{d}{E} \cdot d \tag{2.58}$$

   Where $\alpha = 0.001$ is a normalizing factor, E is the energy expenditure, d is the traveled distance.

2. Maximizing left and rigth step length similarity
   This criterion has been designed to maximize the gait symmetry. It was used at early stage of the project to prevent symmetry issues, but appeared not necessary. The criterion is based on the comparison of left and right steplength. Given two sequences x and y of the same length, the similarity criterion is:

   $$\mathrm{SNR}(x, y) = log\left(\left|\frac{\bar{x}}{var(x)} - \frac{\bar{y}}{var(y)}\right|\right) \tag{2.59}$$

   Where $\bar{x}$ is the mean of the vector x and $var(x)$ is the variance of the vector x The criterion for step length stability is given as :

   $$\mathrm{C}_{left\_right} = \mathrm{SNR}(sl_{left}, sl_{right}) \tag{2.60}$$

   Where sl_{left} is the vector of left limb step lengths, sl_{right} is the vector of right step lengths.

3. Trunk leaning prevention This criterion was designed in order to prevent optimized gait to have their trunk leaning forward when optimizing for high speed or for perturbed environment. The criterion is defined so as to be maximized when $0 < C_{trunk} < 0.105$.

$$C_{trunk} = \begin{cases} |\bar{\theta}_{trunk} - 0.105| & \text{if } \bar{\theta}_{trunk} > 0 \\ 0 & \text{else} \end{cases} \tag{2.61}$$

2.2.3.1 Stage PSO criteria

The adaptation of the previous objective function of stage PSO is straightforward. For each stages a criterion should be chosen among the criterion defined in table 2.7. All stages except the first one should have an "entrance criterion" that says when the previous stages is enough close to the desired value. Note that all criteria for whom a clear desired value is not know (like for example the criterion for energy consumption minimization) can be put at the last stage. Using d_{lim} as SC, the objective function in the previous section can be split into five stages:

- Stage 0 : maximize the traveled distance
- Stage 1 : maximize similarity with human gait
- Stage 2 : bring the speed in a given range
- Stage 3 : maximize step length SNR
- Stage 4 : minimize energy

Stages objective functions and entrance conditions are detailed in table 2.8.

2.2.4 Environments

The robot is evaluated in different environments:

1. Flat ground
2. Unique push on flat ground: one unique push of constant amplitude is applied at a random time to the robot.
3. Random push on flat ground: a serie of random pushes are applied at random time to the robot (see section 2.2.4.1)
4. Wavy ground: the robot walks on an environment made of wave of increasing slope at random length (see section 2.2.4.2).
5. Increasing slope

2.2.4.1 Random push

The pushes are modeled as short forces happening at random time and applied at different position and with different orientations. The force amplitude of the push increases with time. The duration between two pushes is randomly chosen following a F-distribution. The parameters of each push (height, orientation, duration) follow different probability distributions (see figure 2.7 and legend for details). The amplitude is drawn from a normal distribution with mean increasing push after push toward a maximum mean amplitude f.

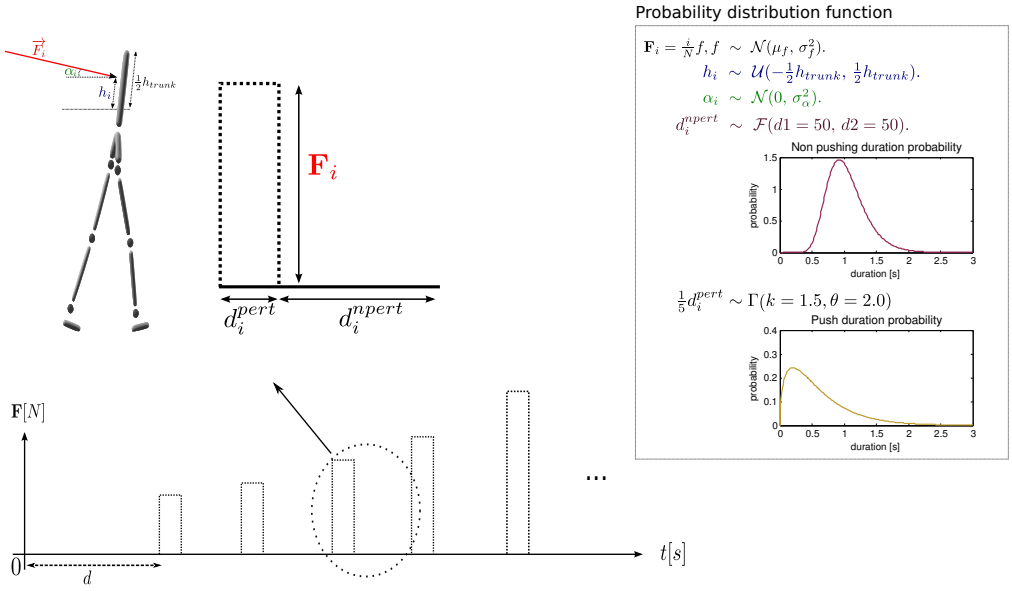

Figure 2.7: The force of the i^{th} push is modeled has a constant input of amplitude $\mathbf{F}_i$ and duration d_i^{pert}, where the amplitude of the force is drawn from a normal distribution. The mean and standard deviation increase linearly push after push. The duration of the push follows a gamma distribution. The angle of the force with respect to the ground follows a normal distribution with mean 0 and standard deviation of $\pi/2$. The height of the push follows a uniform distribution with a range equal to the trunk height. Finally, the duration of the non pushing period follows a F-distribution with parameters chosen so that the push arises approximately each seconds.

2.2.4.2 Wavy ground

The wavy ground is modeled as a serie of small trapezoidal structures. The angle of the structure increases structure after structure towards a maximum angle. The length of each structure and the space between them follow a Gaussian probability distribution. (see figure 2.8 for detail).

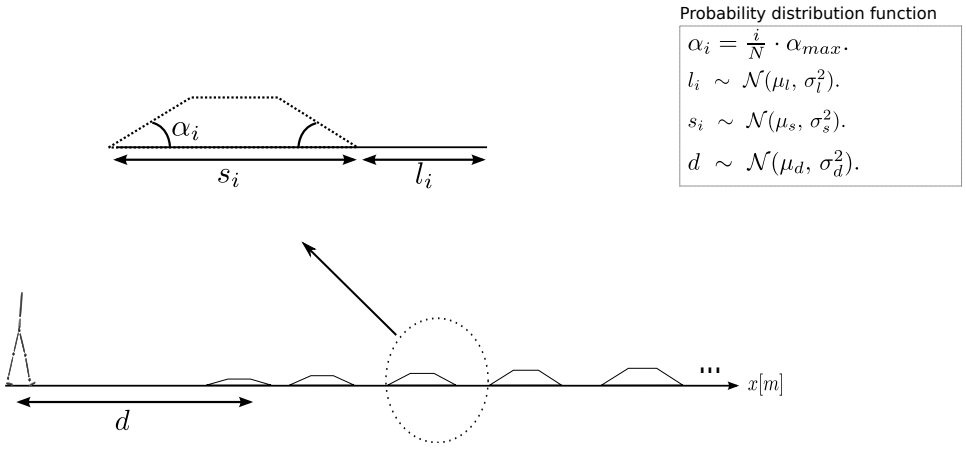

Figure 2.8: The length of each structure and the space between the different structures follow a normal distribution. For each trapezoidal structure, the up and down angles are the same, and increase between structures, toward a maximal angle α_{max}.

2.3 Human Walking Data

Walking experiments on a human have been carried out in Poland at the university of PJWSTK in the laboratory of Prof. Wojciechowski. For each experiments, walking data, ground reaction forces and EMG data of the major limb muscles were extracted. The subject of the experiment was a male of 1.8 m and 80 kg.

2.3.1 Experiments

The experimental setup is shown in figure 2.9. Three different experiments have been carried out:

1. Low speed walking
2. Normal speed walking
3. Slow running

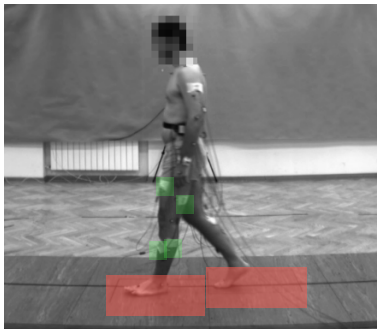

Figure 2.9: Experimental setup of the motion capture system. In yellow are two of the 10 infrared cameras, in red the two plates that record the ground reaction forces and in green the position of limb EMG electrode. The small dots on the body of the subject are the captor detect by the infrared cameras.

2.3.2 Walking data

The walking data was extracted using a Motion Capture Systems from Vicon. 40 captors were placed on the body and their position during walking were recorded using 10 infrared cameras. From the position of the captors, the joint angles of both limb were extracted using the Matlab toolbox *Biomechanical Toolkit*. Figure 2.10 shows the angle movement of the hip, knee and ankle joints in the sagittal plane. We observe that the general shape of the angle evolution curves are similar between all experiments, especially between the slow walking and normal walking (the only significant difference being the maximum amplitude of the hip angle). However, between walking and running, several differences are noted: We observe that the peak of the knee angle during the stance is increasing in amplitude with speed (i.e., very small in the case of slow running, higher for normal walking, and even higher for slow running). This is due to the fact that this peak corresponds to the propulsion of the limb, and thus is more important when the locomotion is faster. We also note that the ankle angle evolution has an extra peak at the limit between swing and stance (i.e. when the foot touches the ground) in the two cases of walking, but not in the case of running. This is due to the fact that when walking, the heel touches the ground first (i.e., the toes are up), which is not the case when running. Moreover, the peak of knee and ankle angle during the stance overlap in the case of running, whereas they are consecutive in the case of walking (first the knee and then the ankle peak). This

is due to the fact, in the case of running, the knee and ankle extend together to better propel the body forward. Finally, We also observe the swing and stance phases have the same durations for the slow and normal walking, whereas they are shorter in the case of running, due to the fact that the whole cycle is shorter. As expected, the duration of the swing is shorter than that of the stance in the case of walking, whereas it is the opposite in the case of running.
Given the similarity between slow and normal walking, we will not further study the slow walking data, and rather focus on the normal walking and running data.

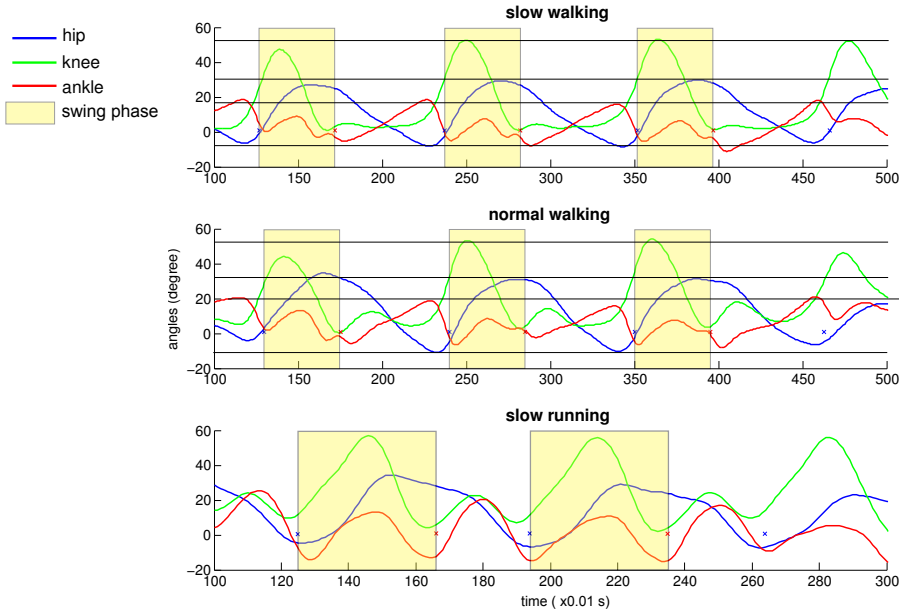

Figure 2.10: Angle recorded during experiment of walking. From top to bottom; angles during slow walking, normal walking and slow running.

2.3.3 Ground Reaction Forces

Ground reaction forces (GRF) were recorded using two plates from Kistler. The figure 2.11 presents a schematic view of a ground reaction forces plate and the different axes (left), as well as the ground reaction forces in the different axes during normal walking and slow running (right). Similarly to what is found in the literature [4], the vertical forces have a double bell shape for walking and a one bell shape for running. Moreover, the forces in the coronal plane present the characteristic sinusoidal shape for both walking and running, with a stiffer slope in the case of walking.

2.3.4 Surface eletromyogram (EMG) data

EMG data of external limb muscles were recorded using the 1400a Surface EMG from Noraxon MyoSystem (16 channels). Recorded muscles are presented in figure 2.12. Compared to the lower limb model presented in section 2.1.2.1, five muscles where recorded for comparison with EMG from [12].

The hip flexor muscles (HF) were not recorded, because this group of muscle is composed of many thin muscles, leading to poor signal. The soleus muscles (SOL) were also not recorded, as they are not accessible from the skin (i.e. they are behind the Gastrocnemius muscle group). The raw data is unusable as it. A common way of processing it is

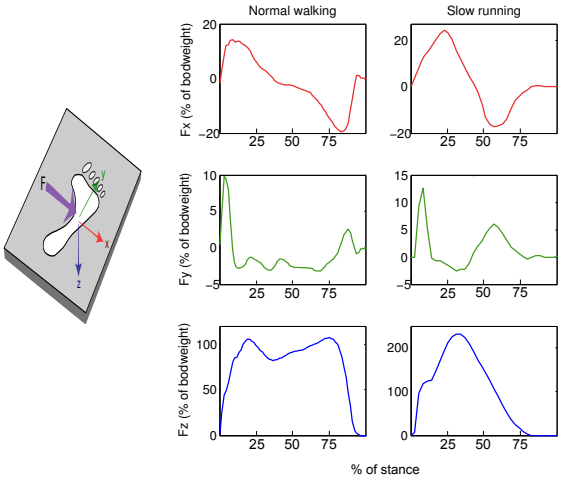

Figure 2.11: LEFT: schematic view of a ground reaction forces plate and the different axes. RIGHT: Ground reaction forces (GRF), presented as percent of the total body weight (from left to right: walking experiment, slow running experiment).

the use of a butterworth filters as explained in [17]. Before applying the butterwoth filter, some preprocessing are done on the signal:

- Low pass filter of order 8 and cut off frequency of 300Hz
- High pass filter of order 2 and cut off frequency of 2Hz
- Band stop filter that removes the 50 Hz and its harmonics (at 100Hz, 150Hz, 200Hz, 250Hz)

After the pre-processing the EMG signal, a low pass butterworth filter of order 4 with 2Hz cut-off frequency is applied to obtain a linear envelope of the signal. The figure 2.12 shows the processed data of the recorded muscles during an experiment of normal walk. Unfortunately, because the maximum force of the muscles has not been recorded, the EMG signal can not be normalized. We are only able to compare the shape of the EMG signal with the muscle activity of the model.

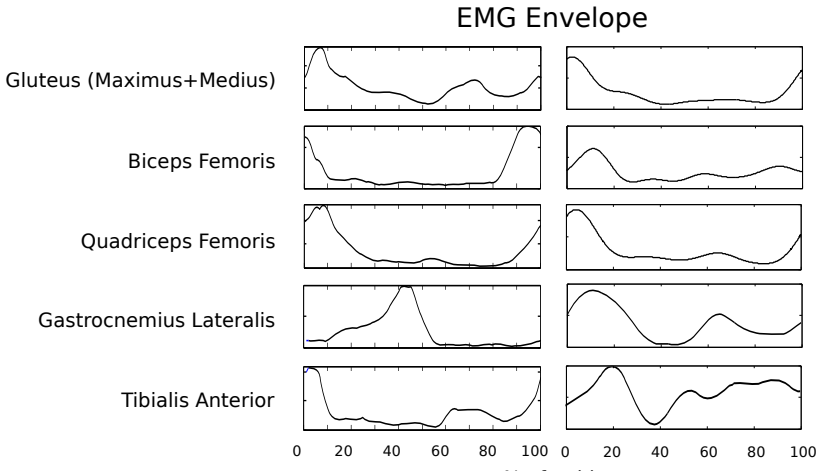

Figure 2.12: LEFT: EMG signal from [12] of a human walking at 1.25[m/s]. RIGHT: processed EMG signal of the corresponding recorded muscles. In the FBL model this corresponds to the GLU, HAM, VAS, GAS and TA muscles (from top to bottom).

Table 2.2: The first table shows the muscles used in the model, the joint onto which they act and the type of movement they induce (flexion or extension), each of which being modeled as one MTU. Two variables θ_{max} and θ_{ref} are also given (values retrieved from the H. Geyer article [9]). The first variable corresponds to the angle at which the force generated by the muscle contributes the most to the joint movement, the second variable is the initial angle of the muscle. The second table gives the muscle parameters, as selected by H. Geyer. The third table gives the segments weight and length based on anthropometric data from [31].

Muscles and joints corresponding to the MTUs

Abbrev.	**Name**	**Action**	$\mathbf{r_0}$	$\theta_{\mathbf{max}}$	$\theta_{\mathbf{ref}}$
GLU	Gluteus	hip extension	0.1	-	150
HF	Hip flexor	hip flexion	0.1	-	180
VAS	Vasilus	knee extension	0.06	165	125
GAS	Gastrocnemius	knee extension	0.05	110	80
TA	Tibialis	ankle flexion	0.04	80	110
HAM	Hamstring	Bi-articular muscle, hip and knee flexion	0.08	- for hip, 180 for knee	155 for hip, 180 for knee
SOL	Soleus	Bi-articular muscle, ankle extension and knee flexion	0.05	110 for ankle, 140 for knee	80 for ankle, 165 for knee

Muscles parameters

	HF	**GLU**	**VAS**	**HAM**	**GAS**	**SOL**	**TA**
Maximal muscle force ($F_{max}[N]$)	2000	1500	6000	3000	1500	4000	800
Maximal speed of the muscle ($v_{max}[m/s]$)	12.0	12.0	12.0	12.0	12.0	6.0	12.0
Optimal length of the muscle ($l_{opt}[m]$)	0.11	0.11	0.08	0.10	0.05	0.04	0.06
Optimal length of the tendon ($l_{slack}[m]$)	0.10	0.13	0.23	0.31	0.40	0.26	0.24
Pennation factor ($\rho[]$)	0.5	0.5	0.7	0.7	0.7	0.5	0.7
Type I fibers percentage	0.5	0.5	0.44	0.54	0.81	0.7	0.5

Lower limbs segments parameters

Segment	**Mass (kg)**	**Length (m)**
Trunk	53.5	0.8
Thigh	8.5	0.5
Shin	3.5	0.5
Foot	1.25	0.16
Ankle	0	0.1
Total body	70	1.8

Table 2.3: Range of joints angle outside of which soft limit engages. The soft limit models the action of ligaments to work against unnatural movement, thus preventing injuries [9].

Joint	$\theta_{\mathbf{min}}$	$\theta_{\mathbf{max}}$
Hip	20°	230°
Knee	45°	175°
Ankle	70°	130°

Table 2.4: Motoneurons signal equations for each MTU. In brown the MTU feedback, in blue the stability feedback and in green the ground feedback. We can see that during swing only MTUs feedback are used except for the hip flexor that has an extra term $k_{lean}(\phi^{TO} - \phi^{ref})$. Where ϕ^{TO} is the angle of the trunk when the limb detaches from the ground, and ϕ^{ref} is the trunk reference angle. This term permits the swing movement to increases with the trunk inclination, simulating the biological reflex of making a larger step to prevent falling. This term thus increases the stability of the model.

Motoneurons signal during stance

$$
\begin{aligned}
s^{st}_{GLU} &= s^{0}_{GLU} + Fb'_{s} \cdot Fb_{g}(ipsi) \\
s^{st}_{HF} &= s^{0}_{HF} + Fb_{s} \cdot Fb_{g}(ipsi) \\
s^{st}_{HAM} &= s^{0}_{HAM} + Fb_{s} \cdot Fb_{g}(ipsi) \\
s^{st}_{VAS} &= s^{0}_{VAS} + w_{VAS,VAS_f} \cdot Fb_{f}(VAS) - w_{VAS,KNEE_o} \cdot Fb_{o}(knee) \\
s^{st}_{SOL} &= s^{0}_{SOL} + w_{SOL,SOL_f} \cdot Fb_{f}(SOL) \\
s^{st}_{TA} &= s^{0}_{TA} + w_{TA,TA_l} \cdot Fb_{l}(TA) - w_{TA,SOL_f} \cdot Fb_{f}(SOL) \\
s^{st}_{GAS} &= s^{0}_{GAS} + w_{GAS,GAS_f} \cdot Fb_{f}(GAS)
\end{aligned}
$$

Motoneurons signal during stance end

$$
\begin{aligned}
s^{st}_{VAS} &-= Fb_{g}(contra) \\
s^{st}_{GLU} &-= \Delta S \\
s^{st}_{HF} &+= \Delta S
\end{aligned}
$$

Motoneurons signal during swing

$$
\begin{aligned}
s^{sw}_{GLU} &= s^{0}_{GLU} + w_{GLU,GLU_f} \cdot Fb_{f}(GLU) \\
s^{sw}_{HF} &= s^{0}_{HF} + w_{HF,HF_l} \cdot Fb_{l}(HF) - w_{HF,HAM_l} \cdot Fb_{l}(HAM) + k_{lean}(\phi^{TO} - \phi^{ref}) \\
s^{sw}_{HAM} &= s^{0}_{HAM} + w_{HAM,HAM_f} \cdot Fb_{f}(HAM) \\
s^{sw}_{VAS} &= s^{0}_{VAS} \\
s^{sw}_{SOL} &= s^{0}_{SOL} \\
s^{sw}_{TA} &= s^{0}_{TA} + w_{TA,TA_l} \cdot Fb_{l}(TA) \\
s^{sw}_{GAS} &= s^{0}_{GAS}
\end{aligned}
$$

Table 2.5: FBL model parameters list and their respective range. The parameters are tuned by optimization (using PSO). Under "others" are presented the parameters related to weight bearing transfer and the knee overextension feedbacks.

Stance phase stability control

Name	Range	Extra information
k_{bw}	$[\ 0.8; 1.4\ ]$	
k_{p1}	$[\ 0.8; 1.4\ ]$	Used for the Fb_s feedback rule
k_{p2}	$[\ 0.5; 1.4\ ]$	Used for the Fb'_s feedback rule
k_d	$[\ 0.8; 1.4\ ]$	Used for the Fb_s and Fb'_s feedback rule
δ_{ref}	$[\ 0.8; 1.4\ ]$	Used for the Fb_s and Fb'_s feedback rule

Muscle force feedback

Name	Range
w_{SOL,SOL_f}	$[\ 0.8; 1.6\ ]$
w_{TA,SOL_f}	$[\ 0.1; 0.8\ ]$
w_{GAS,GAS_f}	$[\ 0.3; 1.6\ ]$
w_{VAS,VAS_f}	$[\ 0.9; 1.8\ ]$
w_{HAM,HAM_f}	$[\ 0.2; 1.0\ ]$
w_{GLU,GLU_f}	$[\ 0.2; 0.9\ ]$

Muscle length feedback

Name	Range
w_{TA,TA_l}	$[\ 1.0; 3.0\ ]$
w_{HF,HF_l}	$[\ 0.2; 1.5\ ]$
w_{HF,HAM_l}	$[\ 0.0; 3.0\ ]$
l^{TA}_{offset}	$[\ 0.0; 1.0\ ]$
l^{HF}_{offset}	$[\ 0.2; 1.0\ ]$
l^{HAM}_{offset}	$[\ 0.7; 1.0\ ]$

Basal activity

Name	Range
s^0_{SOL}	$[\ 0.01; 0.1\ ]$
s^0_{TA}	$[\ 0.01; 0.1\ ]$
s^0_{GAS}	$[\ 0.01; 0.1\ ]$
s^0_{VAS}	$[\ 0.01; 0.1\ ]$
s^0_{HAM}	$[\ 0.01; 0.1\ ]$
s^0_{GLU}	$[\ 0.01; 0.1\ ]$
s^0_{HF}	$[\ 0.01; 0.1\ ]$

Other parameters

Name	Range
k_{lean}	$[\ 0.0; 2.0\ ]$
$k_{\delta knee}$	$[\ 0.0; 3.0\ ]$
$k_{\delta knee_{off}}$	$[\ 2.8; \pi\ ]$
ΔS	$[\ 0.0; 1.05\ ]$

Table 2.6: FBL+ additional parameters list and their respective range.

Swing end phase feedback rules

Name	Range
k_p^{hf}	$[\ 0.0; 2.0\ ]$
k_d^{hf}	$[\ 0.0; 1.0\ ]$
k_p^{glu}	$[\ 0.0; 2.0\ ]$
k_d^{glu}	$[\ 0.0; 1.0\ ]$
k_p^{vas}	$[\ 0.0; 2.0\ ]$
k_d^{vas}	$[\ 0.0; 1.0\ ]$
δ_{ref}^{hip}	$[\ -1.0; 0.0\ ]$
δ_{ref}^{knee}	$[\ 0.0; 1.14\ ]$
st_{end}	$[\ 0.0; 3.0\ ]$
sw_{end}	$[\ -2.5; 0.0\ ]$

Table 2.7: The table summarizes the different evaluation criterion that are used in the optimization process.

Optimization evaluation criterion

EC	Passing criterion
C_{angles}	$C_{angles} > 0.8$
$C_{steplengths}$	$C_{steplengths} > 5$
C_{trunk}	$0.0 < C_{trunk} < 0.105$
$C_{speed}(v_{opt})$	$\lvert v - v_{opt}\rvert < 0.05$

Table 2.8: The five stages defined in the stage PSO of experiment 3, and their associated entrance condition. All evaluated criterion are maximized. If not specified in an experiment of stage PSO, the entrance criterion defined in this table are used

stage	eval. criterion	entrance condition	detail
0	d		d is the distance and d_{lim} is the SC
1	C_{angles}	$d > 0.99 \cdot d_{lim}$	The C_{angles} criterion captures the similarity of the angles compared to human. The criterion is defined in eq. 2.51
2	C_{speed}	$\mathrm{C}_{angles} > 0.8$	
3	$\mathrm{C}_{steplengths}$	$\mathrm{C}_{speed} + v_{desired} < 0.05$	The $\mathrm{C}_{steplengths}$ criterion captures the variability of the step lengths and is defined in eq.2.54.
4	$-E$	$\mathrm{C}_{steplengths} > 6$	E is the energy consumed during the run.

Chapter 3

Results

Here are presented the results of the FBL model optimization on a flat ground, using different optimization criteria (presented in section 2.1). The different experiment are compared, and their similarity to to human gait is evaluated (section 3.1). Then, the robustness of both the FBL and the FBL+ model is tested on two different environments (i.e. pushes and wavy ground, section 3.2).

3.1 Optimization on flat ground

Four different optimization experiments with the FBL model have been carried out on a flat ground (presented in table 3.2). The three first experiments make use of the stage particle swarm optimization (stage PSO, see section 2.2.1.2). Those three stage PSO experiments differs among them by the number of stages that are used (three, four and five). The fourth experiment uses a simple particle swarm optimization (see section 2.2.1) with the multi-objectives function defined in section 2.2.3. The first experiment has three stages: the maximization of traveled distance, the optimization toward a speed of 1.3[m/s] and the minimization of the energy consumption. The second experiment has one additional stage: the maximization of the step length SNR, optimized before the stage of energy consumption minimization. The third experiment has another extra stage, which maximizes the correlation of the computed joint angles with human joint angles, also optimized before the stage of energy consumption minimization (see section 2.2.3.1) The last experiment is a simple PSO experiment which uses the fitness function defined in eq. 2.58, this function tries to optimize all the criteria mentioned above in parallel. For all experiments, the SC used is the distance, with $d_{lim} = 35m$. In order to ensure convergence we used a large number of iterations (150). The experiments were repeated several times (data not shown) to make sure that the obtained results are reproducible. Here we analyze one solution of each experiment. Note that even if some difficulties can arise when using multi-objectives functions (as shown in section 2.2.1.1), the convergence speed is much faster because all criteria are evaluated at the same time.

3.1.1 Experiments comparison

Here we compare the results obtained for the step length SNR, the angle correlation and the energy presented in table 3.2 and figure 3.1. The speed is not studied here since the optimal value of $1.3[m/s]$ was reached in all experiments. Videos are available at [6].

We observe that the step length SNR is smaller in experiment 1, which was expected since this criterion was not considered in the optimization process of this experiment.

Table 3.1: Details of the different experiments. The rows are in order : 1) the experiments id, 2) the environments used for optimization, see 2.2.4, 3) The model used during optimization, either FBL or FBL+, 4) The pso type optimization algorithm used, either stage or standard, 5) The list of stages (only for stage PSO), the prefixes used are the same as those presented in table 2.8 and defined in section 2.2.3, 6) The number of iterations and 7) The number of particle are defined in the last two rows.

Experiments details

Optimization on flat ground

Exp.	Env.	Models	PSO	Stage list	Iter.	Part.
1	1	FBL	Stage	$(d, \mathrm{C}_{speed}, E)$	150	60
2	1	FBL	Stage	$(d, \mathrm{C}_{speed}, \mathrm{C}_{steplengths}, E)$	150	60
3	1	FBL	Stage	$(d, \mathrm{C}_{speed}, \mathrm{C}_{steplengths}, \mathrm{C}_{angles}, E)$	150	60
4	1	FBL	Std.		150	60

Optimization on environments with perturbation

Exp.	Env.	Models	PSO	Stage list	Iter.	Part.
5	2	FBL+	Stage	$(d, \mathrm{C}_{trunk}, \mathrm{C}_{speed}, \mathrm{C}_{angles}, \mathrm{C}_{cot})$	150	60
6a	3	FBL	Stage	$(d, \mathrm{C}_{trunk}, \mathrm{C}_{speed}, \mathrm{C}_{angles}, \mathrm{C}_{cot})$	150	60
6b	3	FBL+	Stage	$(d, \mathrm{C}_{trunk}, \mathrm{C}_{speed}, \mathrm{C}_{angles}, \mathrm{C}_{cot})$	150	60
7a	4	FBL	Stage	$(d, \mathrm{C}_{trunk}, \mathrm{C}_{speed}, \mathrm{C}_{angles}, \mathrm{C}_{cot})$	150	60
7b	4	FBL+	Stage	$(d, \mathrm{C}_{trunk}, \mathrm{C}_{speed}, \mathrm{C}_{angles}, \mathrm{C}_{cot})$	150	60

Table 3.2: Optimization results of the experiments on flat ground. The second row gives the values of energy obtained and the last row the value of step lengths SNR. Speed is not shown because all solutions converged to the optimal speed of 1.3 [m/s]. For clarity purposes, the results concerning the correlation between the computed and human joint angles are presented separately in figure 3.1.

Experiments results on flat ground

Exp.	**Energy**[J/m]	step length SNR
1	131.4	1.5
2	257.1	6
3	148.6	7.5
4	200.0	5

Note also that the step length SNR of experiment 4 (standard PSO with one global multi-objectives function) is lower than the one of experiments 2 and 3. However, since a step length SNR of 5 or more is satisfying (i.e. the step length is stable enough, empirically determined), there is no clear distinction in gait stability between experiments 2, 3 and 4.

Concerning the angle correlation (see figure 3.1), we note - as expected - that the correlation is lower for experiment 1 and 2, where the angle correlation was not a criterion. We also note that when the step length is used as a criterion, the hip joint shows an excellent correlation with human data, meaning that the maximization of step length stability is done mainly at the hip joints level. Overall, we observe that the best results are obtained with the full stage PSO experiment (experiment 3) as expected, see section 2.2.1.2.

Finally, concerning the energy consumption, we observe that even if the results are in the same range in all cases, there is a significant differences between experiments. This can be explained by the fact that, for stage PSO experiment, energy consumption is the last optimized criterion. There is therefore not values below which the optimization of this criterion stops and the optimization enters the next stage, and thus this criteria is optimized until the number of iterations (here 150) is reached. Therefore, depending on the number of stages, the optimization will enter the last stage after different number of iterations and thus there will be more or less iterations devoted to energy minimization. This is confirmed by the increase in energy consumption observed between experiment 1 and 2; experiment 2 having one extra criteria to optimize, the number of iterations devoted to energy optimization is decreased. The same tendency could be expected for experiment 3, as yet another extra criteria is optimized. It is however, not the case; indeed, a lower energy consumption is observed, compared to experiment 2. The net decrease in energy consumption of experiment 3 can be explained by the fact that we add a criterion for similarity with humans. Human gait being optimized to generate movements that minimize the energy consumption, it is expected that a gait resembling that of the human will also spend less energy.

A human with same weight walking at the same speed as our model would consume 210[J/m] [33]. Therefore, the energy consumption model used (defined in section 2.1.2.4) gives an energy consumption (between 131.4[J/m] and 257.1[J/m]) comparable to human.

3.1.2 Human gait reproduction

Here we compare data obtained from human walking with data extracted form the solution of the experiments 1, 2, 3 and 4.

Figure 3.1 and 3.2 compares the joint angles between the human data and the model. We observe that the correlation values are higher in experiment 2 compared to 1. This result suggests that the additional criterion present in experiment 2 (i.e. the step length SNR) significantly influences the resemblance between the model and human walk. Experiment 3 has correlation values higher than experiment 1 and 2. This is expected since the correlation of the joint angle is the additional criterion that is optimized in this experiment. Finally the experiment 4, which uses standard PSO, shows a joint angle correlation similar to what is obtained in experiment 3, suggesting that the number of criterion used, rather than the method (i.e. standard PSO vs. stage PSO) influences the correlation between the model and human walk.

Figure 3.4 compares the vertical ground reaction force (GRF) between the human data and the model. We observe that, for all four experiments, the general shape of the vertical GRF in a cycle is similar to the human data (i.e. the two typical peaks are observed in all cases). However, small differences can be observed; notably, experiment 1 shows a higher amplitude of GRF, meaning that the feet touch the ground with a velocity that is higher

than what is observed in human walking, possibly because it would wear out human joints. Conversely, experiments 2, 3 and 4 show decreasing vertical GRF amplitude, indicating more resemblance to human walking.

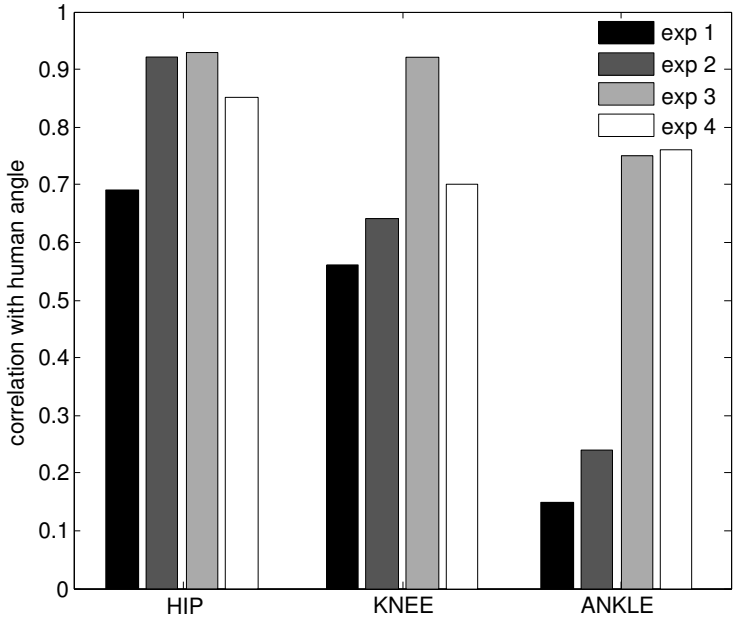

Figure 3.1: Angle correlation between the computed (experiment 1 to 4) and human hip, knee and ankle joint angles.

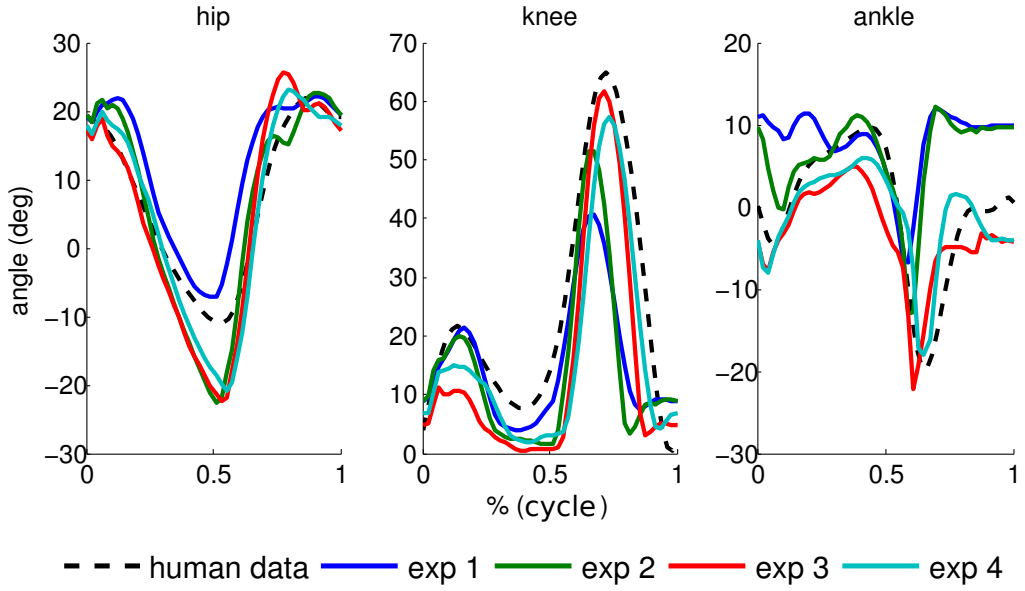

Figure 3.2: Hip, knee and ankle angle comparison between model and human for experiment 1 to 4.

We then compared the muscle activity of the experiments 1 to 4 with a EMG profile of the corresponding muscles of a human walking at 1.25 m/s (data from [12]). It is important to keep in mind that raw EMG data are unusable (several filters are needed to obtain the presented EMG profile see section 2.3.4). Furthermore the quality of the

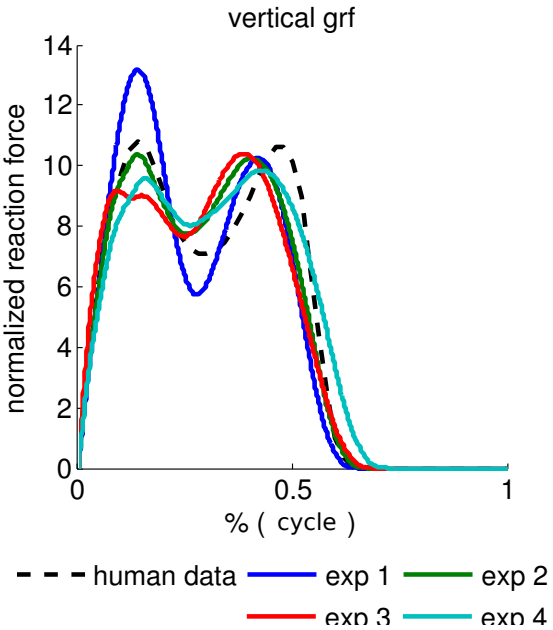

Figure 3.3: Vertical ground reaction forces comparison between model and human for experiment 1 to 4. The data from the models as been filtered with a linear filter of order 100.

data is not excellent, as EMG are recorded on the skin. We thus need to be careful with conclusions made when comparing the muscle activity of the model with human EMG profile.

In agreement with what was observed with the joint angle correlation (see above), the similarity between the human data and the model generally increases with the number of criteria optimized (see figure 3.5 Left). The correlation between human EMG profile and model data (see figure 3.2 Right) shows that, as expected, the best scores are obtained for experiments 3 and 4 for the HF the HAM and the TA muscles. The GLU and SOL muscles correlation is good in all experiments. The GAS shows good correlation for all experiments, although there is a small decrease for experiment 3 and 4. Moreover, there is a clear decrease in correlation for the VAS muscle for experiments 3 and 4, especially for the experiments 3. This differences is confirmed at the level of joint torques where the KNEE torque show a bad correlation with human data (see figure 3.4), but not at the level of joint angles, where the correlation with human is excellent. This low scores can be explained by the lack of both body elasticity and toes in the model. Indeed, in absence of toes and elasticity, which act as spring and damper shocks, the knee will directly absorb forces from the foot contact with the ground, leading to muscle activity and torques at the knee joint that do not resemble human ones. Supporting this hypothesis, this difference is observed mainly during the stance phase, when the toes are most active. Experiments 3 and 4 are more sensitive to this shortcoming, compared to experiment 1 and 2, possibly because they are optimized to have joint angles close to those of human, but the absence of toes do not permit both the joint angles and the joint forces to be consistent with those of human.

3.2 Robustness optimization

The FBL and FBL+ models are optimized on environments 3 and 4, respectively the flat ground with random pushes and the wavy ground (see section 2.2.4 for details on the

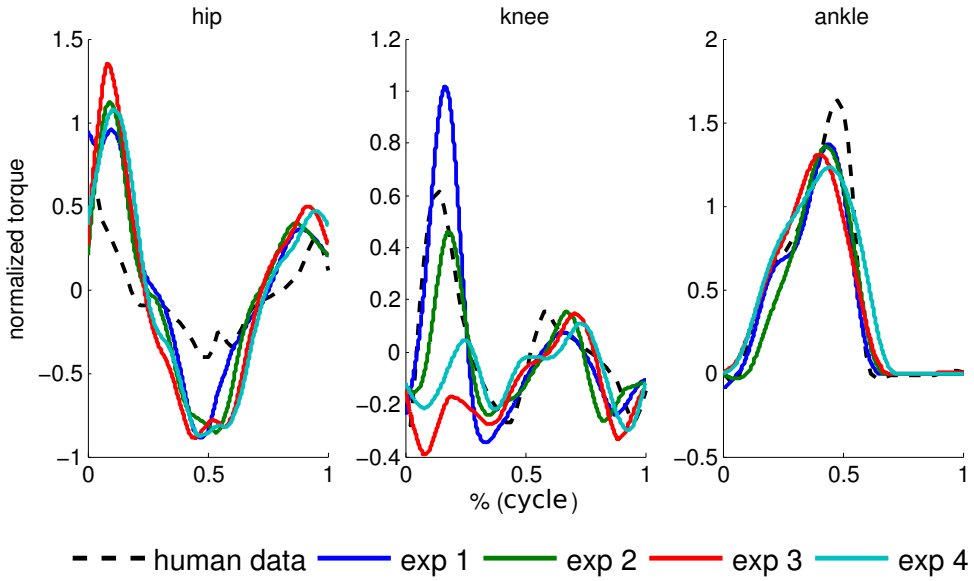

Figure 3.4: Hip, knee and ankle torque comparison between model and human for experiment 1 to 4. The data from the models was filtered with a linear filter of order 100.

environments). In order to avoid false good scores (obtained by chance) each particle is evaluated 5 times with random perturbations and only the worst score is kept. Note that during the optimization on environment 4, a different wavy ground is generated on the fly for each evaluated particles and each iteration, ensuring that the optimization will not optimize for one specific type of wavy ground.

The optimized solutions are then evaluated on three different environments (Note that the experiment 3 is also evaluated for comparison purposes.):

- flat ground for similarity with human assessment
- wavy ground to estimate the wave slope limit
- random push environment to estimate the force limit

The optimization algorithm used is the stage PSO. The stages used for experiment 5, 6 and 7 differs from experiment 3 by several aspects.

- First, instead of using $d > 0.99 d_{lim}$ for the entrance condition of the second stage we now use $d > 10.0$ to ensure that the model can make some steps. Indeed, unlike in experiment 3 (i.e. without perturbations), we don't know how far the model will be able to walk before falling but still want to allow the model to enter the second stage. Note that $d_{lim} = 120$[m] is used.
- Second, the criterion of the last stage becomes minimization of the cost of transport (C_{cot}), instead of the minimization of the energy. This criterion is used because here we use $d > 10.0$ as entrance condition for stage, but we still want the model to go as far as possible, while spending a reasonable amount of energy.
- Third, the stage of step length similarity maximization is not used. Indeed, as we optimize on a perturbed environment, the step length can significantly vary, due to the perturbations, while being stable when evaluated on a flat ground. We can therefore not use this criterion to ensure stable gait. However, we can assume that the perturbations themselves play the role of gait stability criterion. In fact, the

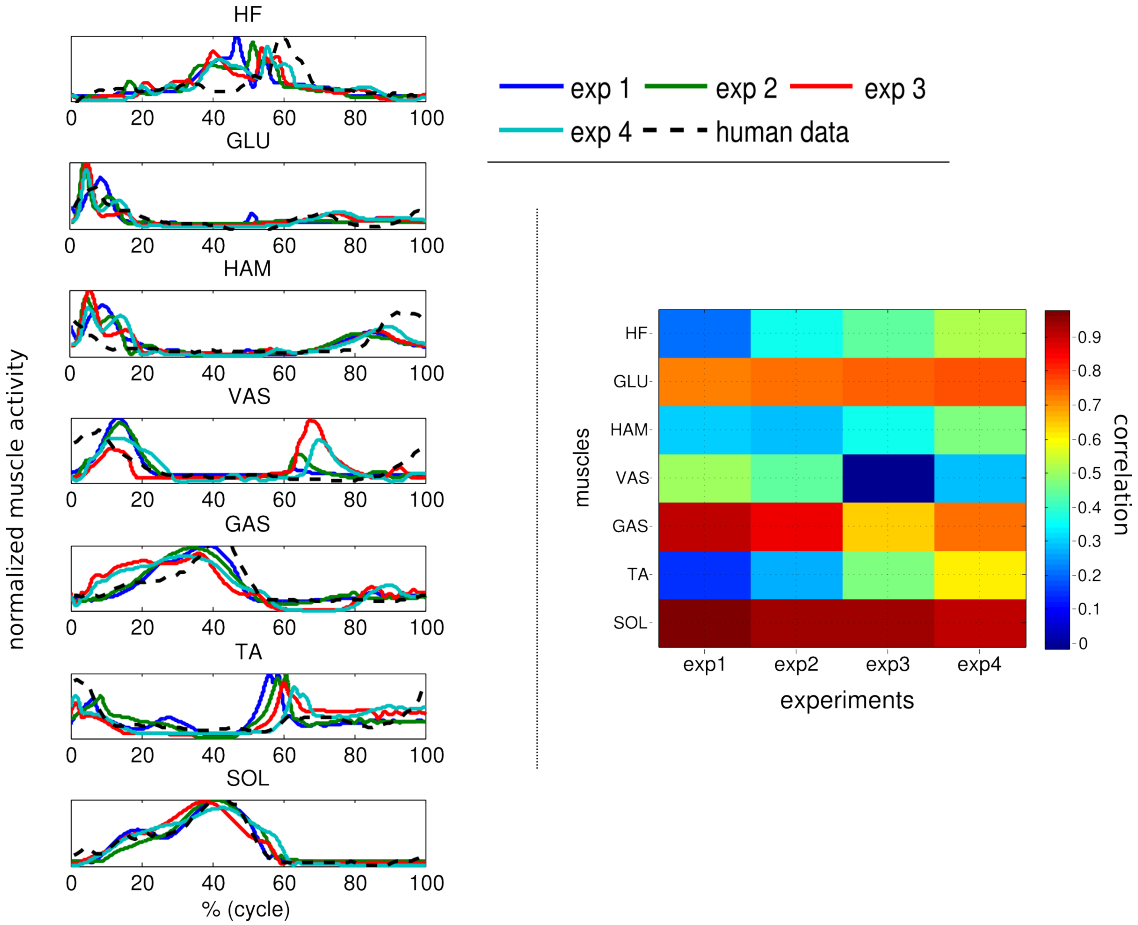

Figure 3.5: Muscle activity of the model (experiments 1, 2, 3 and 4) compared to EMG profile of a human walking at 1.25 m/s (data from [12]). The recorded muscle are in order (from top to bottom): rectur femoris (HF), gluteus maximus + gluteus medius (GLU), biceps femoris (long head)+semitendinosus (HAM), vastus medialis+vastus lateralis (VAS), gastrocnemius medialis+gastrocnemius lateralis (GAS), tibialis anterior (TA), soleus (SOL) (see figure 2.5 for anatomical localization). LEFT: muscles activity of the model compared to EMG profile (dashed black line). RIGHT: correlation between muscles activity of the model and human EMG profile for each experiment. Most of the activities show similarity in shape, with increasing similarity with increasing number of criteria optimized. .

obtained gaits are always stable when evaluated on flat ground, which makes sense because perturbation resistance can be viewed as a stability criterion, but instead of having it encoded in the fitness function, it is now directly encoded in the interaction of the model with the environment.

- Finally, a new stage is added to prevent the model of having the trunk leaning forward, resulting in gait with unnaturally large steps. The selection of gaits making large steps (which in the model often implies leaning forward) is often favored during the optimization process on environment with random pushes, because it increases the ability of the model to resists to strong pushes. The stage is added just after the first stage. It uses the C_{trunk} criterion and the passing criterion is: $0 < \bar{\theta}_{trunk} < 0.105$, where $\bar{\theta}_{trunk}$ is in [rad] and corresponds to the mean trunk angle with respect to the vertical axis.

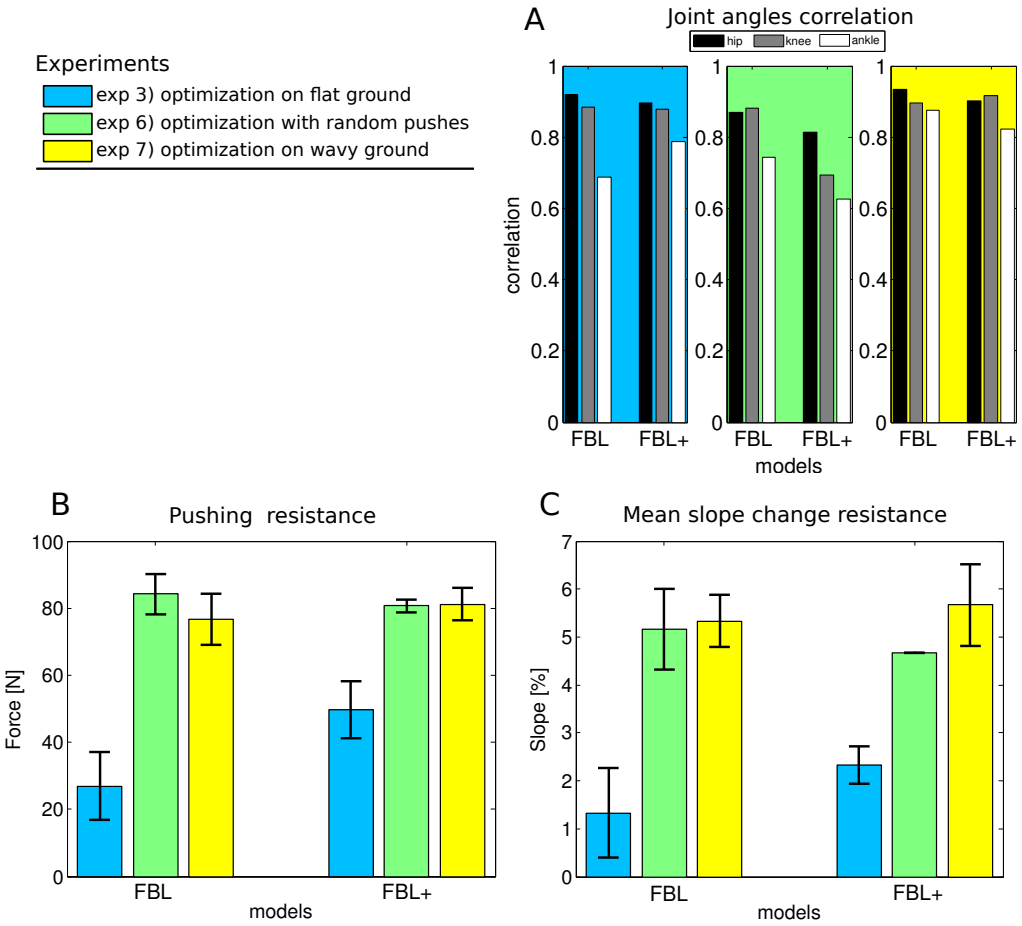

Figure 3.6: Results of evaluation of experiment 3, 6, 7. A) Joint angles correlation with human for the different experiments and the two FBL models. B) Mean maximum push force amplitude resistance. C) Mean maximum slope change (in %) resistance .

3.2.1 Human similarity assessment

To assess the quality of the gait obtained on perturbed environments, we start by looking at how similar to humans the different optimized gaits are. Indeed, as we optimize on environments presenting different kinds of perturbations, we want to make sure that the optimization do not lead to unnatural gaits that managed to maximize their resistance, at the cost of a decrease in the quality of the gait. In other words, we want to verify that the gait did not specialize to much.

As expected, when evaluated on flat ground, all optimized gaits are visually good (videos available at [6]) and show a good correlation of joint angles compared to human (approximately 0.8), see Figure 3.6 A. The correlation of the activity of the muscles is also comparable to what was found in previous section (data not shown). We can thus conclude that the gaits are not to over-specialized.

3.2.2 Resistance to pushes

There is a clear increase in the maximum push force amplitude from which the gait can recover for gaits optimized on the random pushes environment, compared to gaits optimized on flat ground, see Figure 3.6 B. It is interesting to note that gaits optimized on

the wavy ground are also good when evaluated against resistance to pushes. This holds true for both FBL and FBL+ models. The gait optimized on perturbed environment can resists to 80 [N] pushes of 0.25[s] mean duration (to visually appreciate the effect of pushes of different amplitude see videos available at [6]).

In order to give an idea of the kind of perturbation applied to the robot let's use the law of conservation of momentum and its relation to impulses. Given the mean push duration of 0.25[s], the perturbation is an impulse of $J = F \cdot \Delta T = 15$ [Ns]. Since impulse is related to the change in momentum by $J = \Delta p = m \cdot v_1 - m \cdot v_0$, we can estimate the speed of the robot after the push. Assuming that, during the push, the robot is a point object moving at constant speed with no other resistance, we have: $v_1 = J/m + v_0 = 1.4875$ [m/s]. Using the conservation of momentum we can make the correspondence with another robot walking at constant speed and pushing the robot by the back. Lets assume that the other robot as the same mass $m = 80$ [kg], then using conservation of momentum, we can say that the momentum at the beginning of the push and at the end are the same. Assuming that at the end of the push the second robot as a speed equals to the speed of the robot we have:

$$m_a v_{a0} + m_b v_{b0} = v_1 \cdot (m_a + m_b) \tag{3.1}$$

$$v_{b0} = \frac{v_1 \cdot (m_a + m_b) - m_a v_{a0}}{m_b} \tag{3.2}$$

$$v_{b0} = \frac{1.4875 \cdot (80 + 80) - 80 \cdot 1.3}{80} \tag{3.3}$$

$$v_{b0} = 1.675\text{[m/s]} \tag{3.4}$$

Thus, under the mentioned conditions, the change in momentum of the system would be equivalent to the effect of a collision with an other robot coming by the back with a speed 30% higher.

3.2.3 Resistance to wavy ground

As with the resistance to pushes, there is a clear increase in the maximum slope from which the gait can recover for gaits optimized on the wavy ground environment, compared to gaits optimized on flat ground, see Figure 3.6 C. As noted with the resistance to pushes, gaits optimized on wavy ground are as good as gaits optimized on random push environment. Thus there is no clear distinction in the resistance to perturbations for both experiment 6 and 7 and both perturbations.

We can also note that the maximum slope is only of 5% which is not really high. When looking at the optimized gait walking on this environment (see attached video available at), the robots falls because the feedbacks used do not take into account the necessity to give more energy when going up. What changes between the gait optimized on flat ground (experiment 3) and gaits from experiments 6 and 7 is more the shape of the gait.

We observe that, generally, the FBL+ model do not show more stable gaits, compared to the FBL model. We will therefore not further investigate this extended model, so as not to complicate the model for non significantly gains.

3.3 FBL extensions

3.3.1 Discovering running gait with the FBL+ model

It has be showed by J.Wang that the addition of the 3 feedbacks rules to prepare the limb position before landing and the addition of new sub cycle phases (see section 2.1.3) are

enough to give the FBL the ability to generate running gait. This extension has been implemented in the FBL+ model, and as expected some running gait were found (see example video at [6]). The experiment 5 has been designed to generate running gait. It uses the FBL+ model defined in section 2.1.3. The optimization algorithm used is the stage PSO. The stages used are the same as the one of experiment 2. The only differences is that the model is optimized for a walking speed of 2.5 m/s (i.e. the passing criterion for the second stage is changed from $v > 1.3$ to $v > 2.5$ m/s). The figure 3.7 shows the ground reaction forces differences between a running gait (results of experiment 5) and a walking gait (results of experiment 3).

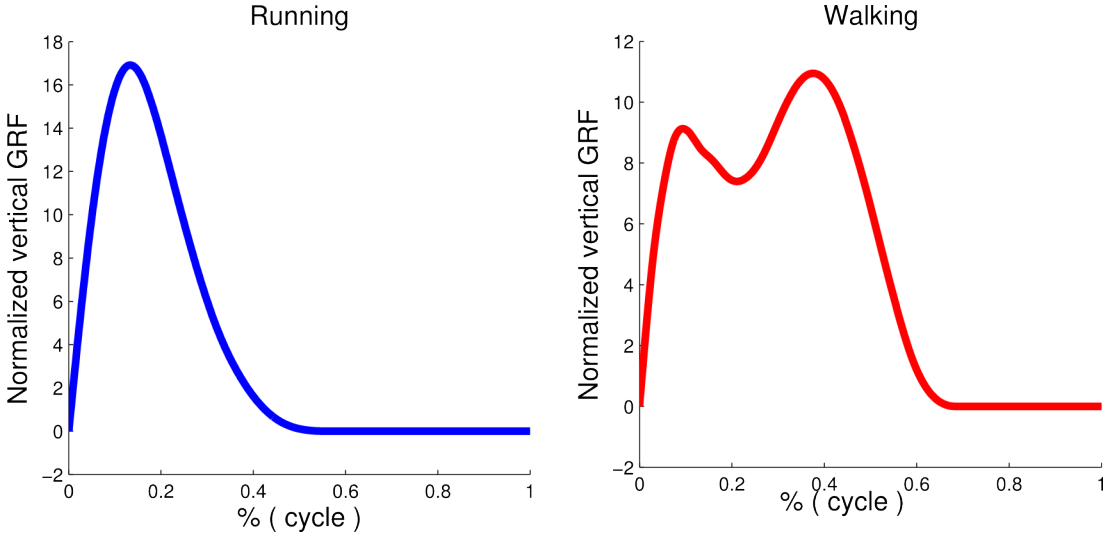

Figure 3.7: Vertical ground reaction forces between a running FBL+ model (LEFT) and a walking one (RIGHT). The data has been filtered with a linear filter of order 100.

Chapter 4

Discussion

4.1 Optimization of the FBL model

It has been shown in the results that the addition of criterion accounting for the quality of the gait are necessary to discover good gait (i.e. steplength SNR, joint angles correlation with human). The minimization of the step length variation is crucial for finding stable gait, this is shown when comparing the step length SNR value of experiment 1 and 2 (see table 3.2). This can be more appreciated when comparing video of experiment 1a (without the criterion accounting for the stability of the step length) with video of experiment 2a (with the criterion accounting for the stability of the step length) [6]). The addition of the criterion accounting for similarity with human gait improved remarkable the shape of the gait, especially for the KNEE and ANKLE joint (see figure 3.1). However the gait didn't show a good correlation of forces acting at the level of the knee joint during the stance phase (see figure 3.4). This can be explained a) by the absence of toes that can play the role of absorbing the shock arising from foot ground contact and b) because the body segments have no elasticity (except at their junction where joint soft limit are used to model the effect of ligaments).

4.2 FBL Similarity with human

Human limbs are made of many muscles whose actions overlaps. More than 20 different muscles act on the hip joint, 10 on the knee and 10 on the ankle [19]. The model used here only include 7 modeled muscles, i.e., the minimal subset of muscles necessary to drive the different limb joint in the sagittal plan (flexion and extension). In this model, the only overlap in actions comes from the two bi-articular muscles (SOL and HAM muscles). Even with this small number of muscles, produced gaits are visually very close to real human gait. This visual observation is confirmed by the good correlation of muscle activity, angles and torques compared to human data (see figures 3.2, 2.10, 2.9).

Main differences are observed for the VAS and GAS muscles, which seems to have an effect only at the knee torques level. However, this difference is not visible at the angles level (see figure 3.2). As the force applied on the knee joint is not comparable to humans, whereas the shape of the knee joint angles is really close to humans, it is very likely that this discrepancy is due to model simplifications at different levels (e.g. modeling of body segments, lack of several structures (such as toes, cartilages and bones), interactions between the model and the environment, reduction of muscles number). The fact that the differences appears at the knee joint is thus not surprising. Indeed, the shock arising from foot - ground contact is mainly absorbed by the knee joint. This shock - in the physical

simulator - is overestimated because the elasticity of the body is not modeled and, maybe most importantly, because toes are not modeled. In order to circumvent this issue, a simple passive toe could be added, modeled as an overdamped spring. Furthermore, the contact could be amortized by adding damping at the contact point between foot and ground (as it was the case in [9]).

4.3 Model robustness

An important feature of the FBL model is certainly its ability to resist to pushes of remarkably high amplitude, (80 [N] during 0.5 [sec] applied at the trunk level, see section 3.2.2). This is of crucial importance when thinking about the possible applications of this kind of model. Indeed, if applied to intelligent lower limb prosthesis, the device would benefit from this intrinsic high robustness to pushes.

However, when looking at the ability of the FBL model to adapt to slope changes, the results are quite disappointing. Indeed, the best experiment is only able to resist to change in slope of 5% and walk upward on a slope of 7.0%. However, as it will be shown in the next part of the report, the addition of a feed-forward component inspired by CPG can greatly improve this results (after introduction of the feed forward component the so-called 3FBL model is able to walk upward on slope of 30%).

4.4 J. Wang based extensions

In the FBL + model, 3 reflex rules are added to prepare the limb position before landing, and a new sub cycle phases (see section 2.1.3) is also added. Contrary to what could be expected, preparing the limb before touching the ground did not significantly improve the resistance of the gait toward perturbation (see section 3.2). The introduction of the new feedback rules acting on the HF, GLU and VAS muscles in order to bring the hip and knee joint of a limb toward a reference angle just before touching the ground did not improved the robustness of the gait to the designed perturbations. However, these additional rules were proved to be useful in other situations. Indeed, it has be showed by J.Wang that those extensions are enough to give the FBL the ability to generate running gait. This extension has been implemented in the FBL+ model, and as expected, running gait were observed (see example video at [6]). The bell shaped characteristic vertical ground reaction forces observed (see figure 3.5) is comparable to ground reaction forces found in human running [18].

Part II

FBL extension : addition of a Central Pattern Generator (CPG)

Chapter 5

Introduction

In this second part, we add a feedforward component to the FBL model described in the first part. The feedforward component is modeled by constant inputs acting on an interneuron network made of sensory interneurons, basal interneurons and cpg interneuron mimicking the action of a central pattern generator (CPG).

First, we give a mathematical description of the CPG model that is used (section 6.3). Then we describe how the CPG is generated (section 6.4). Since the FBL model can generate stable locomotion, we decided to add a feedforward component that minimizes the differences with the FBL model by mimicking the signals generated by the the feedback loops (i.e. interaction between the body and the environment). Indeed, as locomotion can be viewed - in a dynamical system point of view - as a limit cycle, it makes sense to assume that most of the sensory information will also be represented by a limit cycle. The CPG will thus mimic the oscillatory pattern generated by the sensors of the FBL model that are the most stable among periods. In order to analyze those patterns, the simple feedback rule of the FBL model is explicitly split into three stages: the sensory input, the sensory interneurons (IN_{SEN}) and the motoneurons MN stages (see section 6.1).

The addition of the intermediary IN_{SEN} stage is a step toward the modeling of the spinal cord, that will be complemented by two kinds of feedforward interneurons (IN_{FF}): the interneurons of the CPG (IN_{CPG}) and the basal interneurons (IN_{BAS}) . These IN_{FF} will mimic the signals of certain IN_{SEN}. In order to choose which IN_{SEN} signals the feedforward component will replace, a periodical stability assessment method will be used (section 6.4.2). When applied to the IN_{SEN} signals, it will be shown that most IN_{SEN} are - as expected - almost invariant between cycles. The signal of the INs_{SEN} presenting the smallest variations will be then modeled as a IN_{BAS} in the model named FBL- and as IN_{CPG} and IN_{BAS} in a model called 3FBL (see section 6.2.1)

In the FBL-, the IN_{BAS} simply replaces the IN_{SEN} that showed the least variation. It will be shown that even if a large part of the sensory information is lost, the model is still able to generate stable locomotion comparable to the FBL model. In the second model a CPG component is added to replace IN_{SEN} with low variation acting on proximal limbs. This second models combine the three type of interneurons: IN_{SEN}, IN_{CPG} and IN_{BAS}.

Then control variables will be added to the model to mimick the action of upper brain structures, like the reticular formation. The online modification of the control variables will allow gait modulations (changes in speed and steplength) and gait adaptation such as adaptation to increasing slope. The added control variables are inspired from neurobiology. In particular, we attempt to model neural control of locomotion, whose biological relevance is presented below,

5.1 Neural control of locomotion

5.1.1 Vestibular system

The vestibular system acts in the management of balance and conveys information about body orientation and movements to the CNS. The vestibular system is made of two main structures: the otolith organs and the semi-circular canal. The otolith is sensitive to linear acceleration and can thus detect the direction and magnitude of the gravity, as well as other linear accelerations due, for example, to movements. The semi-circular canals are sensitive to angular acceleration [23]; there are three semi-circular canals that are oriented orthogonally to each other. By combining the information from the three different canals the CNS generates a 3D representation of the head instantaneous speed [14]. The action of the vestibular system on movements is made through the vestibulospinal tract whose neurons are located in the vestibular nuclei (see figure 5.2). It acts on motoneurons of extensor muscles. It also innervates muscles of the trunk, thus helping in coordinating postural adjustment [21].

5.1.2 Cerebellum

The cerebellum is located at the base of the brain (see figure 5.1). It receives information from higher brain structures (through the cerebrocerebellum) and has afferent and efferent to the spinal cord; some direct through the spinocerebellum and others direct through reticular formation. The direct connections play role in movement fine tuning. The indirect connections (passing through the reticular formation) play an important role in motor control, as well as in balance (it is also involved - to a lesser extent - in cognitive functions such as emotions, attention or event pain [32]).

The cerebellum is made of several modules (enumerated below), each of which having a specific role. The role of the cerebellum in motor control can be appreciated by looking at the effects of injuries on the cerebellum. Depending on the damaged module of the cerebellum different effects results:

- vestibulocerebellum The Vestibulocerebellum (by its connection to the vestibular system) regulates balance and eye movements. When damaged, it can cause equilibrium dysfunction and difficulties in balancing, apparent when walking, as an unnaturally large stance and gait asymmetry.

- cerebrocerebellum The Cerebrocerebellum plays roles in planned movements execution and skilled movements generation. When damaged, patients develop difficulties in reaching task, judging distances and sometimes also show tremor.

- Spinocerebellum The spinocerebellum plays role in whole-body movements coordination and fine movements. Damages to this part of the cerebellum can also have consequences in the psychology and cognitive functions of the patient. Patients with damaged spinocerebellum often show deficits in their ability to experience emotions and are more likely to present depression [32].

The group of symptoms related to motor disfunction due to damages of the cerebellum is called cerbellar ataxia. It has been suggested that the difficulties to coordinate movements in cerebellar ataxia is due to an inability to manage the interaction between torques during movement involving multiple joints movements [1].

5.1.3 Reticular Formation

The reticular formation is part of the brain stem (located at the base of the brain, see figure 5.1). It is involved, for example, in sleep phases control, pain modulation and consciousness. Breathing and swallowing CPG are also located there. It has an important role during locomotion; its descending pathway to the spinal cord (so-called reticulospinal tract) has a major role in maintaining the body posture during locomotion, by acting on the proximal limbs muscles and trunk muscles [7].

5.1.3.1 The Reticulospinal Tract

Some of the neurons of the reticular formation involved in locomotion project to the α and γ motoneurons of the spinal cord through the reticulospinal tract. Their actions on motoneurons of spinal cord can be both excitatory and inhibitory [7].

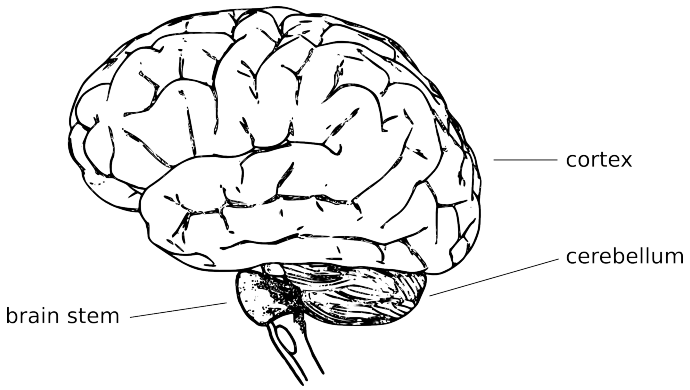

Figure 5.1: Schematic view of a brain together with the cerebellum and the brain stem.

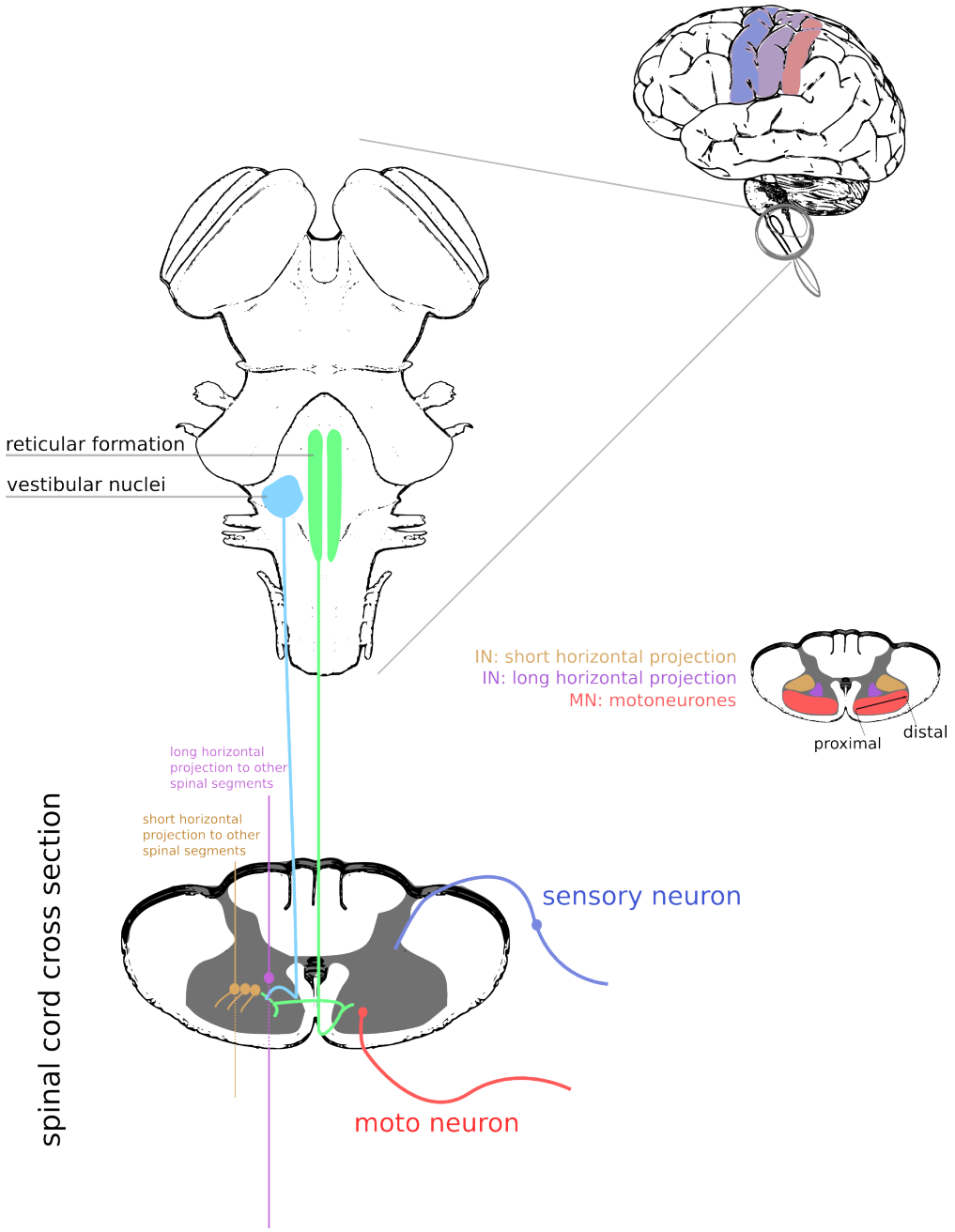

Figure 5.2: Schematic view of the effect of vestibulospinal and reticulospinal tract on the spinal cord [21]. The sensory information enters the spinal cord by the dorsal part while motoneurons project to muscles through the ventral part of th spinal cord. Small interneuron network exists in the spinal cord with vertical projections to other segments. Figure inspired from [21].

Chapter 6

Methods

6.1 Sensors to muscles mapping reorganization

As mentioned in the introduction, the first step toward the addition of a feedforward component is the analysis of the sensory signals present in the FBL model. In order to permit an in depth analysis of the sensory signal generated by the FBL model, the direct connection that exists between sensors and actuators in the FBL model is split into three more realistic steps, presented in figure 6.1:

- SEN: The same four types of sensory inputs used in the model of H. Geyer (see section 2.1.2.3) are here explicitly defined; each type of sensor output is isolated and individually sent to interneurons.
- IN_{SEN}: The sensors described above send signals to sensory interneurons. Each interneuron receives either one input (from either the muscles, the overextension prevention or ground feedbacks) or two inputs for the stability feedback (i.e. the ground and trunk posture feedbacks).
- MN: Each motoneurons receives a combination of inputs from a set of IN_{SEN}.

Note that this reorganization does not modify *per se* the FBL model. Indeed, the muscles output remains the same, but the splitting performed is more biologically relevant and allows analysis of sensory, inter- and motorneurons separately, providing depth analysis of the feedback generated by the model (see section 7.3.3).

The connection between signals sent from sensors and received by IN_{SEN} and the connection between the signal sent from IN_{SEN} and received by motoneurons are modeled by a first order differential equation, similar to equation 2.40. One concern of this reoganization is that it introduces two delays; one between sensors and IN_{SEN} and one between IN_{SEN} and motoneurons. However, these changes will not affect the behavior of the model if the delays are small enough.
Since input to motoneurons depends on whether the limb is on stance, swing phase, on the double stance support finishing stance phase, or whether the joint is moving to fast (for overextension feedback), three state-dependent interneurons (IN_{SD}) are added: one that is active during stance, one that is active during swing and one that is active when a joint is moving faster than its limit. Those interneurons are coupled to the previously defined IN_{SEN}, with inhibitory connections. They can thus turn on/off IN_{SEN} activity when needed. The table 6.1 presents the different IN_{SEN} of the FBL model.

Table 6.1: List of the sensors used in the model. If not specified, the muscle onto which the sensor acts is on the same side as the sensor (i.e. ipsilateral).

Sensors

Abbreviation	Sensor(s) type	From	To	Active in
GAS←GAS MFF, ST	Muscle force	GAS	GAS	Stance
GLU←GLU MFF, SW	Muscle force	GLU	GLU	Swing
HAM←HAM MFF, SW	Muscle force	HAM	HAM	Swing
SOL←SOL MFF, ST	Muscle force	SOL	SOL	Stance
VAS←VAS MFF, ST	Muscle force	VAS	VAS	Stance
TA←TA MLF CY	Muscle length	TA	TA	Cycle
HAM←HF MLF SW	Muscle length	HAM	HF	Swing
HF←HF MLF SW	Muscle length	HF	HF	Swing
HF←GIF ST	Contact, Joint	iFoot,Trunk	HF	Stance
HAM←GIF ST	Contact, Joint	iFoot	HAM	Stance
GLU←GIF ST	Contact, Joint	iFoot	GLU	Stance
VAS←GCF STend	Contact	cFoot	VAS	Stance end
HF TL SW	Trunk lean	Trunk	HF	Swing
VAS←KNEE OPF	Overext. prev.	KNEE	VAS	Swing

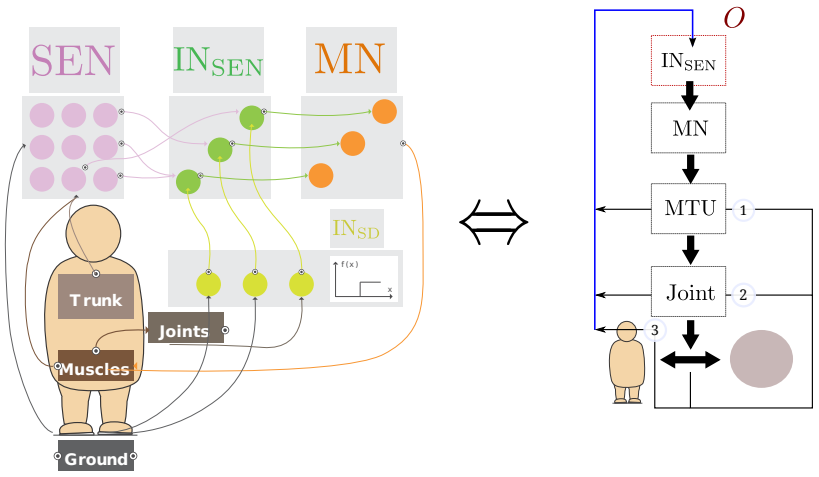

Figure 6.1: Extension of the H. Geyer model by explicitly splitting the reflex loop into sensors (SEN), interneurons (IN_{SEN}) and motorneurons (MN)

6.2 Feedforward extension of the FBL model

As mentioned in the introduction, modifications on the FBL model are made at the level of the interneurons (IN). In the FBL model, all signals sent to motoneurons (MN) are coming from sensors. Here, based on the conclusion of the analysis of the IN_{SEN} signals (see section 7.3.3), two new kind of biologically inspired feedforward interneurons (IN_{FF}) are created, replacing selected IN_{SEN}:

- IN_{BAS}: interneurons generating signals of constant output, which are sent to selected MN. Biologically, these signals of constant input can be viewed as those generated by the reticular formation and sent to the motoneurons, acting on limb muscles through the reticulospinal tract (see section 5.1.3).
- IN_{CPG}: interneurons generating signals whose shape is inspired from signal of the IN_{SEN} signals they replace, acting as central pattern generators. This kind of CPG for controlling the locomotion of humans is purely speculative. Motor CPG, located in the reticular formation, exists in humans for controlling. for example, breathing or swallowing. As the reticular formation has efferent to motoneurons in the spinal cord, it is a possible location for locomotor CPG. An other possible location is in the gray matter of the spinal cord, where interneurons networks that projects to different segments of the spinal cord exists (see section 5).

The properties of the feedforward units IN_{FF} are fully inspired by their IN_{SEN} counterpart. Indeed, the IN_{BAS} have a constant input whose level equals the mean level of the corresponding IN_{SEN} and the IN_{CPG} have a shape mimicking the one of the corresponding IN_{SEN}. Figure 6.2 A shows the different type of sensory interneurons (note that state-dependent interneurons (IN_{SD}) are not shown).

6.2.1 Sensory interneuron replacement

Based on the analysis of the IN_{SEN} signals, two new models are introduced:

- FBL- : Reduced FBL
- 3FBL : Feedforward and Feedback based locomotion

The figure 6.2 describes the differences between the FBL, the FBL- and the 3FBL models. The FBL- and 3FBL models differ from the FBL model by the structure of the IN network. Both models removes 70% of the sensory information coming from muscles. The FBL- model replaces the removed IN_{SEN} by IN_{BAS}, whose output levels equals the mean activity of their corresponding IN_{SEN}. The 3FBL model replaces the removed IN_{SEN} by IN_{BAS} and IN_{CPG}. As the CPGs are introduced for controlling properties of the gait (such as speed and step length), they are used for IN sending connections to MN acting on proximal limb muscles (i.e. GLU and HF muscles). Figure 6.2 B shows the information flow from IN to MTU through MN, and highlight the differences between models at the IN level. The differences between the three models can be most appreciated in figure 6.2 C. The tables summarizes the IN used in each model. They show which IN_{SEN} are removed in the FBL- and 3FBL model (see gray crosses in the table) and by what kind of IN_{FF} they are replaced.

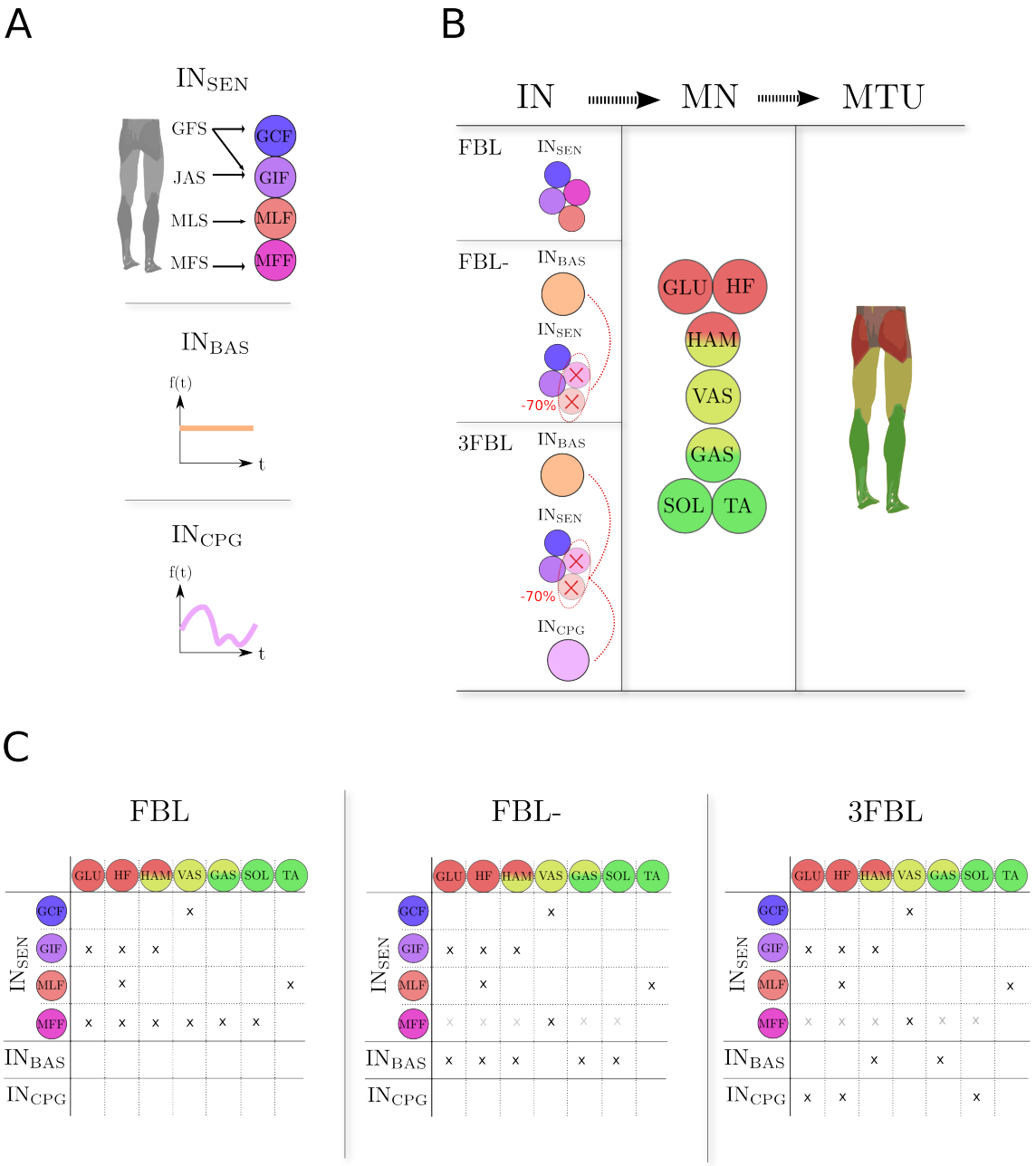

Figure 6.2: A: The different kind of interneurons; the sensory interneurons (IN_{SEN}), the basal activity interneurons (IN_{BAS}) and the CPG interneurons (IN_{CPG}). B: the information flow from IN to MTU through MN; the FBL, FBL- and 3FBL models only differ at the IN level. C: table describing the relationships between IN and MN for the three models (columns: MN, lines: IN) Left: the initial FBL model. Middle: the reduced FBL model (FBL-). Right: the 3FBL model.

6.2.2 System control parameters

In this section, we introduce two biologically inspired control laws applied at the level of the interneurons. The two different types of control variables introduced are:

1. A: variable acting on the connection strength between two neurons. It models an inhibitory connection acting on the axon of the postynaptic neuron (see figure 6.3 left) and controls the connection strength between the postsynaptic neuron and the neuron on which it acts. Its effect is thus proportional to the activity of the postsynaptic neuron.
2. O: variable adding a constant input to a neuron. It models a simple excitatory connection between two neurons, where the presynaptic neuron has a constant activity and act close to the soma of the postsynaptic neuron (see figure 6.3 right).

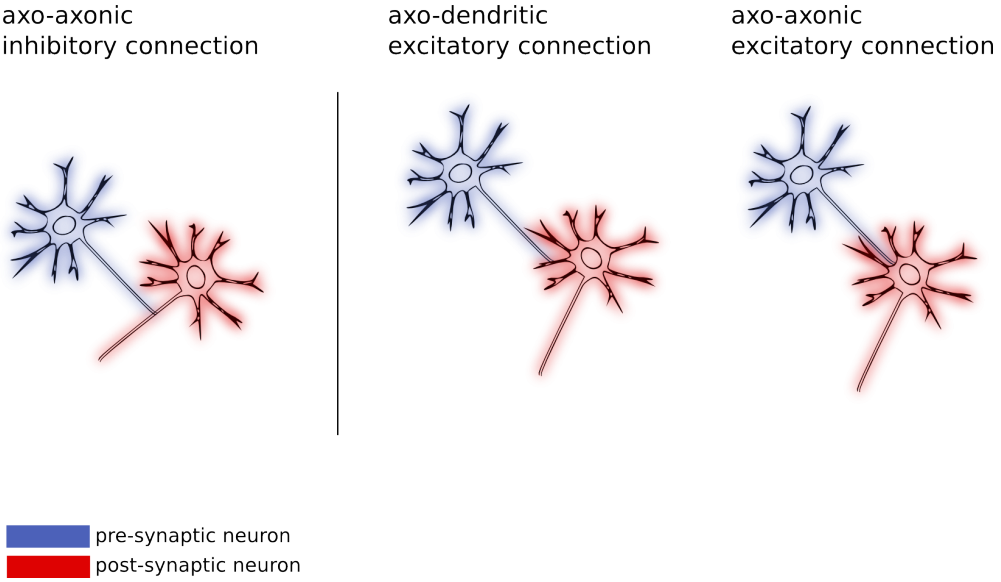

Figure 6.3: Schematic view of simple connection between neurons. LEFT: axo-axonic inhibitory connection. RIGHT: axo-dendritc and axo-somatic excitatory connection.

Based on the those two control variables, 3 different control rules pairs are defined:

- A control rule pair acting on $\mathrm{IN}_{\mathrm{SEN}}$ relaying information from ground feedback (GCF), ground and stability feedback (GIF) and the most variable muscle length feedbacks (MLF) and muscle force feedbacks (MFF), noted:
  $A_{\mathrm{IN}_{\mathrm{SEN}}}, O_{\mathrm{IN}_{\mathrm{SEN}}}$
- A control rule pair acting on $\mathrm{IN}_{\mathrm{SEN}}$ relaying information from the least variable MLF and MFF acting on HIP muscles and, for the 3FBL model, their associated $\mathrm{IN}_{\mathrm{CPG}}$, noted:
  $A_{\mathrm{IN}_{\mathrm{CPG}}}, O_{\mathrm{IN}_{\mathrm{CPG}}}$
- A control rule pair acting on $\mathrm{IN}_{\mathrm{SEN}}$ relaying information from the other least variable MLF and MFF (i.e. those not acting on the HIP muscles) and, in the FBL- and 3FBL models, their associated $\mathrm{IN}_{\mathrm{BAS}}$, noted:
  $A_{\mathrm{IN}_{\mathrm{BAS}}}, O_{\mathrm{IN}_{\mathrm{BAS}}}$

The summary of the pair of rules used by each model is shown below. One extra control rule, called ω and controlling the frequency of $\mathrm{IN}_{\mathrm{CPG}}$ is also added to the 3FBL

model. A set of control variable value is called a control vector and is noted C. Each model has an associated C^{trl}:

$$\begin{aligned} C^{trl}_{\text{FBL-}} &= \{A_{\text{IN}_{\text{SEN}}}, O_{\text{IN}_{\text{SEN}}}, A_{\text{IN}_{\text{BAS}}}, O_{\text{IN}_{\text{BAS}}}\} \\ C^{trl}_{\text{FBL}} &= \{A_{\text{IN}_{\text{SEN}}}, O_{\text{IN}_{\text{SEN}}}, A_{\text{IN}_{\text{CPG}}}, O_{\text{IN}_{\text{CPG}}}, A_{\text{IN}_{\text{BAS}}}, O_{\text{IN}_{\text{BAS}}}\} \\ C^{trl}_{\text{3FBL}} &= \{A_{\text{IN}_{\text{SEN}}}, O_{\text{IN}_{\text{SEN}}}, A_{\text{IN}_{\text{CPG}}}, O_{\text{IN}_{\text{CPG}}}, A_{\text{IN}_{\text{BAS}}}, O_{\text{IN}_{\text{BAS}}}, \omega\} \end{aligned}$$

If not specified, the control vectors used for each model are:

$$C^{trl}_{\text{FBL-}} = \{1.0, 0.0, 1.0, 0.0\} \tag{6.1}$$

$$C^{trl}_{\text{FBL}} = \{1.0, 0.0, 1.0, 0.0, 1.0, 0.0\} \tag{6.2}$$

$$C^{trl}_{\text{3FBL}} = \{1.0, 0.0, 1.0, 0.0, 1.0, 0.0, 0.85\} \tag{6.3}$$

Note that the control presented here is specifically designed for the FBL- and 3FBL models, but in order to determine whether the observed effects are due to the combined effect of the added structures (i.e. the IN_{FF}) and the separation of the control variables into the three control rules pairs, or whether it is simply a consequence of the latter, we also test the FBL model. This means that the names chosen for the control rules (i.e. IN_{CPG} and IN_{BAS}) do not implies - in the case of the FBP model - the actual presence of a feedforward component. It simply refers to the corresponding IN_{SEN} in the FBL model.

The control variables are chosen based on biological observations. The introduction of offset signals is in agreement with constant bursts sent by the reticular formation to the spinal cord. The change in signal amplitudes is in agreement with the existence of inhibitory connections sent by the cerebellum, and the vestibular nuclei to the spinal cord. Here the inhibitory connections are assumed to acts on the connection weight between two neurons. Finally, the control of frequency follows the assumption of the existence of locomotor CPG [21].

6.3 CPG model

6.3.1 Arbitrary wave oscillator (AWO)

The dynamical system used to model signals generated by spinal circuits is an arbitrary wave oscillator (AWO)[15]. This oscillator is able to produce any shape, as long as this shape can be represented by a function that is both 1-periodic and is derivable. The differential equation governing the oscillator is the following:

$$\dot{\theta} = \omega \tag{6.4}$$

$$\dot{x} = \gamma(g(\theta) - x) + \frac{dg}{\theta} \cdot \dot{\theta} + K \tag{6.5}$$

where :

- $\dot{\theta}$ is the frequency of the oscillator, see section 6.3.2 for details on how the frequency is calculated.

- K is a perturbation term (set to zero).

- γ controls the speed of convergence of the oscillator output x toward the shaping function $g(\theta)$. γ is set to 100.
- $g(t)$ is the nominal function that shapes the output of the oscillator.

$x(t)$ is the output of the oscillator. This output has a shape given by the $g(t)$ function. Since several signals will be modeled, different AWO oscillators (noted awo_i) are used, each of them having its own $g_i(t)$ function.

6.3.2 Frequency control

Since the $g(t)$ functions will be modeled from sensory signals, and that all signals have been chosen to start at the same moment (i.e. at the swing/stance transition), there is by definition no phase shift between the oscillators. The different oscillators can thus be controlled by the same $\dot{\theta}$ phase differential equation (called central clock).

We construct this central clock, step by step. Let's start with a clock with a constant frequency:

$$\dot{\theta} \quad = \quad \omega \tag{6.6}$$

Where the frequency ω is estimated from the speed of the underlying FBL model. In order to account for the variation of the cycle duration two different strategies are used, depending on whether the clock is too slow or too fast compared to the walking frequency:

1. If the central clock is too slow compared to the walking frequency, the phase of the central clock is simply restarted (i.e. all oscillators acting on motoneurons of one side are restarted when the corresponding limb touches the ground).

2. If the central clock is going to fast compared to the walking frequency, a slowing down mechanism enters in action. It ensures that signals generated by the AWOs will not start a new cycle before they should, i.e. before the limb touches the ground. With the slowing down mechanism the frequency has the form:

$$\dot{\theta} \quad = \quad \begin{cases} \omega & \text{if } t < p \cdot \frac{1}{w} \\ c'(t) & \text{else} \end{cases} \tag{6.7}$$

   Where:

   - p is the percentage of the phase at which the slowing down mechanism is turned on
   - $c'(t)$ is a slowing down function that ensures that $\theta \leqslant 1.0, \forall t \epsilon \mathbb{R}$

   In order to find a satisfying $c'(t)$ function, we looked at the evolution of θ. We want:

$$\theta = \begin{cases} \omega t & \text{if } t < p \cdot \frac{1}{w} \\ c(t) & \text{else} \end{cases}$$

   With, $c(t)$ monotonically increasing and $\lim_{t \to \infty} c(t) = 1.0$. We can for example take the class of exponential functions :

$$c(x) = 1 - exp\left(-\beta x + \gamma\right), \beta > 0$$

   In order to find the β and γ parameters we can enforce that, when $t = p \cdot \frac{1}{w}$:

   (a) There is a unique solution to $t = c(t)$: $1 - exp\left(-\beta p/w + \gamma\right) = p/w$
   (b) The transition from t to $c(t)$ is continuous, i.e. $c'(t) = w$: $c'(p) = a \cdot exp(-\beta \cdot p + \gamma) = w$

The second condition can be easily solved for γ, we get :

$$\gamma = ln(\omega/\beta) + \frac{\beta \cdot p}{\omega}$$

Using this result in the first condition, we obtain

$$\begin{aligned} 1 - exp\left(-\beta p \cdot \frac{1}{w} + ln(\omega/\beta) + \frac{\beta \cdot p}{\omega}\right) &= p \\ 1 - \frac{\omega}{\beta} &= p \\ \beta &= \omega \frac{1}{1-p} \end{aligned}$$

If we want the slowing down mechanism to enters in action after 90% of the period of the oscillator (e.g. $p = 0.9$) we get $\beta = 10\omega$ and $\gamma = -ln(10) + 9$, it follows that :

$$c(t) = 1 - exp\left(-10\omega x - ln(10) + 9\right) \tag{6.8}$$

$$c'(t) = 10\omega \cdot exp(-10\omega x - ln(10) + 9) \tag{6.9}$$

6.4 CPG : pattern generation

Here we describe the method used to model signals generated by the IN_{SEN} as a dynamical system. The method is based on the use of Arbitrary Wave Oscillator (AWO), which are simple oscillators able to follow an arbitrary shape (see section 6.3.1 for details on the AWO).

We first extract a normalized periodic functions named *nominal functions* from the signals generated by the IN_{SEN}, based on a clear splitting criterion (here the transition time between swing and stance phase). Then the periodic stability is verified, and only the signals considered stable enough are selected to be modeled using AWOs. Indeed, to be modeled as an AWO, the signal needs to be periodic with small variability between periods. We therefore developed a method to assess the periodic variability of the signals (see section 6.4.2 for a description of the variability assessment method). Finally, the mean and standard deviation of the original signals combined with the normalized functions are used to generate the AWOs.

6.4.1 Nominal function extraction

The first step towards the generation of the nominal function is thus the separation of the signal $S(t)$ into cycles split at the swing/stance transition. The swing/stance transition is found using the ground sensors. Assuming that there are M transitions, the same number of sub-signals $S_i[t]$ with $i\epsilon\{1, .., M\}$ are generated.
The second step consists in the generation of the stereotyped function starting from the $S_i[t]$. This is achieved by normalizing each cycle so that they have a mean (i.e. offset) of zero and a standard deviation of one.

$$\tilde{S}_i^n(t) = \frac{S_i[t] - \mu_i}{\sigma_i} \tag{6.10}$$

where μ_i and σ_i are respectively the mean and standard deviation of the sub signal i.
In order to obtain sequences of same lengths, a continuous version of the discrete $\tilde{S}_i^n[t]$ sub signals is generated using spline interpolation. Then, the sub signals are split into N

equally spaced point. A set of discrete normalized sub-signal with the same length are thus generated (noted $S_i^n[t]$). The length of the sub signals can be recorded for studying the variability of the periodic pattern duration.

6.4.2 Periodical stability assessment

As previously mentioned, the signals need to be stable enough among periods in order to be represented as an AWO and thus to be modeled in our CPG. Here we use two different methods to ensure that this requirement is fulfilled:

Comparison with a reference signal S_{ref}
A method to estimate the periodical stability is to compare each sub signal with a reference signal S_{ref}, and calculate a normalized stability factor s, that represents the error between the reference signal and each sub signals. Here we use the mean of the normalized sub signals as the the reference signal: $S_{ref}[i] = \overline{S^n[i]} = \frac{1}{M}\sum_{k=1}^{M} S_k^n[i]$ with $i\epsilon\{1, .., N\}$ where N is the number of data points and M the number of sub signals. The sum of squared distances between the reference signal S_{ref} and the different sub signals is then calculated:

$$s = \frac{\sum_{i=1}^{M}\sum_{j=1}^{N}(\overline{S^n[j]} - S_i^n[j])^2}{M \cdot N} \tag{6.11}$$

When the value of the normalized stability factor s is below an empirically determined value, the signal is considered as periodically stable. To determine this limit value, we investigated the value of the normalized stability factor s in different controlled situations. We start with discrete reference signal S_{ref} extracted from a M periods (with $M = 1000$) of a full periodic pattern governed by $y = sin(2\pi t)$. N data points are extracted per period. Then different versions of this signal are generated by adding white noise, i.e.:

$$S_\sigma[i] = S_{ref}[i] + X_\sigma \ , \text{ where } X_\sigma \ \sim \ \mathcal{N}(0, \sigma^2) \tag{6.12}$$

Where S_σ^n is a noise-contaminated version of $S_{ref}[t]$ generated by adding a random noise generated by the random variable X drawn from a Gaussian distribution with a mean of zero and a standard deviation σ. Starting from the definition of the normalized stability factor we have:

$$\begin{aligned} s &= \frac{\sum_{i=1}^{M\cdot N}(S_{ref}[i] - S_\sigma[i])^2}{M \cdot N} \\ &= \frac{\sum_{i=1}^{M\cdot N}(S_{ref}[i] - (S_{ref}[i] + X))^2}{M \cdot N} \\ &= \frac{\sum_{i=1}^{M\cdot N} X^2}{M \cdot N} \end{aligned}$$

Remembering that the mean of the random variable X is 0 (i.e. $\mathrm{E}[X] = 0$) and that the variance is equal to the mean of the square minus the square of the mean we (i.e. $\mathrm{Var}(X) = \mathrm{E}[X^2] - \mathrm{E}[X]$) we can write:

$$\begin{aligned} \mathrm{Var}(X) &= \mathrm{E}[X^2] - \mathrm{E}[X] \\ &= \mathrm{E}[X^2] \end{aligned}$$

Then, given that $lim_{N\to\infty}\frac{\sum_{i=1}^{N} X^2}{N} = \mathrm{E}[X^2]$, s is an estimation of the variance of X_σ :

$$s \approx \sigma^2 \tag{6.13}$$

Figure 6.4 shows the normalized stability factor s of S_σ signals with different level of noise. From bottom to top the noise is generated from a distribution with 10%, 25%, 50% and 75% of the standard deviation σ of the reference signal S_{ref}.
Because the purpose of the measure s is to help us define whether or not a signal can be modeled properly by an AWO, the periodic pattern needs to be clearly stable. Visually, we observe that the functions with a normalized stability factor $s > 0.1$ are not clearly stable. We therefore consider that a signal needs to have a $s < 0.1$ to be properly modeled by an AWO.

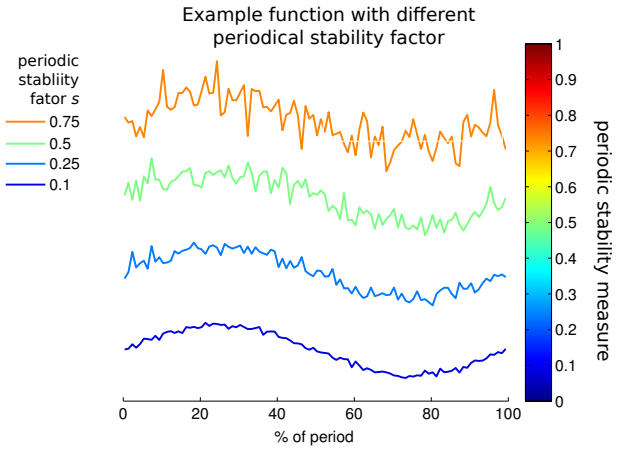

Figure 6.4: Example dataset with different periodic stability: S_{ref} is a sine function, the noise is generated from a distribution with 10%, 25%, 50% and 75% of the standard deviation σ of S_{ref}. A color scale is associated with the value of s. When $s > 0.1$, the normalized stability of the function is considered low.

Variation of the periodic pattern
The value of normalized stability factor s is obtained on a normalized signal, and thus does not take into account the potentially high variations in offsets and amplitudes between different periods. In order to circumvent this issue, the values of μ_i and σ_i are compared among cycles to determine their variability. The variability is assessed using the standard deviation of the μ_i and σ_i and is noted v_μ and v_σ.

$$v_\mu = std(\mu) \tag{6.14}$$
$$v_\sigma = std(\sigma) \tag{6.15}$$

With μ being the vector of μ_i of each sub signal and σ being the vector of σ_i of each sub signal $S_i(t)$.

6.4.3 Generation of differentiable functions

Since the final goal is the implementation of AWOs, another requirement need to be fulfilled by the functions. Indeed, the function obtained need to be differentiable, since the derivative of the function is needed in the implementation of the AWOs. To satisfy this criterion, the normalized nominal function $g^n(t)$ is generated using a spline interpolation of degree three of the mean of the fully normalized sub signals $\overline{S^n(t)}$. The number of regularly spaced knots used for the interpolation controls the quality of the interpolation (here we

considered 100 knots per cycle, which was empirically proven to be largely sufficient to perfectly reproduce the stereotyped function).

Chapter 7

Results

7.1 Pattern extraction from sensory information

7.1.1 Sensory signal periodic variability

For the sensory variability study, we use the methodology presented in section 6.4; we calculate the periodical stability of a normalized signal using the normalized stability factor s and then determine the variations in offsets and amplitudes using the two momentum variability factors v_μ and v_σ. This analysis is crucial to determine which IN_{SEN} are periodically variable and thus should remain modeled as feedbacks, and which ones are stable enough to be replaced either by IN_{BAS} or IN_{CPG}. This analysis is performed on the FBL based experiments presented in the first part of the report (list of the experiments and specificities can be found in table 3.1).

The figure 7.1 presents the stability scores s (top panel), the standard deviation of first momentum stability factors v_μ (middle panel) and the standard deviation of second momentum stability factors v_σ (bottom panel) of the different IN_{SEN} (see section 6.4.2 for how the different factors are calculated, and table 6.1 for the list of IN_{SEN} used by the FBL model, their abbreviations and action on the muscles).

The IN_{SEN} relaying information from ground and trunk angles and responsible for maintaining the body upright generate the most variable signals (the three stability factors are large compared to others). Generally the IN_{SEN} relaying information from the muscle sensors are really small. An exception is the IN_{SEN} relaying information from the VAS muscle, that has the largest variability factor s. This result correlates with the observation made in the first part of the report (section 3.1.2) that the model VAS muscles activity poorly correlates with the human one. Indeed, it is likely that the missing structures (i.e. elasticity and toes) not only affects similarity with human muscle activity, but also the signal variability, as the shock is mainly absorbed at the knee level and might significantly change between cycles.

7.1.1.1 Minimal FBL : FBL reduction

In this section, we reduce the sensory information used by the FBL model to its minimal (called FBL-) and we compare FBL and FBL- gait characteristics. The experiment 7a is used as starting point. The IN_{SEN} that show the least variability (red star on the figure 7.1) are removed from the system and replaced by constant signals (of amplitude equaling the mean of the signal). When tested on exp 7a, the resulting gait (see video [6]) looks similar to the original gait in many regards (see figure 7.2 for a comparison between FBL and FBL- models regarding joint angles correlation with human and vertical ground

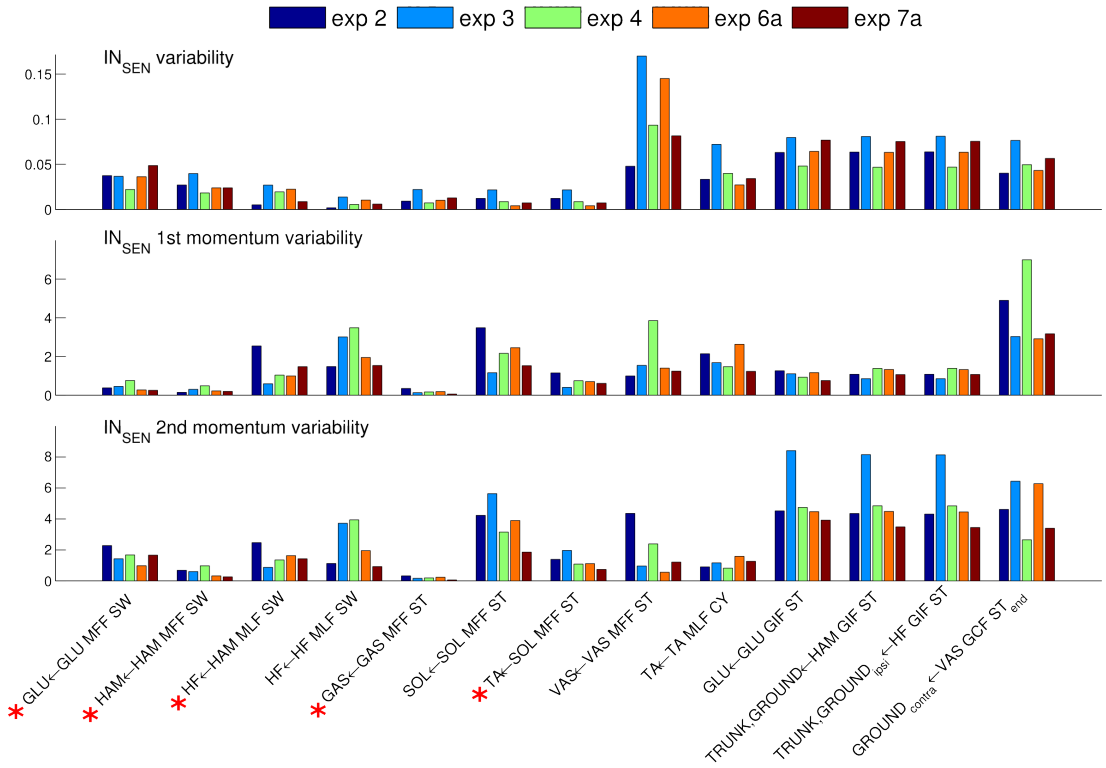

Figure 7.1: IN_{SEN} signals variability of experiment 2, 3, 6, 7. Experiment 1 is not shown because the variability was much to high compared to other experiments. .

reaction forces). The only notable difference between the two gaits is a decrease in speed from 1.3 to 1.2 [m/s] for the FBL- gait. It is also interesting to note that there is no clear decrease in robustness between the FBL and FBL- model (see section 7.2).

7.1.2 Pattern signal extraction

After analyzing the variability of the IN_{SEN} signals (see figure 7.1), we extract the nominal pattern of each IN_{SEN} (see section 6.4.1 for the nominal function extraction method). The figure 7.3 shows the IN_{SEN} nominal patterns of IN_{SEN} from experiment 3 (solid line) and 7a (dashed line) evaluated on flat ground. It is interesting to note that nominal patterns from experiment 3 and 7a correlate for the most periodically stables IN_{SEN}. Low correlation is observed for the VAS ← VAS MFF ST IN_{SEN}, the only IN_{SEN} acting on the VAS muscle (knee extensor). This IN_{SEN} is active only during stance phase and is important for generating the forward movement of the body. Low correlation is also observed for all IN_{SEN} responsible for postural control (IN_{SEN} from the joint trunk sensor and force sensor on the foot). The model from experiment 7a differs from experiment 3 mainly at the level of the IN_{SEN} related to stability sensors (i.e. GCF and GIF), while muscle IN_{SEN} are generally not modified, except the ones acting on VAS and TA, which are important during stance (VAS and TA) and stance preparation (VAS). Based on the fact that the most variable signals within one gait are also the ones that are modified in gaits optimized on perturbed environments (exp 7a) compared to flat ground optimization without perturbations (exp 3), we can make the hypothesis that the least periodically stable IN_{SEN} are the one that are important for gait stability.

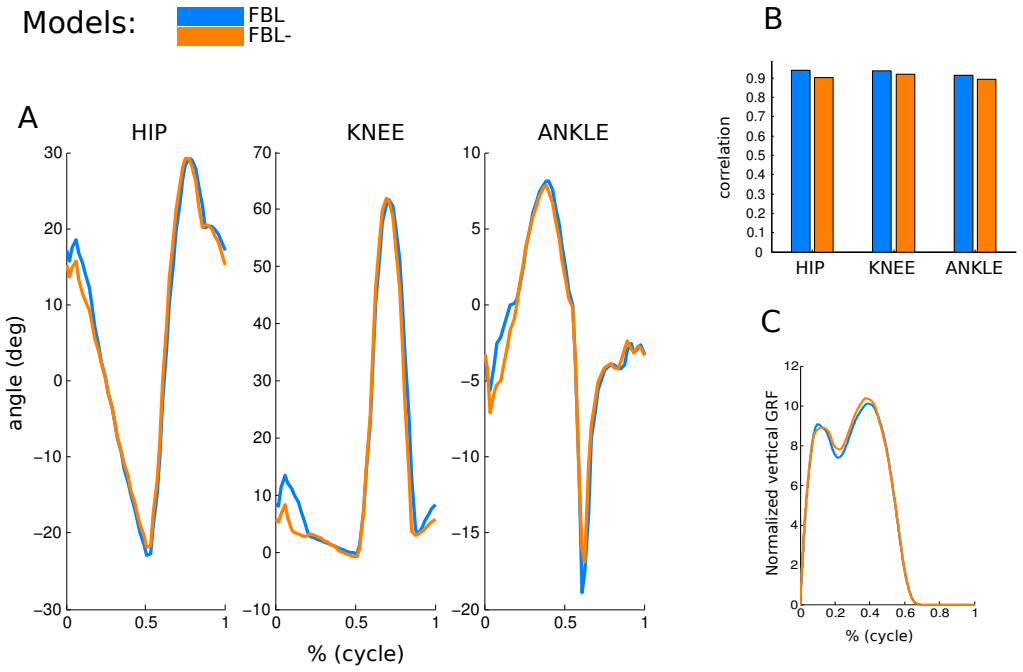

Figure 7.2: Comparison of FBL (blue) and FBL- (green) models for experiment 7a. The FBL- model has 5 IN_{SEN} removed from the initial 13 (see figure 7.1). A: HIP, KNEE and ANKLE angle comparison. B: HIP, KNEE and ANKLE angle correlation with corresponding human joints angles. C: Normalized vertical ground reaction force comparison..

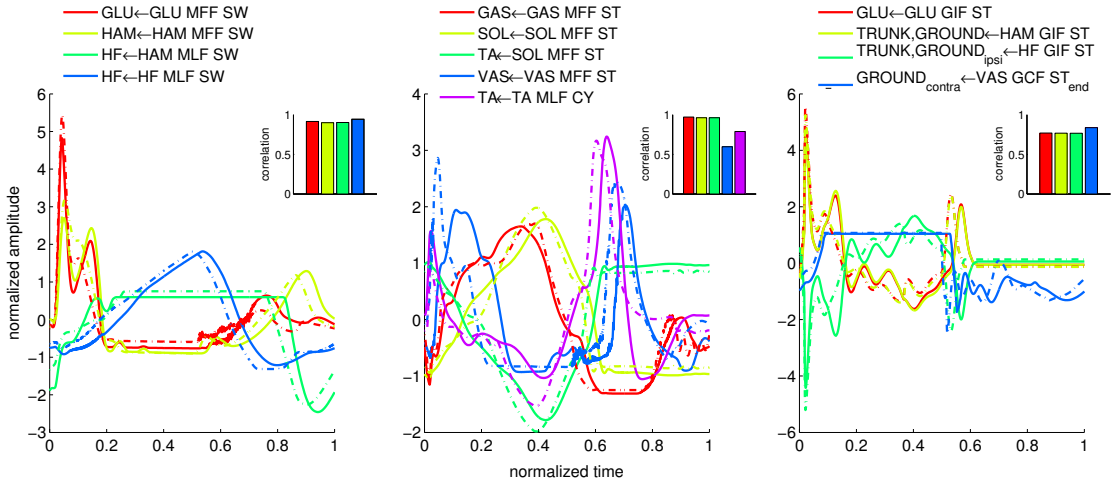

Figure 7.3: Normalized IN_{SEN} signals comparison between a solution of experiment 3 (solid line) and a solution of experiment 7a (dashed line). See table 6.1 for IN_{SEN} signal details. The correlation between corresponding signals of each experiment is shown in the top right of each graph. LEFT: Muscle feedback active during swing. MIDDLE: Muscle feedback active during stance or whole cycle. RIGHT: Ground and Trunk feedback

7.2 Robustness comparison

In this section we compare the robustness of the 3 different models (FBL, FBL-, 3FBL). Here we use the solution of experiment 7a for the FBL model (note that similar results are obtained when using the solution of experiment 6a, data not shown). See figure 6.2 for FBL- and 3FBL model composition and comparison with the FBL model. The robustness

is evaluated without on-line control, the default control vector is used (see eq. 6.1).

The results of the robustness evaluation are shown in the figure 7.4. We can see that there is no clear difference between the different models regarding their correlation with humans. There is a slight decrease in correlation at the level of the KNEE and ANKLE joints for the 3FBL model. When inspecting the gait of the 3FBL model with the C^{trl}_{std} we see that it is going more slowly than the FBL and FBL- models, both of which are going at the same speed as the human gait used for comparison. This could explains the 3FBL lower joint correlation, since a difference in speed is expected to modify the joints movements. Regarding the resistance to pushes, all models are in the same range (80[N]). Same holds for the resistance to slope change. We can note, however, that the variation in the results is larger for the 3FBL and FBL- models, possibly because both models have 30% less sensors than the FBL model (they have less IN_{SEN} and therefore less information about the body/environment interactions).

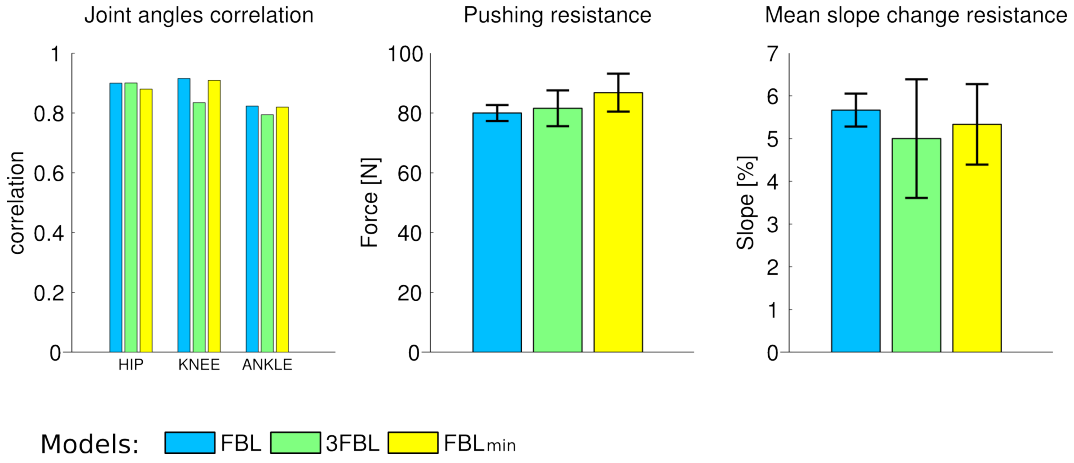

Figure 7.4: LEFT: Joint angles correlation with human for the the FBL, FBL- and 3FBL models. MIDDLE: Mean maximum push force amplitude resistance. RIGHT: Mean maximum slope change (in %) resistance

7.3 Online gait control

In this section we look at the new feature that an online control can bring to the different models. The online control is made through the modification of the C^{trl} control vector (defined in section 6.2.2). The online control will be evaluated for changes in speed and adaptation to increasing slope.

7.3.1 Walking on upward increasing slope

In this section, we look at the ability of the different models to negotiate an environment with increasing slope (see figure 7.5 A, for a representation of the environment). The slope increases from 0 to 30% in 160 meters. Each model is evaluated with and without online control. The online control is made manually by a person trained to this task.

It seems logical that without controlling the gait, the maximum slope successfully managed by the model can not be too steep, since changes in gaits are necessary to adapt to increasing slope. This is indeed confirmed by the results (see blue bars on figure 7.5 B). As expected (and mentioned in the previous section), without online control, the best model is the FBL model, since it uses more sensory information. However when varying

the component of the C^{trl} vector the results reverts. The best results are obtained with the 3FBL model. The control of the internal frequency of the CPGs is crucial in negotiating slope steeper than 10%, as a decrease in frequency forces the movements to slow down and thus provide sufficient force to climb up. Here, the online control is done manually, and results are very promising. The next step regarding the online adaptation would be the implementation of a neural network that uses different kind of feedbacks to control value of the C^{trl} control vector.

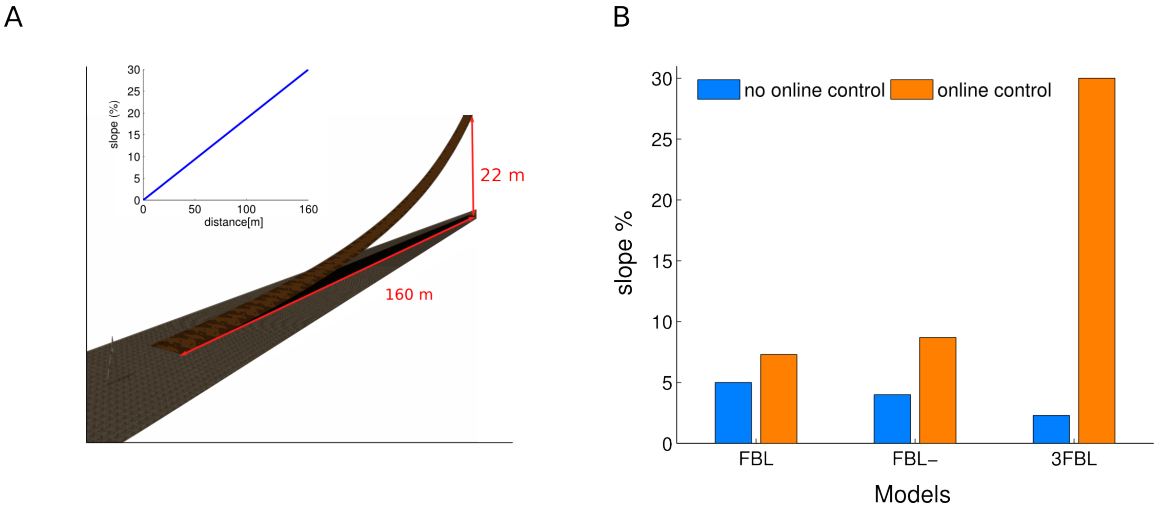

Figure 7.5: A: view of the increasing slope, the slopes increase from 0 to 30% in 160 meters. B: maximum successfully managed slope percentage of the FBL, FBL- and 3FBL without online control (blue) and with online control (orange).

7.3.2 Speed changes

In order to look at the effect of the modification of the C^{trl} control vector on the characteristics of the gaits, we implemented a simple systematic search algorithm that iteratively modifies the C^{trl} control vector. During one systematic search, only two components of the C^{trl} vector are modified and the others are kept constant. After each modification of the C^{trl}, we wait a certain amount of time (to ensure that the gait as stabilized) before recording the gaits characteristics.

In this analysis, we focus on the 3FBL model, since the slope management experiment showed that it can successfully negotiate slope up to 30%, which is more than three times better than scores obtained by the two other models (i.e. FBL, FBL-). However, in the future, an in depth analysis and comparison with the two other models would be interesting.

The figures 7.6 and 7.7 shows two examples of systematic searches that lead to interesting changes in the gait characteristics of the 3FBL model. Each figure is made of 4 sub-figures, each of which showing a specific gait characteristic (top-left the mean speed, top-right the energy consumption, bottom-left the mean double stance duration per cycle and bottom-right the mean cycle length).

When looking at the figure 7.6 where the amplitudes of both basal and CPG interneurons are modified (i.e. $A_{\mathrm{IN}_{\mathrm{BAS}}}$ and $A_{\mathrm{IN}_{\mathrm{CPG}}}$), we observe speed changes from 1.2 m/s to 1.5 m/s. It is interesting to note that changes in $A_{\mathrm{IN}_{\mathrm{CPG}}}$ have almost no effect; neither on the speed, nor on the energy consumption of the gait. However, we note that $A_{\mathrm{IN}_{\mathrm{CPG}}}$ values seem to have an effect on the double stance duration. Interestingly, some fast gaits show

very small double stance durations, which indicates that the gait spent almost no time with both foot on the ground, thus indicating that we are going toward a change in regime from walking to running. However running gait could not be found using this model. It is possible that the addition of a rule for entering in the end stance phase based J.Wang works (see section 2.1.3) could help generating this change in regime.

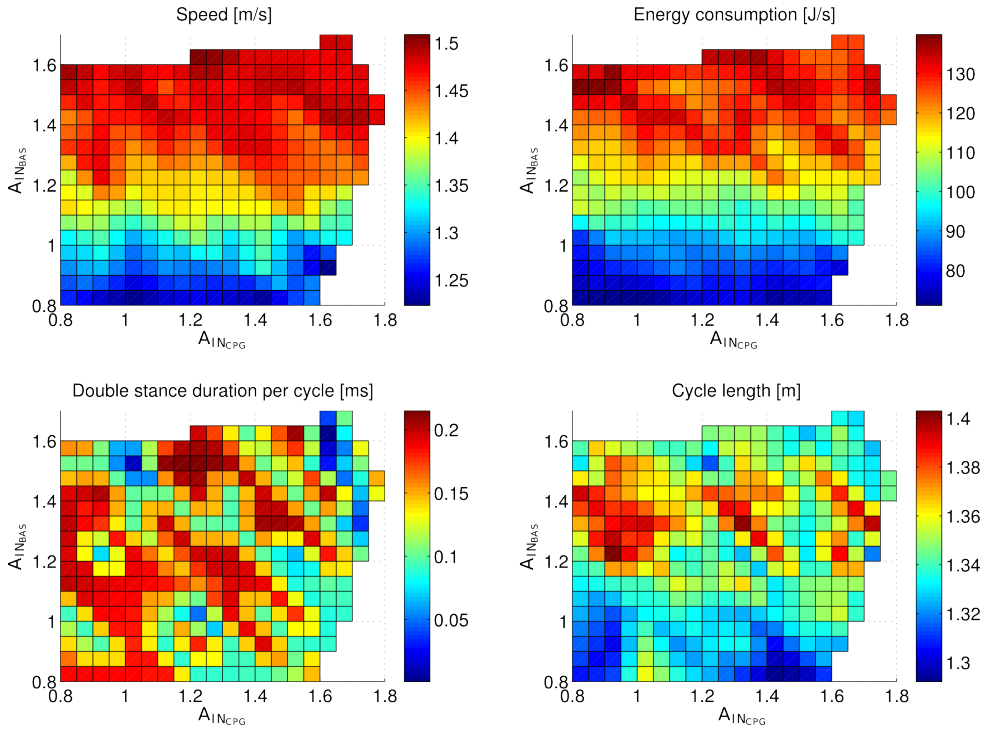

Figure 7.6: Systematic search made by varying the $A_{\mathrm{IN_{BAS}}}$ and $A_{\mathrm{IN_{CPG}}}$ components of the C^{trl}. Others component are the same as for the C^{trl}_{std} except the $O_{\mathrm{IN_{CPG}}}$ that is set to -0.2. Top left: Speed, Top right: Energy consumption, Bottom left: Double stance duration, Bottom right: Cycle length.

The figure 7.7 shows the results of a systematic search on the frequency of the CPG interneurons and on the offset of the basal interneurons (i.e. ω and $O_{\mathrm{IN_{BAS}}}$). The first thing that can be noted is the correlation that exists between those two control variables and the speed. We can draw a simple linear relationship that would bring the robot from its the minimal speed of 0.8 to almost 1.4 m/s. Using a linear multidimensional minimization (Nelder-Mead method implemented in the fminsearch Matlab function) we obtained the following linear relationship :

$$f(O_{\mathrm{IN_{BAS}}}, \omega) = a_1 O_{\mathrm{IN_{BAS}}} + a_2 \omega + a_3 = \mathrm{S} \tag{7.1}$$

Where S is the speed, and $(a_1, a_2, a_3) = (4.40, 0.57, 0.63)$. This relationship can satisfactory predict the speed of the model.

It is also interesting to note that the energy consumption does not always increases with increasing speed, as it was illustrated in figure 7.7. Indeed, the gait of highest speed is not the one that consumes the most energy. We can also note a clear and brutal decrease in cycle length for frequency between 0.7 and 0.85 and $O_{\mathrm{IN_{BAS}}}$ smaller than -0.05.

7.3.3 Impact of basal interneurons in controllability

In this section we propose to test the effect of removing the basal interneurons in the controllability of the gait (i.e. effects of changes in the control variables). A simple

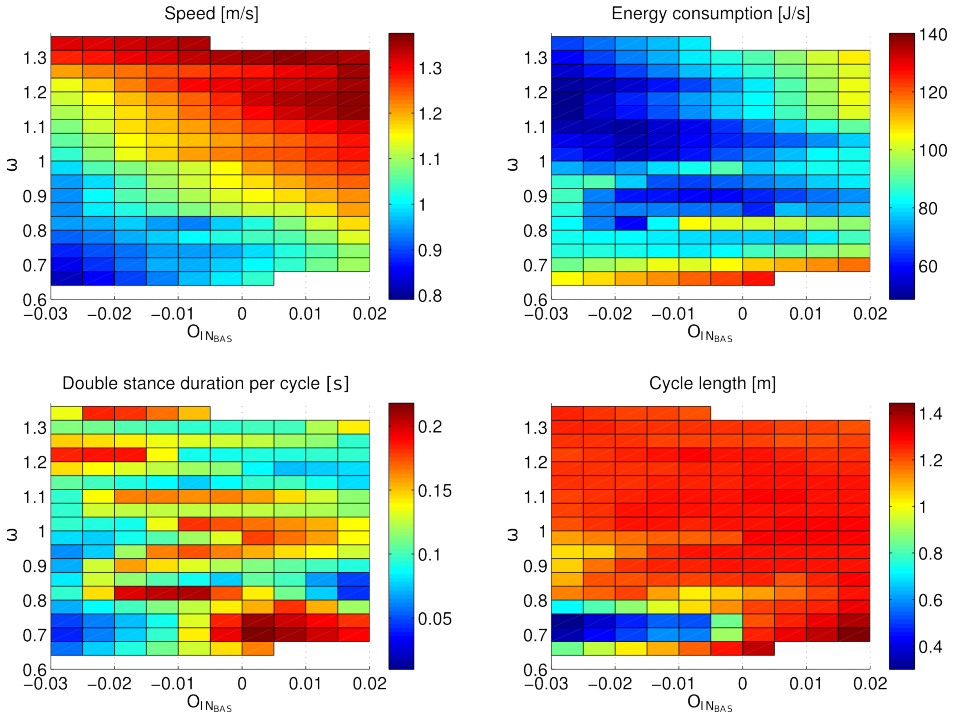

Figure 7.7: Systematic search made by varying the ω and $O_{\mathrm{IN_{BAS}}}$ components of the C^{trl}. Others component are the same as for the C^{trl}_{std}. Top left: Speed, Top right: Energy consumption, Bottom left: Double stance duration, Bottom right: Cycle length.

systematic search experiment is designed. The search space is limited as follow: a) we fix the $A_{\mathrm{IN_{SEN}}}$ and $O_{\mathrm{IN_{SEN}}}$ variables to their default value, this is motivated by the fact that we don't want to modify $\mathrm{IN_{SEN}}$ that showed an importance in stability (see section), b) variables 1 to 4 (respectively $O_{\mathrm{IN_{BAS}}}$, $O_{\mathrm{IN_{CPG}}}$, $A_{\mathrm{IN_{BAS}}}$, $A_{\mathrm{IN_{CPG}}}$) are tested to by two for 49 different pair values in the range defined in figure 7.8, c) for each pair values 6 different frequency (ω) are tested. The search is made online. The control vector is updated each ten seconds. Gait characteristics are collected during the last seconds seconds (four seconds are devoted to gait stabilization after parameter changes).

Two different models are tested with this systematic search scheme. The 3FBL and 3FBL' model. As we are interested in the impact of basal interneurons in controllability, the 3FBL' model is equivalent to the 3FBL model except that $\mathrm{IN_{BAS}}$ are replaced by $\mathrm{IN_{SEN}}$ which are still controlled by their own variables: $O_{\mathrm{IN_{BAS}}}$ and $A_{\mathrm{IN_{BAS}}}$).

The results of the systematic search with the 3FBL and 3FBL' model are shown on figure 7.9 and figure 7.10. Each quadrants shows one gait characteristic recorded (top left: mean speed, top right: step length variance, bottom left: double stance support duration, bottom right: gait frequency). In each cells, the white part indicate that the set of variable is unstable and make the robot fall.

By comparing the white part on each cells, the first thing we can note is that the 3FBL model (figure 7.9) is stable against changes in parameters in a larger range than the 3FBL' model (7.10).

When looking at the variance of the step length (top right quadrant), which is a measure of the gait stability, we can note that the variance of both 3FBL 3FBL' models in general increase with a decrease in frequency. However there are still set of parameters that are stable even at low frequency.

When looking at change in speed we can see that in general the 3FBL goes slower than

the 3FBL'. Which could be explained by the fact that some of the MFF and MLF IN_{SEN} play the role of positive feedback rules. Especially some MFF and MLF IN_{SEN} projects to the same muscles than they receives input from. If positive this kind of auto-feedback increases the response of muscle, i.e it the same burst will generate a bigger response due to the positive feedback loops and hence a faster gait.

The 3FBL speed vary from 0.70 to 1.35 [m/s] while the 3FBL' speed vary from 0.70 to 1.60. Although the 3FBL model can be stable in all speeds the 3FBL' is stable only between 1.0 to 1.60 [m/s].

An interesting effect can also be observed at the level of double stance duration. Indeed as it is visible on the 23 columns of the bottom left quadrants of figure 7.9 with frequency of 1.11, the increase of the variable 2 and 3 ($O_{\text{IN}_{\text{CPG}}}$,$A_{\text{IN}_{\text{CPG}}}$ respectively) shows a decrease of the double stance duration from 0.2 while increasing the the frequency the double stance duration decreases from 0.2 to almost zeros second possibly indicating that a change of regime (from walking to running) could be possible in those region. However the model like that seems impossible to run as this decrease in the double stance duration correlates with an increase in the instability of the gait (indicating that some structure are possibly missing, the implementation of the feedforward component on the J.Wang model (see section 2.1.3) could be interesting).

To conclude, it is interesting to note that even if the frequency of the CPG as an impact on the gait it is in not linked with its frequency as it could be expected. Indeed, increase in speed can be observed without changing the gait frequency (combine column 24 of top left and bottom right quadrants on figure 7.9). This indicates that in this model the effect of the CPG is not the usually modeled one, where the system frequency synchronizes to the one of the CPG. This indicates that our model of CPG is more like a vestige of CPG network.

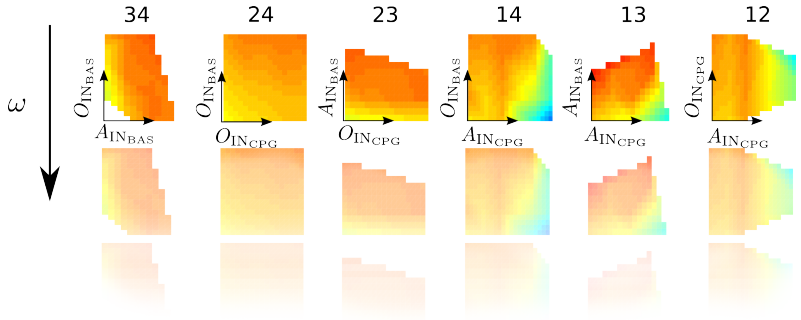

Control Variable

Id	Name	Range	Std.
1	$O_{\text{IN}_{\text{BAS}}}$	$[-0.01; 0.01]$	0.0
2	$O_{\text{IN}_{\text{CPG}}}$	$[-0.01; 0.01]$	0.0
3	$A_{\text{IN}_{\text{BAS}}}$	$[0.7; 1.6]$	1.0
4	$A_{\text{IN}_{\text{CPG}}}$	$[0.7; 1.6]$	1.0
0	ω	$[0.65; 1.8]$	0.85

Figure 7.8: TOP: description of the organization of figures 7.10 and 7.9. Each column corresponds to the variation of two control variables (shown as axis name). The title of each column is in the format id_1id_2 where id_1 is the id of the control variable on the x-axis and id_2 is the id of the control variable on the y-axis. Each line corresponds to a different frequency in ascending order. BOTTOM: table showing the different control variable name, id, default values, and the range used in the systematic search.)

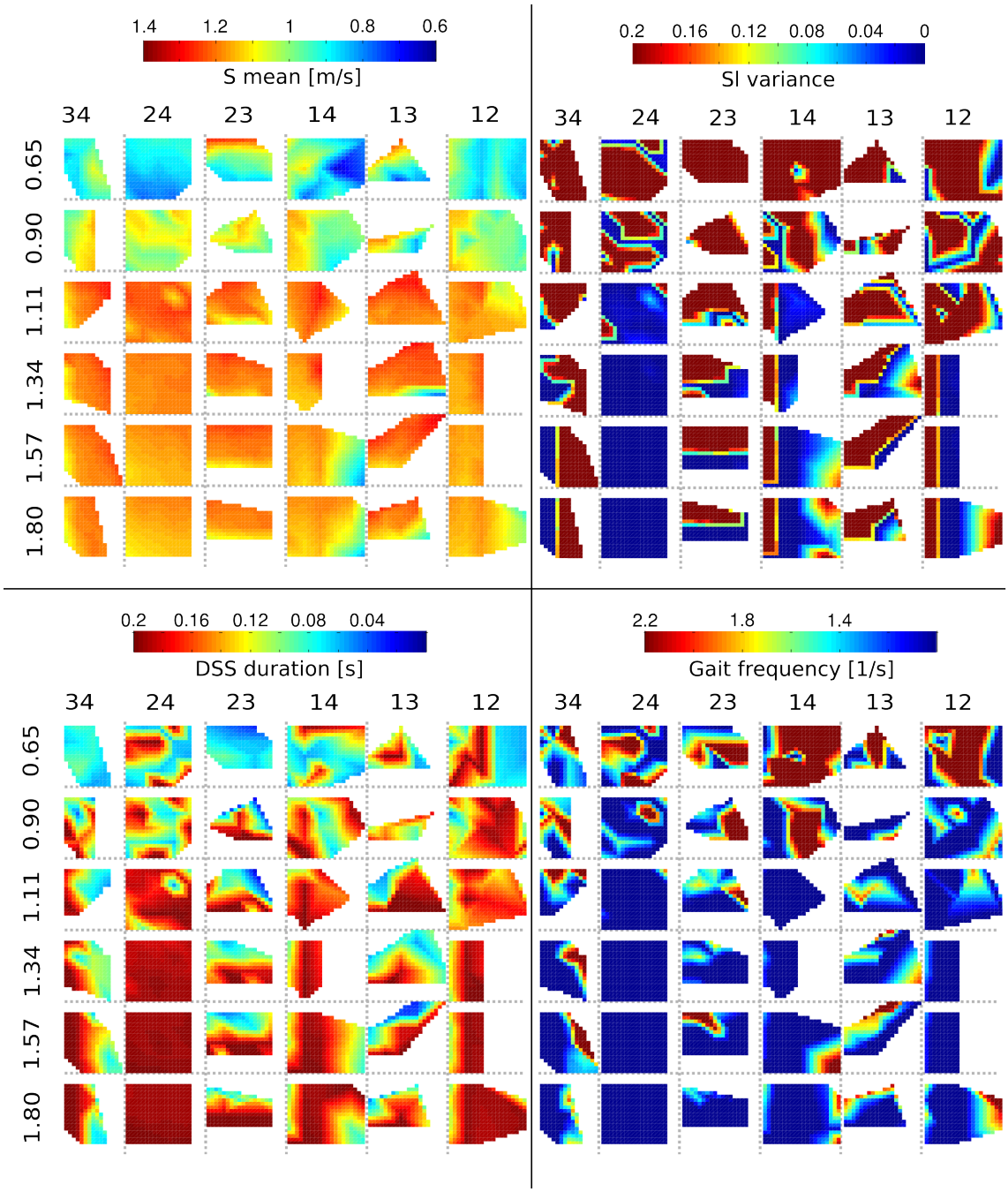

Figure 7.9: Systematic search on the control variable (shown on figure 7.8) of the 3FBL model. The parameters are modified two by two (each column), while each line corresponds to different frequency of the CPG. On each quadrants a different gait characteristics is shown TOP LEFT: Mean speed [m/s]. TOP RIGHT: Step length variance. BOTTOM LEFT: Double stance support duration [s]. BOTTOM RIGHT: Gait frequency [1/s].

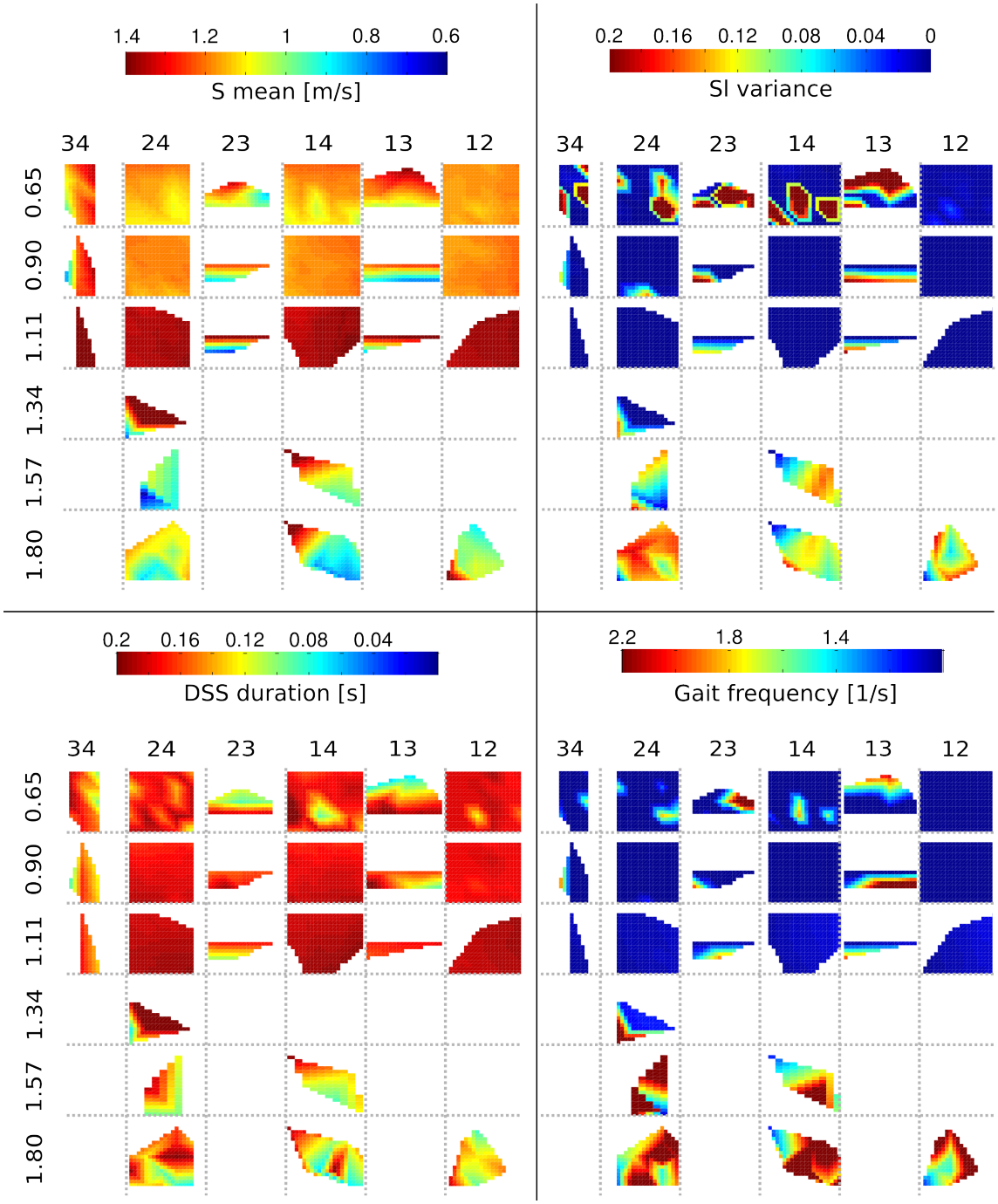

Figure 7.10: Systematic search on the control variable (shown on figure 7.8) of a slightly different version of the 3FBL model (where $\mathrm{IN}_{\mathrm{BAS}}$ are replaced by $\mathrm{IN}_{\mathrm{SEN}}$ which are still controlled by their own variables: $O_{\mathrm{IN}_{\mathrm{BAS}}}$ and $A_{\mathrm{IN}_{\mathrm{BAS}}}$). The parameters are modified two by two (each column), while each line corresponds to different frequency of the CPG. On each quadrants a different gait characteristics is shown TOP LEFT: Mean speed [m/s]. TOP RIGHT: Step length variance. BOTTOM LEFT: Double stance support duration [s]. BOTTOM RIGHT: Gait frequency [1/s].

Chapter 8

Discussion

8.1 Model modifications

Given the quality of the results obtained with the FBL model despite its simplicity compared to the complexity of the brain (see section 3), its use as starting point for the addition of a biologically inspired feedforward component is fully justified. Therefore, motivated by the goal of adding this component, the FBL model was dissected (see section 6.1) in order to understand the relative importance of each of its components. Using the simple methodology described in section 6.4.2 we showed that almost all signals generated by muscles feedbacks were perfectly periodic, (i.e. small variation between cycles, see figure 7.1).

When comparing the signals generated by gaits resulting from experiment 3 and 7a (see figure 7.3). Most of the feedbacks had similar shapes. Main differences came from the stability feedbacks and muscle feedbacks controlling the VAS and TA muscles. This is fully consistent with the sensors variability assessment within one gait (see figure 7.1). Meaning that the feedbacks that shows the biggest differences between experiment 3 and experiment 7a or 6a are also the one that are the most variable among cycles of a given gait. The conclusion we can draw from this observation is that the feedbacks that are the more variable during locomotion are the one responsible for brining stability to the model. Indeed, when optimizing the gait for robustness and comparing the generated feedbacks signals, only the one that were the more variable during locomotion are adapted to increase the robustness of the gait. This confirms the importance of the ground and trunk feedbacks in the stabilization of the gait.

Most interestingly, when replacing those less variable signal by constant input (5 from the 13 feedback rules per limb where removed like that), the obtained reduced gait (so-called FBL- model) showed characteristics remarkably close to the FBL model (see figure 7.2).

Those results opened the way toward the addition of a feedforward component, as the possibility of using constant input signals is consistent with biological characteristics of some descending neural pathways (see section 5.1). Furthermore, as the replaced signals were almost periodical, they could be replaced by oscillators. These observations permitted the implementation of a new model: 3FBL models (sensory + basal + CPG activity) (see figure 6.2 for details).

The results obtained by the two new models (FBL- and 3FBL) without any other changes than the replacement of some of the sensory interneurons by feedforward interneurons did not show significant decrease in the quality of the gait (both in term of human similarity and robustness).

8.2 Online control

In order to verify the validity of the added feedforward component, a set of control rules needed to be implemented. Inspired from biological facts, two basic control rules were added (see section 6.2.2). Those rules give raise to a set of 6 control variables. The 3FBL model had also an extra control variable to set the frequency of the CPG. By varying those control rules, interesting properties were observed. Indeed, the models were able to adapt their speed by varying only one or two control variables. Notably, the 3FBL model showed capacity to go from 0.8 to almost 1.6 [m/s]. Some values set to control variables also led to significant decreases in double stance support duration, bringing it close to 0. When visually inspecting the gait, they were almost running.

Furthermore, the online adaptation of the control variables also permitted to walk on slope up to 30% with the 3FBL. Whereas only slopes of 10% were manageable with an online control on the FBL or FBL- model.

By combining the two characteristics of the online control (e.g. adaptation to environment change and control of gait characteristics), the next stage would be the implementation of an artificial neural network taking as input sensory information (to adapt to environment changes) and desired gait characteristics (such as speed changes), where the output of the network would be the control variables. This artificial neural network could corresponds to some higher brain structures such as the cerebellum or the reticular formation, which are known to work has modular structures during locomotion.

Chapter 9

Conclusion

In this project, we confirmed that the FBL model could reproduce human gait with satisfactory similarity (see section 3.1.2). These results are particularly striking, as this model is exclusively controlled by reflexes. We then showed that optimization of the gaits on perturbed environments (i.e. wavy grounds and pushes, see section 3.2) could drastically increase the gait resistance to pushing perturbations. Notably, only feedbacks associated with gait stability were modified (i.e. those related to ground sensors and trunk position, see section 7.1.2).

However, this model has its limitations: missing physical properties and elements, such as toes or body elasticity still prevent the model to totally recapitulate the main features of human gait (see section 3.1.2). Moreover, because of the simplicity of the model, both robustness and adaptability to changes in slope were relatively limited (see section 3.2). It is therefore clear that human walking is not simply generated through feedback, but that other circuits are necessary.

This is why, after an in depth analysis of the FBL model, we moved toward the implementation of different types of extensions that could provide the model with increased capacities and similarity with real human gaits.

The first step was a reorganization of the model into three more realistic steps; the sensory inputs (SEN), the sensory interneurones (IN_{SEN}) and the motoneurons (MN). Interestingly, the sensory interneurones that were shown to vary during robustness optimization, are also the ones that were the most variable during walking.

The IN_{SEN} that were shown not to vary among walking cycles (30% of the total IN_{SEN}, as determined by the periodical stability assessment method described in section 6.4.2), were modeled - based on their cyclic behavior- either as a constant input (both in the FBL- and 3FBL models) or as CPGs (in the 3FBL model only), introducing a feedforward component to the initial feedback based model.

Replacement of the selected IN_{SEN} by constant signals (i.e. the FBL- model, see section 7.1.1.1) showed no significant differences in gait characteristic and robustness to perturbations, as compared to the initial model, although 30% of the feedbacks (corresponding to 70% of the muscle feedbacks) were removed. This result indicates that the selected signals (i.e. those not involved in gait stabilization) do not have a crucial role in gait generation and stabilization.

Moreover, in the 3FBL, where selected IN_{SEN} (acting on proximal limb muscles) were replaced by CPG, the implementation of an online control of a set of variables successfully allowed adaptation to changing environments (i.e. increasing slope) and speed modifications (see section 7.3). This results is mainly due to the creation of a variable that controls CPGs frequency (ω), which could be related to the control of hypothetic oscillatory struc-

ture present in interneurons networks of the spinal cord and modulated by input from the reticular formation. An other variable controlling the amplitude of the signal generated by interneurones was also shown to be important (see section 7.3.2), this control could be related to inhibitory connection from the cerebellum, controlling the amplitude of the spiking frequency of spinal cord interneurons. This result suggests that even simple control circuits in upper brain structure like the reticular formation are enough to modulate the generated movement, which would be almost fully encoded at the spinal cord level. Online modulation of the set variable together with the control of the CPG frequency generated modification of the gait permitting to walk on slope up to 30% (see section 7.3.1). These results suggest the existence of a secondary layer of sensory control, acting closer to the CNS. For instance, in humans, the cerebellum plays exactly this role of sensory integrator, by adapting the gait to change in environment (see section 5.1.2). In the future, it would be interesting to investigate further whether gait transition could be found by simply varying the high level control variables. Indeed, preliminary results indicates an emerging change in regime when the basal activity of some of the interneurons is modified. Indeed, the duration of the double stance support phase was observed to decrease proportionally to the increase in basal activity, while it was visually observed that the robot tried to run (see section 7.3.2). It would be interesting to implement the feedforward component to the J. Wang's extension of the FBL model, to test the hypothesis of gait changes while uniquely changing the global offset of the system.

Taken together, the results presented in this report show that simple extensions of the H. Geyer feedback based model allows the implementation of a control that could have various applications in medical field, such as intelligent prostheses and orthoses. Indeed, the possibility of controlling gait characteristics (of a model generating movement comparable to human walking) by simple signals could allow adaptation to the contently changing environment that humans face while walking (e.g. slope, uneven ground, steps, pushes). Therefore, the implementation of such prosthesis/orthosis could be of tremendous interest in the medical field, where, up to now, no prosthesis possesses such adaptive capabilities.

Bibliography

[1] A J Bastian, K M Zackowski, and W T Thach. Cerebellar ataxia: torque deficiency or torque mismatch between joints? *Journal of neurophysiology*, 83(5):3019–3030, May 2000. PMID: 10805697.

[2] Steve Berger. Energy consumption optimization and stumbling corrective response for bipedal walking gait, 2011.

[3] Lindsay J. Bhargava, Marcus G. Pandy, and Frank C. Anderson. A phenomenological model for estimating metabolic energy consumption in muscle contraction. *Journal of Biomechanics*, 37(1):81–88, January 2004.

[4] Mohsen Damavandi, Philippe C. Dixon, and David J. Pearsall. Ground reaction force adaptations during cross-slope walking and running. *Human Movement Science*, 31(1):182–189, February 2012.

[5] N. Dominici, Y. P. Ivanenko, G. Cappellini, A. d'Avella, V. Mondi, M. Cicchese, A. Fabiano, T. Silei, A. Di Paolo, C. Giannini, R. E. Poppele, and F. Lacquaniti. Locomotor primitives in newborn babies and their development. *Science*, 334(6058):997–999, November 2011.

[6] Florin Dzeladini. Implementation of a human feedback based locomotion and its control by means of a biologically inspired feedforward component http://biorob.epfl.ch/page-36403-en.html, 2013.

[7] M. J. T FitzGerald, Gregory Gruener, and Estomih Mtui. *Clinical neuroanatomy and neuroscience*. Saunders/Elsevier, [Edinburgh?], 2012.

[8] H. Geyer, A. Seyfarth, and R. Blickhan. Positive force feedback in bouncing gaits? *Proceedings of the Royal Society B: Biological Sciences*, 270(1529):2173–2183, October 2003.

[9] Hartmut Geyer and Hugh Herr. A muscle-reflex model that encodes principles of legged mechanics produces human walking dynamics and muscle activities. *IEEE Transactions on Neural Systems and Rehabilitation Engineering*, 18(3):263–273, June 2010.

[10] A M Gordon, A F Huxley, and F J Julian. The variation in isometric tension with sarcomere length in vertebrate muscle fibres. *The Journal of physiology*, 184(1):170–192, May 1966. PMID: 5921536.

[11] A. V. Hill. The heat of shortening and the dynamic constants of muscle. *Proceedings of the Royal Society B: Biological Sciences*, 126(843):136–195, October 1938.

[12] A.L. Hof, H. Elzinga, W. Grimmius, and J.P.K. Halbertsma. Speed dependence of averaged EMG profiles in walking. *Gait & Posture*, 16(1):78–86, August 2002.

[13] Matthias Hoffmann, Moritz Mühlenthaler, Sabine Helwig, and Rolf Wanka. Discrete particle swarm optimization for TSP: theoretical results and experimental evaluations. In David Hutchison, Takeo Kanade, Josef Kittler, Jon M. Kleinberg, Friedemann Mattern, John C. Mitchell, Moni Naor, Oscar Nierstrasz, C. Pandu Rangan, Bernhard Steffen, Madhu Sudan, Demetri Terzopoulos, Doug Tygar, Moshe Y. Vardi, Gerhard Weikum, and Abdelhamid Bouchachia, editors, *Adaptive and Intelligent Systems*, volume 6943, pages 416–427. Springer Berlin Heidelberg, Berlin, Heidelberg, 2011.

[14] M Igarashi, T O-Uchi, and B R Alford. Volumetric and dimensional measurements of vestibular structures in the squirrel monkey. *Acta oto-laryngologica*, 91(5-6):437–444, June 1981. PMID: 7270114.

[15] Jesse Van Den Kieboom. Arbitrary Wave-Form Oscillator. *Building*, (4):1–3.

[16] C. Maufroy, H. Kimura, and K. Takase. Towards a general neural controller for quadrupedal locomotion. *Neural Networks*, 21(4):667–681, 2008.

[17] Roger G.T. Mello, Liliam F. Oliveira, and Jurandir Nadal. Digital butterworth filter for subtracting noise from low magnitude surface electromyogram. *Computer Methods and Programs in Biomedicine*, 87(1):28–35, July 2007.

[18] Carolyn F. Munro, Doris I. Miller, and Andrew J. Fuglevand. Ground reaction forces in running: A reexamination. *Journal of Biomechanics*, 20(2):147–155, January 1987.

[19] Werner Platzer. *Color atlas of human anatomy.* Thieme, Stuttgart ; New York, 6th rev. and enlarged ed edition, 2009.

[20] A Prochazka and M Gorassini. Ensemble firing of muscle afferents recorded during normal locomotion in cats. *The Journal of physiology*, 507 (Pt 1):293–304, February 1998. PMID: 9490855.

[21] Dale Purves and Jean-Marie Coquery. *Neurosciences.* De Boeck, Paris [etc.], 2005.

[22] Sandeep Rana, Sanjay Jasola, and Rajesh Kumar. A review on particle swarm optimization algorithms and their applications to data clustering. *Artificial Intelligence Review*, 35(3):211–222, November 2010.

[23] H. Reisine, J. I. Simpson, and V. Henn. A geometric analysis of semicircular canals and induced activity in their peripheral afferents in the rhesus monkey. *Annals of the New York Academy of Sciences*, 545(1 Representatio):10–20, December 1988.

[24] L. Righetti. Programmable central pattern generators: an application to biped locomotion control. *Proceedings 2006 IEEE International Conference on Robotics and Automation, 2006. ICRA 2006.*, (May):1585–1590, 2006.

[25] Kenneth S. Saladin. *Anatomy & physiology: the unity of form and function.* McGraw-Hill, New York, NY, 6th ed edition, 2012.

[26] Stephen H. Scott and David A. Winter. Biomechanical model of the human foot: Kinematics and kinetics during the stance phase of walking. *Journal of Biomechanics*, 26(9):1091–1104, September 1993.

[27] W Scott and J Stevens. Human skeletal muscle fiber type classifications. *Phys Therapy*, 81:1810–1816, 2001.

[28] XH Shi, Y. Zhou, LM Wang, QX Wang, and YC Liang. A discrete particle swarm optimization algorithm for travelling salesman problem. *Computational methods*, pages 1063–1068, 2006.

[29] Shoubao Su, Xibin Cao, and Xukun Zuo. Traveling salesman problems on a cuboid using discrete particle swarm optimization. In Rongbo Zhu and Yan Ma, editors, *Information Engineering and Applications*, volume 154, pages 404–411. Springer London, London, 2012.

[30] Jack M. Wang, Samuel R. Hamner, Scott L. Delp, and Vladlen Koltun. Optimizing locomotion controllers using biologically-based actuators and objectives. *ACM Transactions on Graphics*, 31(4):1–11, July 2012.

[31] David A. Winter. *Biomechanics and Motor Control of Human Movement.* John Wiley & Sons, Inc., Hoboken, NJ, USA, September 2009.

[32] Uri Wolf, Mark J Rapoport, and Tom A Schweizer. Evaluating the affective component of the cerebellar cognitive affective syndrome. *The Journal of neuropsychiatry and clinical neurosciences*, 21(3):245–253, 2009. PMID: 19776302.

[33] Wolfram Alpha LLC. 2010. Wolfram—Alpha. Human walking, 2012.